ANODIC TITANIUM DIOXIDE: ELECTROCHEMICAL SYNTHESIS OF CORE-SHELL AND HONEYCOMB NANOSTRUCTURES

A Thesis

Presented in Partial Fulfilment of the Requirements for the

Degree of Master of Science

with a

Major in Materials Science and Engineering

in the

College of Graduate Studies

University of Idaho

by

Steven J. Sitler

December 2013

Major Professor: Krishnan S. Raja, Ph.D.

AUTHORIZATION TO SUBMIT THESIS

This thesis of Steven J. Sitler, submitted for the degree of Master of Science with a Major in Materials and Science Engineering and titled "Anodic Titanium Dioxide: Electrochemical Synthesis of Core-Shell and Honeycomb Nanostructures," has been reviewed in final form. Permission, as indicated by the signatures and dates given below, is now granted to submit final copies to the College of Graduate Studies for approval.

Major Professor: _____ Date: _____
Dr. Krishnan Raja

Committee Members: _____ Date: _____
Dr. Indrajit Charit

_____ Date: _____
Dr. Thomas Williams

Department Administrator: _____ Date: _____
Dr. Wudneh Admassu

Discipline's College Dean: _____ Date: _____
Dr. Larry Stauffer

Final Approval and Acceptance by the College of Graduate Studies:

_____ Date: _____
Dr. Jie Chen

ABSTRACT

Growth of metal/oxide nanowires inside of semiconducting nanotubes has several applications for energy storage and energy conversion. In this study, growth of copper/copper oxide through electrodeposition techniques was studied as a method to fill TiO_2 nanotube arrays. Specifically, emphasis was placed on the study of copper containing electrolyte solution kinetics. This was necessary due to the differences between TiO_2 and anodic aluminum oxide (AAO) as the substrate. AAO has been well-studied and successfully filled with metal/oxide nanowires. The difficulty with TiO_2 is that unlike AAO it is not an insulator; this makes electrodeposition of the copper difficult as it is not inherently attracted to the bottom of the nanotubes. Another area of study was the morphology of the TiO_2 substrate. Through different anodization techniques a new self-ordered morphology of TiO_2, called Super Honeycomb was discovered. Applications of the Super Honeycomb nanostructure as well as a similar process on Ti-Mn alloy are reported.

ACKNOWLEDGEMENTS

I would like to thank, foremost, my loving and beautiful wife for her dedication and support. I would also like to thank my parents who have been supportive in so many ways. I am also very grateful for all the help and time my major professor, Krishnan Raja, has given me, and for the time and advise that my thesis committee has given me along the way. I would especially like to thank Dr. Williams for all his help using the electron microscopy lab. I would also like to thank the department of Chemical and Materials Engineering for funding my education and research. Thank you all.

TABLE OF CONTENTS

LIST OF FIGURES

CHAPTER 1: INTRODUCTION TO THESIS WORK

1.1 Electrochemical Growth of Copper Nanowires Inside of Semiconducting TiO_2 Nanotubes

Core-shell nano-composite structures, consisting of metal/semiconductor nanowires surrounded by oxide nanotubes, show interesting physical, electrical and catalytic properties. Therefore, these nano core-shell materials are extensively investigated for applications in next generation thermo-electrical, photovoltaic, sensor and energy conversion and storage devices.

Most of the reported core-shell nanostructures in the literature pertain to semiconductor cores from groups I-VI, II-IV or group III-V compounds on the periodic table with metal-oxide or carbon nanotube shells. TiO_2 nanotubes have been considered by many investigators as a shell structure with different core materials such as TeO_2, Cu_2O, ZnO, CdS, CdSe, Fe_2O_3, SnO_2, ZnTe, CdZnTe, etc. All these semiconductor core-shell structures are considered for photovoltaic, photocatalytic, and photoluminescence applications.

Metal-TiO_2 heterogeneous nanostructures such as Pt-TiO_2, Au-TiO_2, Ag-TiO_2, Ni-TiO_2 and others have been synthesized for importing enhanced catalytic/photocatalytic properties in oxidation of CO, Methanol, dyes, as well as photo water splitting, and fast energy storage. The metal-TiO_2 core-shell structures have been synthesized in various ways such as coating the TiO_2 onto the metal nanoparticle colloids by sol-gel method [1], reverse micelle systems containing aqueous solutions of core metal salts and $TiCl_3$ [2], exposing metal nanorods to a pH controlled $TiCl_3$ solution and hydrolyzing $TiCl_3$ into TiO_2 [3], electrodeposition of a metal core into TiO_2 nanotubes, and by wet chemical or hydrothermal synthesis of metal nanowires after filling the TiO_2 nanotubes with metal salt and calcining in a reducing atmosphere.

From the preceding discussion, it is noted that metal-TiO_2 core-shell nanostructures can be synthesized using several methods, and each method has its own merits and limitations. Therefore, choosing a particular synthesis method depends on the end-use for which the core-shell structure is to be applied. If the material is going to be used as a catalyst in a chemical reaction, such as oxidation of carbon monoxide, then it would be used in a particulate form. In such a case, a one-pot synthesis method based on reverse-micelle would be the most economical manufacturing route. If the intended use is for electrodes of an energy storage device, then the core and the shell materials each should be in contact with a current collector. Particulate core-shell nanomaterials require metal foil, such as copper or aluminum, to be coated as in the case of Li-ion battery anodes or ultra-capacitors electrodes. This results in an additional manufacturing step. Therefore, considering electrodeposition of core nanowires into TiO_2 nanotubes formed by anodization of titanium foil will be economically more viable. Electrochemical synthesis of metal-TiO_2 core-shell structures offers the following advantages. First, TiO_2 nanotubes are synthesized by electrochemical anodization of titanium foil. The diameter, tube wall thickness, and tube length can be easily controlled or tuned to desired values by adjusting the anodization parameters. Second, the oxide nanotubes are vertically oriented and self-ordering. Therefore, enhanced electrical properties are observed. Third, the vertical orientation and self-ordering structure lead to more 1-dimentional pathways for diffusion and transportation of ions and charge carriers. Lastly, the titanium substrate acts as a current collector, eliminating an additional manufacturing step in electrode preparation for photovoltaic, sensor and energy storage applications.

Electrodeposition of metal nanostructures within TiO_2 has not been reported widely in literature because of the limitations relating to wetting and conductivity issues. Most of the available reports on electrodeposition of metal nanowires pertain to aluminum oxide nanoporous templates. The nanoporous aluminum oxide is prepared by anodization of aluminum. Therefore,

the aluminum oxide template is generally referred to as anodic aluminum oxide template or AAO. Since AAO is an insulator, one side or surface of the AAO is coated with a conducting metal thin film by physical vapor deposition. When immersed in the electrolyte, the deposition current is therefore made available only through this conducting metal thin film which results in a bottom-up growth of metal nanowires through the insulating AAO nanopores. However, when a similar process is carried out using TiO_2 nanotubes as a template, nanowire growth of the metal is not easily achieved because TiO_2 is a semiconductor. Nucleation of metal electrodeposition is not localized at the bottom of the TiO_2 nanotube, since current distribution is present throughout the TiO_2 nanotube surface. Furthermore, one end of the nanotube is closed, which results in incomplete filling of the nanotube by the electrolyte. In order to achieve a uniform core-shell structure using TiO_2 nanotube shells, the following issues must be solved. First, in order to have bottom-up growth of nanowires, the conductivity of the TiO_2 nanotubes should be higher at the bottoms than on the sidewalls and top surface. Second, the inside of the TiO_2 nanotube walls should have higher surface energy than any other surface for better wettability by the electrolyte. Third, the surface energy of the electrolyte should be low enough to completely fill the nanotubes. Lastly, nucleation and growth of metal deposits on the walls of the nanotubes should be minimized so that the openings of the nanotubes are accessible for the electrolyte to enter the nanotubes at all times, thus enabling complete filling of the nanotubes.

The reports available in literature on metal-TiO_2 core-shell are very limited and do not address the above issues in detail. Schmuki's group [4] reported on controlling the electrochemical conductivity of the nanotubes by partial reduction of the bottom of the nanotubes by applying a cathodic pulse in an $NH_4(SO_4)_2$ solution. However, localized increase in the conductivity of the nanotubes did not result in uniform growth of nanowires.

In this present work, several strategies have been implemented to overcome these issues in order to achieve a uniform metal-TiO_2 core-shell nanostructure throughout the sample. The target was to obtain at least 50% coverage of complete filling of TiO_2 nanotubes with metal nanowires in a 1.5 cm^2 sample.

The following methods were investigated to modify the electrical conductivity of the nanotubes in order to achieve a bottom-up growth of copper nanowires. First, the conductivity of the nanotubes was modified by annealing in different environments. Second, the conductivity of the bottom of the nanotubes was locally increased by applying cathodic potentials for short durations in an $NH_4(SO_4)_2$ solution.

The surface energies and wettability of TiO_2 and the electrolytes were modified by the following methods: first, by decreasing the temperature of the electrolyte; second, by adding surfactants in the electrolyte solutions; third, by soaking the TiO_2 nanotube template in methanol under ultrasonication; fourth, by illuminating the TiO_2 nanotube template with UV light and lastly, by ultrasonication during the electrodeposition process.

In this work, a Cu-TiO_2 core-shell structure has been investigated as a model system. The reason for choosing copper as a core is two-fold; first, because electrodeposition of copper in high aspect ratio nanochannels has been investigated for electronic packaging applications such as 3-D integrated electronic circuits as trenches and vias; secondly, because Cu-TiO_2 core-shell structures can be used as an electrochemical sensor or catalyst. Copper nanowires can also be oxidized to Cu_2O or CuO and form a p-n semiconductor junction with TiO_2, which can be used in thermoelectric and photovoltaic applications.

The details of this work are given in this report. The report has 8 chapters. Chapter 2 gives an overview of the previous work reported by other researchers on the electrodeposition of copper pertaining to electronic packaging and formation of TiO_2 nanotubes. Chapter 3 summarizes the

objectives and scope of the work. Experimental details are given in chapter 4. Results and discussion are available in chapter 5. Chapter 6 gives conclusions and suggestions for future work. Chapter 7 is a paper submitted for publication on copper deposition into TiO_2 nanotubes. Chapter 7 is summarized in section 1.2.

1.2 Super Honeycomb: A New Highly Ordered Morphology of TiO_2

Super Honeycomb TiO_2 was discovered while trying to fine tune the morphology of TiO_2 for copper deposition through different types of anodization. The procedure of anodizing in an organic electrolyte, removing the oxide layer and re-anodizing in an aqueous electrolyte led to a new, highly self-ordering, unpublished morphology of TiO_2.

Because the new morphology had never before been seen or studied, many electrochemical characterization tests were performed including cyclic voltammograms (CVs), Electrochemical Impedance Spectroscopy (EIS), and Mott-Schottky (MS).These were performed on samples that had been annealed in O_2 and N_2 atmospheres. The tests were also performed in two different electrolyte solutions including 0.1 *M* NaOH and 0.1 *M* LiCl + 0.1 *M* HCl. A complete and thorough coverage of the subject can be found in chapter 8.

1.3 Super Honeycomb: Applications on Ti-Mn Alloy Capacitance

It was thought that the super honeycomb structure could be replicated on a Ti-Mn alloy in order to achieve a much higher capacitance. The same procedures were followed; anodizing in an organic electrolyte, removing the oxide layer and re-anodizing in an aqueous electrolyte. The oxide layer was not the same Super Honeycomb structure, but did have a nanotubular structure.

Again, several electrochemical characterizations tests were performed including cyclic voltammograms (CVs), Electrochemical Impedance Spectroscopy (EIS), Mott-Schottky (MS) and Cyclic Charge/Discharge (CDC). These tests were performed on samples that had been annealed in

O_2, N_2 and air atmospheres, as well as as-anodized samples. The tests were also performed in four different electrolyte solutions including 0.1 *M* NaOH, 1 *M* H_2SO_4, 0.1 *M* LiCl and 0.1 *M* LiCl + 0.1 *M* HCl.

CHAPTER 2: BACKGROUND

2.1 Nanowire Growth within TiO_2 Nanotubes

TiO_2 nanotubes have been used as a template for synthesizing nanorods/nanowires of compound semiconductors such as CdZnTe [5] and ZnTe [6]. In these studies, the compound semiconductor nanowires were deposited onto the TiO_2 template by pulsed electrodeposition using an organic non-polar aprotic electrolyte at relatively high temperatures (around 150 ˚C). The organic aprotic electrolyte showed several advantages. First, the electrolyte excluded the hydrogen evolution reaction that would have interfered with deposition of the more active Zn. Second, complex metal cations were formed which narrowed the difference in the redox potentials of individual components; and lastly, the surface energy of the electrolyte was lower, which resulted in increased wettability of the nanotubes.

Hydroxy apatite (HA) nanorods have been electrodeposited into TiO_2 nanotubes using aqueous electrolytes. In order to have the HA deposition occur inside of the nanotubes, the TiO_2 nanotubes were prepared by anodization in a phosphoric acid electrolyte. This was so that the walls of the TiO_2 nanotubes would already have PO_4^{3-} species adsorbed on the wall to start the nucleation of calcium phosphate. The TiO_2 nanotubes were also pretreated with NaOH to aid in the deposition of $Ca_5(PO_4)_3(OH)$ [7].

Greene, et al. [8] compared ZnO wire based solar cells with the potential of TiO_2 coated ZnO based solar cells and maintains that the efficiency of the “solar cells can be improved 5-fold” (pg. 18452). Unfortunately, this method grows the TiO_2 shell after making the ZnO core, which leaves a gap in the research regarding what types of modifications need to be made to the electrolyte solution to grow nanowires inside of the nanotubes. They used a homemade traveling wave ALD system to grow 0.9 angstroms of coating on their wires using $TiCl_4$.

In another paper, Wei Zhu, et al. [9], describe a 1–step process to create both the nanotubes and the wires inside them. As such, they only report that they used TiF_4 and $NiCl_2 \bullet 6H_2O$ in the solution for electrodeposition. It is assumed that the solution also had accelerators and/or inhibitors that were not mentioned, but the author cannot say for certain as he has not attempted to reproduce this experiment. The experiment nonetheless was successful and created beautiful Ni-TiO_2 core-shell nanotubes. But once again thier paper does not report or research what is required in the solution to fill an already made TiO_2 nanotube with a metal nanowire.

Another interesting paper by Jan M. Macak, et al. [4] explains that by using electrochemical self-doping, a bottom-up filling approach can be successful. By self-doping the TiO_2 nanotubes, the band gap is reduced from 3.2 eV to 2.4 eV. Once this step was taken, they placed the TiO_2 nanotube in a Cu solution bath but did not mention that it contained anything other than $CuSO_4$, only that "conditions must be adjusted to minimize H_2 evolution" (pg. 3029). While the self-doping step may be an important one, the accelerators and inhibitors used in the solution are also important.

Susanta Mohapatra, et al. [10] also performed experiments that dealt with filling TiO_2 nanotubes, this time with iron. They report being able to fill the TiO_2 nanotubes with iron in a single-step process. They do record what they put into the solution, but it does not appear to contain any accelerators or inhibitors, which seems incorrect. They only report four things in the solution: ascorbic acid, amidosulfonic acid, boric acid and the iron. T.P. Mofat,[11] a well-published author on the subject of nanotrench (40-100 nm) filling, believes that in order to have void free feature filling from the bottom up, inhibitors and accelerators must be added to the solution. He has published many papers to this effect, but all of them have to do with nanotrench filling and not nanotubes. Mohapatra, et al. either did not use any such accelerators or inhibitors or do not list them. In either case, this leaves a gap in research that needs to be filled.

Wei Zhu, et al. [12] once again published a paper about filling TiO_2 nanotubes with various metals, this time with a two-step process. They used an AAO template to make the core-shell structure. In the section which dealt with the second step, the metal deposition into the nanotubes, they reported only the metals used in the solutions, but made no mention of any accelerators or inhibitors used. It is noteworthy to state that their nanotubes were between 200 and 250 nm wide, as this is larger than normal. Once again, either no additives were used in the solution or they were not reported, which leaves a gap in research that must to be filled in order to better understand how the accelerators and inhibitors can improve the quality of deposition.

Gayatri Sahu, et al. [13] have published their work on Au nanowires inside TiO_2 nanotubes and their application for solar cells. They used the same basic two-step process as Wei Zhu, et al. [12] with one difference: the TiO_2 nanotubes were grown to be open at both ends. Silver was sputtered on one side to create a back for the gold wires to be grown on. The solution (Orotemp 24) in which the electrodeposition took place was purchased from a company called Technic, Inc. The solution is listed as a "proprietary mixture" which makes its chemical makeup unavailable for review. This is the first paper reviewed to admit that there is a proprietary blend in the solution used. The experiment was successful, and they obtained Au nanowires deposited into TiO_2 nanotubes via bottom-up deposition. The accelerators and inhibitors used in the purchased solution are still unknown, demonstrating that there is a gap in the research which needs to be filled.

Dong Fang, et al. [14] researched copper deposition inside of double open-ended TiO_2 nanotubes. They grew the TiO_2 nanotubes by deposition onto pure titanium foil. They then used ultra-sonication to remove the TiO_2 nanotube layer from the titanium substrate. One end of the TiO_2 nanotubes was covered with a silver coating. The copper was then deposited into the nanotubes via constant current electrodeposition from a $CuSO_4$ solution. No other chemicals are

reported to be in the solution. The conclusion of their paper showed that some copper was deposited on the sidewalls of the TiO_2 nanotubes, which means that it was only partially a bottom-up process. This leads to the conclusion that if their solution did in fact contain no other chemicals, then adding the correct ones may have helped the deposition process to be a bottom-up deposition.

2.2 Electrodeposition of Copper in Vias and Trenches

Electrodeposition of copper in nanometer-sized (<40nm) trenches and vias is typical of silicon chip electrical interconnects. The on-chip metallization by copper electrodeposition is also known as the Damascene process, developed by the IBM Corporation in the early 1990's.

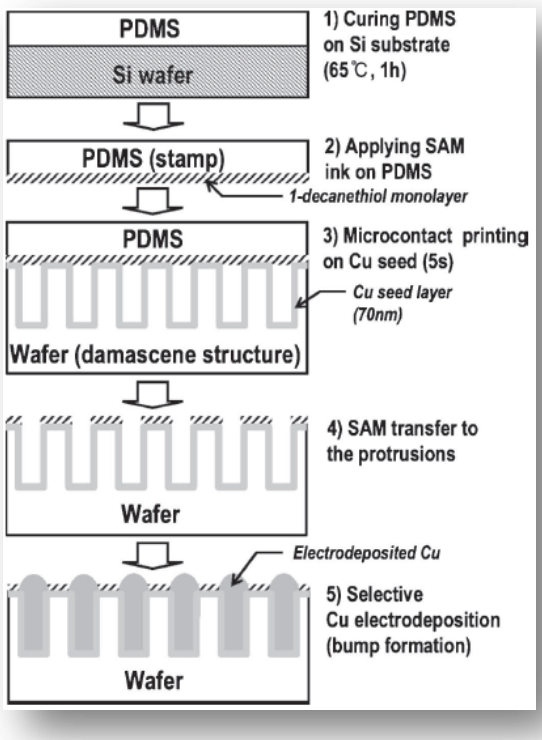

Figure 2.1: Damascene copper metallization process

Figure 2.1 [15] schematically illustrates the various steps involved in the Damascene copper metallization process. In this process, a low dielectric material is deposited on the silicon wafer.

Then a photoresist is deposited on to the dielectric material to form the required pattern. The dielectric is etched according to the defined photoresist pattern. A barrier layer, such as Ta or Ru thin film, is then deposited on the etched dielectric material. A thin (~75 nm) copper seed layer is then deposited on top of the barrier layer. The trenches and vias are then filled with copper by an electrodeposition process. After copper deposition the excess bumps are removed by a planarization process called chemical-mechanical-planarization (CMP).

It is important to note that the electrodeposition of copper within the nanochannels of the electronic chip cannot be directly correlated with the electrochemical growth of copper nanowires within the TiO_2 nanotubes. The first reason is because the Damascene process of copper plating is carried out onto a copper seed layer, whereas no metal seed layer is present on the TiO_2 nanotube walls. Secondly, the height to width aspect ratio of the trenches and vias of electronic chips are almost always less than 10; and in most cases, the width of the vias is greater than 40 nm. The aspect ratio of the TiO_2 nanotubes is generally greater than 10 and has a diameter in the range of 40-100 nm. Lastly, and perhaps most importantly, in the absence of a copper seed layer, the chemistry of the electrolyte cannot be translated to electrodeposition of copper into TiO_2, which will be the focus of discussion in this section.

The electrolyte for copper deposition of integrated circuit (IC) interconnects contains the following components [16]: $CuSO_4$, H_2SO_4, accelerators or brightening agents, such as bis(sodium sulfopropyl)disulfide (SPS), inhibitors or suppressors, such as polyethylene glycol, polyethyleneimine or polypropylene glycol, a leveling agent such as thiourea, benzotriazole (BTA) or Janus Green B (JGB) and finally, trace amounts of chlorides.

It is widely reported that a small amount of chloride is essential to activate both the inhibitor and the accelerator. The superfilling or super conformal plating of the vias and trenches is

achieved by the actions of the additives of the copper sulfate electrolyte system. Figure 2.2 schematically illustrates the superfilling mechanism as proposed by Vereeckeu, et al. [16].

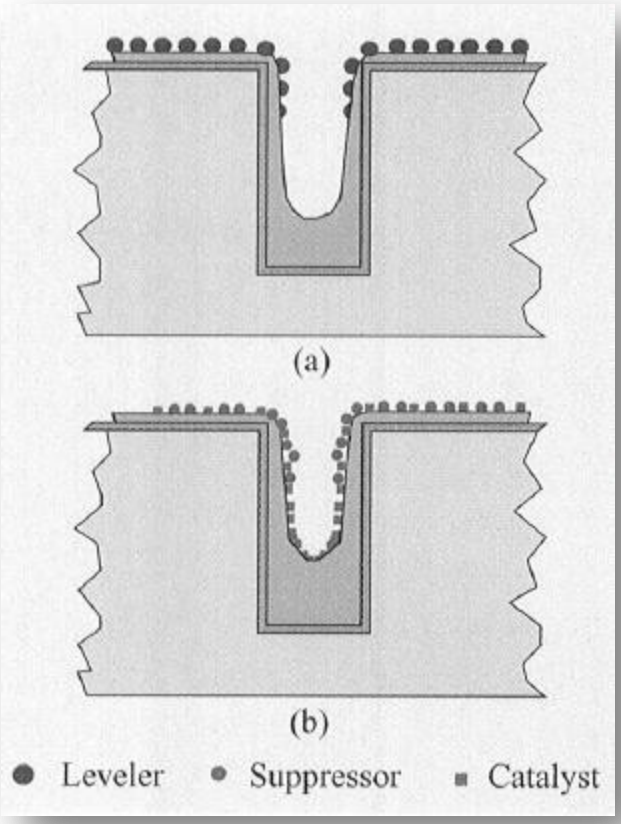

Figure 2.2: Illustration of superfilling mechanism

The aromatic nitrogen-based molecule or polymer, used as a leveler, is adsorbed on the planar surface or mouth of the trench and minimizes the electrodeposition of copper. The suppressor and accelerator are completely adsorbed on the surface. This differential adsorption results in superfilling of the structure.

The differential adsorption of levelers and suppressors is attributed to the diffusional flux of the additives in narrow regions and their consumption during the electrodeposition process. The accelerator and inhibitor compete for adsorption sites, which is attributed to the superfilling of the narrow channels. When the copper seed layer is exposed to an electrolyte containing a suppressor

(PEG) and an accelerator (SPS), initially, a thin passive layer of PEG-based film forms on the copper seed layer surface [17]. Subsequently, the accelerator interacts with the electrode surface. The disulfide/thiol tethers to the copper seed layer by displacing the PEG. The tail of the accelerator molecule-sulfonate terminal group prevents reformation of the passivating PEG layer on the surface. The adsorption of the SPS and displacement of PEG is observed to be an exponential function of potential [18]. Furthermore, the surface area change to the copper also plays a major role in the segregation of inhibitor molecules promoting electroplating of copper in the required locations. The curvature-enhanced accelerator coverage (CEAC) mechanism proposed by Moffat, et al. [19] predicts that when the copper deposit electrolyte interface is non-planar and concave, the surface area is reduced. This change in surface area results in an expulsion of the weakly-bound species such as PEG, which in turn leads to enrichment of the accelerator species at the growing front [20].

The bump formation after filling the trenches is controlled by the addition of levelers which deactivate the accelerators that are accumulated on the advancing surface of the copper deposit [21].

The electrochemistry of copper deposition of the IC interconnects using an acid copper sulfate system with additives is summarized in the following system. It is noted that the addition of anions, such as chlorides, plays a crucial role in the adsorption of suppressors and accelerators. It is further emphasized that, in the absence of chloride ions, adsorption of PEG has been reported to be negligible [22].

When $CuSO_4$ is dissolved in an aqueous electrolyte containing sulfuric acid, the salt solution contains ions of Cu^{2+} and SO_4^{2-} as well as H_3O. The aquo-Cu^{2+} species can be represented as $Cu^{2+}(H_2O)_x$. Historically, the Cu^{2+} was considered to have octahedral co-ordination with water molecules, such as $Cu^{2+}(H_2O)_6$ or a combination of $Cu^{2+}(H_2O)_6$ and $Cu^{2+}SO_4^{2-}(H_2O)_5$, depending on the

concentration of $CuSO_4$ and H_2SO_4 [23]. However, recent studies indicate that the co-ordination with water varies from 4-6. This is because the Cu^{2+} complex is considered to be labile with reference to water exchange, the water exchange time being on the order of 200 ps. [24]

Moffat and Jossell have proposed that the reduction of cupric (Cu^{2+}) ions to elemental copper (Cu^0) occurs in two steps as shown below [25].

$$\mathbf{Cu^{2+}(H_2O)_x(SO_4^{2-})_y + e^- \rightarrow Cu^+(H_2O)_z(SO_4^{2-})_n + (x\text{-}z)\,H_2O + (y\text{-}n)\,SO_4^{2-}} \quad [1]$$

$$\mathbf{Cu^{+}(H_2O)_z(SO_4^{2-})_n + e^- \rightarrow Cu + z\,(H_2O) + n\,(SO_4^{2-})} \quad [2]$$

When considering only the Cu^{2+} species, the redox reactions and standard potentials are given as:

$$\mathbf{Cu^{2+} + e^- \rightleftarrows Cu^+ \qquad E^\circ = 0.153 + 0.059 \log [Cu^{2+}]/[Cu^+]\ V_{SHE}} \quad [3]$$

$$\mathbf{Cu^{+} + e^- \rightleftarrows Cu^0 \qquad E^\circ = 0.521 + 0.059 \log [Cu^+]\ V_{SHE}} \quad [4]$$

$$\mathbf{Cu^{2+} + 2\,e^- \rightleftarrows Cu^0 \qquad E^\circ = 0.337 + 0.0285 \log [Cu^{2+}]\ V_{SHE}} \quad [5]$$

The standard potential for the reaction in equation 5 is the average of the redox potentials of the reactions that occur in equations 3 and 4. It should be noted that the reduction potential of the cuprous ion is more noble than that of the cupric ion. Therefore, formation of the cuprous ion is considered rate limiting. The importance of the formation of Cu^+ as the rate limiting step can also be elucidated by considering the chloride adsorption reaction.

2.3 Role of Anion Adsorption

The adsorption of the anion is related to the strength of anion hydration and its interaction with the electrode. The stronger the solution is (i.e. larger hydrated species), the weaker the adsorption will be [26]. Therefore, ions, such as F^- and ClO^{4-}, that have a strongly bound hydration sheet, will weakly adsorb anions. On the other hand, weakly hydrated anions show higher Gibb's Free Energy of adsorption onto FCC metal surfaces following the order $I^->Br^->Cl^->SO_4^{2-}>F^-$ [27]. Anions adsorption has a catalytic effect on the copper electrodeposition rate by formation of the

anion-bridged activated surface complex $CuCl_{ads}$. The adsorbed layer helps overcome the electron transfer barrier for the reaction in equation 3 which is a rate limiting step in copper plating [28], [29].

The $CuCl_{ads}$ layer is formed by the reaction given below [30]:

$$\mathbf{Cu^{2+} + Cl_{ads}^{-} + e^{-} \rightleftarrows CuCl_{ads} \qquad E^{\circ} = 0.338\ V_{SHE}} \qquad \mathbf{[6]}$$

The monolayer of $CuCl_{ads}$ is then reduced to form copper deposits by the reaction:

$$\mathbf{CuCl_{ads} + e^{-} \rightleftarrows Cu^{0} + Cl^{-} \qquad E^{\circ} = -0.063\ V_{SHE}} \qquad \mathbf{[7]}$$

It is noted that the copper deposition reactions in equations 6 and 7 run parallel to the two stage reduction reactions of Cu^{2+} in equations 3 and 4. Therefore, copper deposition is considered to be accelerated by the adsorption of Cl^{-}. Formation of bulk CuCl phase could form if the potential was held above the equilibrium reaction of equation 6 for a very long time [28]. The bulk CuCl phase is not observed under normal plating conditions. It is important to note that the halide ions adsorb on the copper surface much faster than other additives. All ionic and non-ionic additives interact with the halide ions adsorbed on the copper surface for blocking or catalyzing the reactions [31].

2.4 Adsorption of Suppressors

Polyethoxylated compounds such as polyethylene glycol (PEG), Polyethyleneimine (PEI) and Polypropylene glycol (PPG) are used as suppressors. These are water-soluble polymers that form a dense polymer network at the copper electrolyte interface and are linked by the halide ions adsorbed on the copper surface as shown in Figure 2.3 [32]. Figure 2.4 [32] shows a molecular representation of the different types of additives.

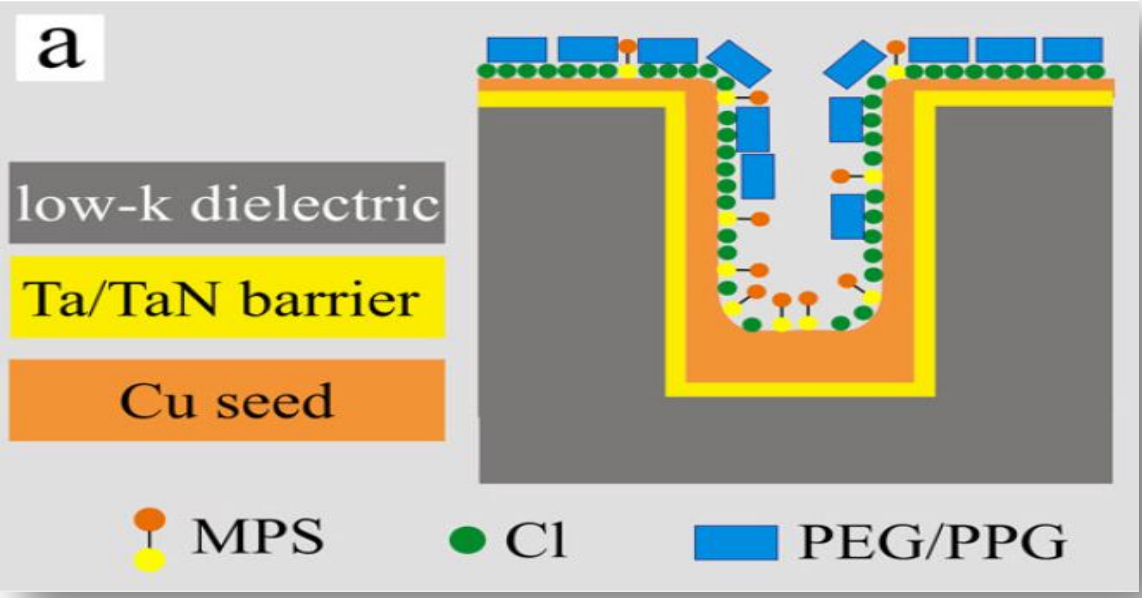

Figure 2.3: Copper electrolyte interface halide adsorption illustration

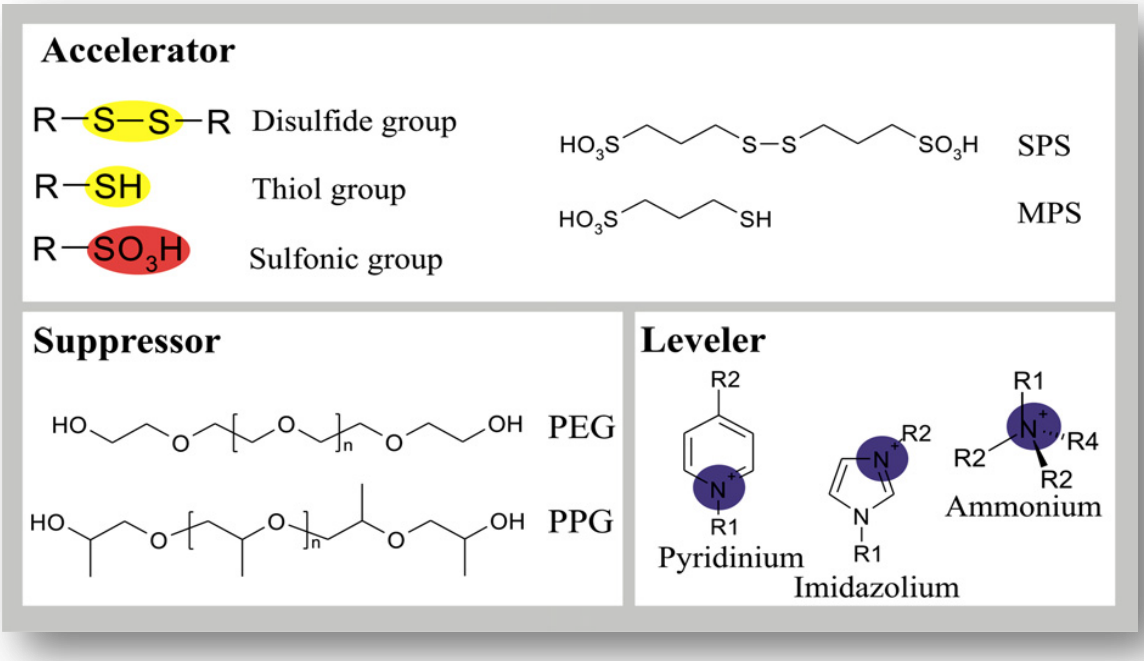

Figure 2.4: Molecular examples of accelerators, suppressors and levelers

A diffusion barrier is formed on the copper surface by the polymer network which physically blocks the access of cupric ions and other additives. Broekmann, et al. [32] identified

three types of suppressors based on their functionalities. Figure 2.5 [32] schematically illustrates the different types of suppressors.

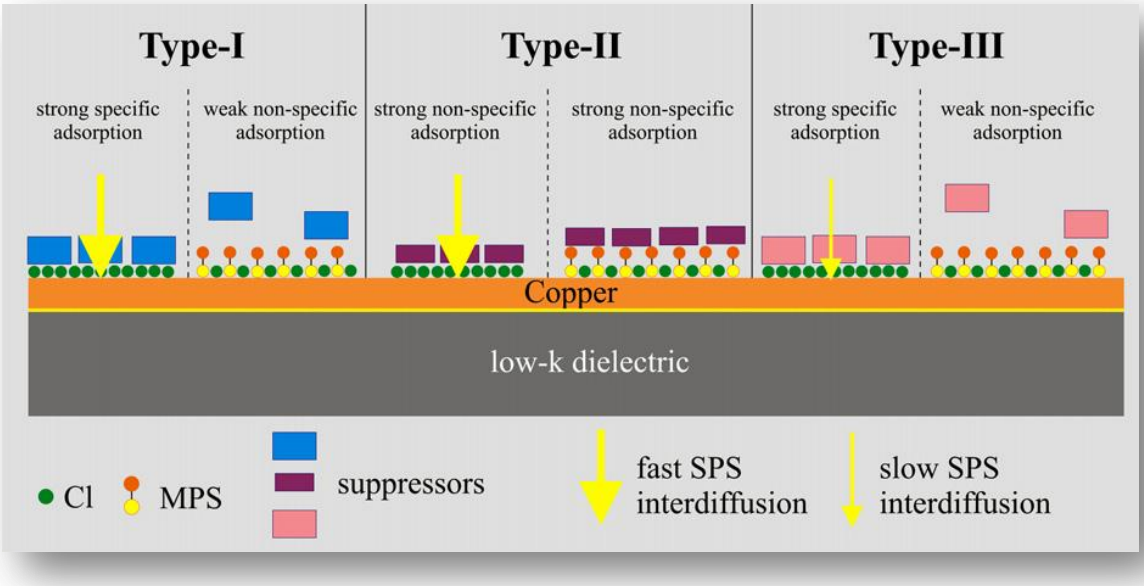

Figure 2.5: Comparison of the behaviors of the three types of suppressors

Type-I suppressors form a strong diffusion barrier for cupric ions but are permeable for SPS inter-diffusion. This type of suppressor has a strong specific adsorption on the chloride lattice. Type-II suppressors have non-specific adsorption on any anion modified surface. They are a barrier to cupric ions but permeable to SPS. Leveling agents of the Damascene Process belong to this category. Type-III suppressors are similar to type-I as far as their selectivity and barrier activity to cupric ions is concerned but with a difference in permeability to SPS. The diffusion of SPS is impeded by the presence of a type-III/Cl^-ensemble.

Since PEG is a large molecule, diffusion into narrow vias and trenches is difficult. Therefore, the inhibiting effect will be predominant in wider areas. Since adsorption of PEG is modified by Cl^- adsorption, at more negative potentials (below the point of zero charge) the adsorption of PEG will be minimal. The adsorbed PEG reportedly appears as flat-cone shaped clusters with a bottom diameter of several tens of nanometers and a height of several nanometers at open circuit

potentials. Upon cathodic polarization to copper plating conditions, the size of the PEG clusters increases and the shape is distorted [20], [33].

Polyethyleneimine (PEI) is a highly-branched nitrogen-bearing polymer. The nitrogen with lone electron pairs present in PEI may interact with copper species of different valences including Cu^0. The imine group present in the PEI could go through protonation and acquire a positive charge. The PEI may impact the copper deposition as a cationic adsorbate and strongly bind to Cl^-adsorbed on the copper surface [21].

2.5 Role of Accelerators

The sodium salts of bis(sulfopropyl)disulfide ([SPS], $Na_2[S(CH_2)_3SO_3]_2$ and mercaptopropane sulfonic acid ([MPS], $HS(CH_2)_3SO_3H$) are used as accelerators. These accelerators are small linear molecules compared to the suppressors PEG, PPG and PEI. Accelerators are present in micromolar concentrations in the copper deposition electrolytes and are adsorbed on the copper surface as either thiolates (R-SH) or disulfides (R-S-S-R). When attached to the copper surface with the SH_3 end, the passivating/inhibiting layer of the PEG-CL-Cu^+ ensemble is disrupted [34]. The thiol and disulfide species are strongly chemisorbed, especially to the variable area of the growth-front with a concave surface. This leads to the superfilling of vias and trenches by the curvature enhanced accelerator coverage mechanism [34].

According to Vereecken et al. [16], the adsorption of SPS onto copper can be given as:

$$\mathbf{2\,Cu^0 + SPS \rightleftarrows 2\,Cu^+(thiolate)_{ads}} \qquad \mathbf{[8]}$$

These authors pointed out that the above reaction will be fast and will only occur when preceded by the following reaction:

$$\mathbf{Cu^0 + Cu^{2+} \rightleftarrows 2\,Cu^+} \qquad \mathbf{[9]}$$

The suppressor/accelerator competitive adsorption process is given by Vereecken et al. [16] as follows. The reaction for the suppressor adsorption is:

$$n\ CuCl_{ads} + HO[(CH_2)_xO]_yH \rightleftarrows \{HO[(CH_2)_xOCuCl]_n[(CH_2)_xO]_{y-n}H\}_{ads} \quad [10]$$

The redox reaction between SPS and Cu^+ is:

$$2\ Cu^+ + SPS + 2\ H^+ \rightleftarrows 2\ Cu^{2+} + 2\ MPS \quad [11]$$

The equation that describes the disruption of the suppressor adsorption by the accelerator is:

$$\{HO[(CH_2)_xOCuCl]_n[(CH_2)_xO]_{y-n}H\}_{ads} + n\ MPS \rightleftarrows HO[(CH_2)_xO]_yH + n\ Cl^- + n\ Cu^+(Thiolate)_{ad} \quad [12]$$

Moffat et al. [34] noted that when the accelerator was added in the form of SPS, during electrolysis, the SPS was converted to MPS by cuprous ions formed at the anode following the reaction:

$$4\ Cu^+ + SPS^{2-} \rightleftarrows 2\ Cu^+(MPS^{2-}) + 2\ Cu^{2+} \quad [13]$$

The above complex could further oxidize to form free MPS according to the following reaction:

$$4\ Cu^+(MPS^{2-})_n + O_2 + (4+4n)\ H^+ \rightarrow 4\ Cu_{2+} + 4n\ MPS^- + 2\ H_2O \quad [14]$$

The MPS thus formed can be converted back into SPS by the reduction of cupric ions in the plating solution according to the oxidative dimerization reaction:

$$2\ Cu^{2+} + 2\ MPS^- \rightarrow SPS^{2-} + 2\ Cu^+ + 2\ H^+ \quad [15]$$

2.6 Copper Deposition in Alkaline Solutions

Alkaline copper electroplating solutions were developed in order to directly electroplate copper onto the barrier layer without having a copper seed layer. Alkaline solutions have higher throwing power and are capable of inducing a high density of copper nuclei on the ruthenium or cobalt diffusion barrier layer [35]–[37].

The alkaline electrolyte solutions consist of $CuSO_4 \bullet 5H_2O$ as the source of copper, a complexing agent in the form of ethylenediamine [35] or potassium tartrate [37], and a pH in the range of 8-12 by the addition of NaOH or Tetra-methyl ammonium hydroxide. The alkaline electrolyte is normally used without the addition of additives such as accelerators and suppressors.

The alkaline electrolyte is often used for depositing a seed copper layer onto the barrier layer. After the seed layer has formed to a nominal thickness of 75 nm, the plating solution is changed to an acid copper plating electrolyte with conventional additives to fill vias and trenches [36]. Landau and his group [37] studied the effects of additives on alkaline electrolytes. The additives they studied were PEI, PEG and SPS. The behaviors of the additives in alkaline solutions were drastically different from those of the conventional acidic electrolytes of the Damascene process [37].

In the previous section, the role of chloride ions on the adsorption of accelerators and suppressors was discussed. It is noted that without chloride ions, both the suppressors and the accelerators are less effective [38]. In alkaline electrolytes no chloride is added. However, the presence of OH^- could determine the adsorption of the additives. Landau, et al. [37] observed that SPS acted as a suppressor in alkaline electrolytes containing tartrate and that PEG acted as a weak suppressor.

In the conventional acid-Cu electrolyte, PEI functions as a leveler and will not be deactivated by the SPS, unlike PEG. On the other hand, in alkaline solutions, PEI acts as an anti-suppressor [37]. However, the reason for such inverse behavior of the additives in alkaline electrolytes remains largely unexplained.

2.7 Electrochemistry of Tartrate Complex in Copper Deposition

Tartaric acid can exist in $C_4H_5O_6^-$ and $C_4H_4O_6^{2-}$ forms in the aqueous solution depending on the pH. The equilibrium of the tartrate species is given as [39], [40]:

$$\mathbf{C_4H_6O_6 \rightarrow C_4H_5O_6^- \rightarrow C_4H_4O_6^{2-}}$$

$$\mathbf{\text{or where T= } C_4H_4O_6 \ (H_2T) \rightarrow (HT^-) \rightarrow (T^{2-})} \qquad \mathbf{[16]}$$

The first rate constant, K_1, for H_2T to HT^- is:

$$\mathbf{K_1 = [HT^-]\,[H^+]/[H_2T] = 2.60} \qquad \mathbf{[17]}$$

The second rate constant, K_2, for HT^- to T^{2-} is:

$$\mathbf{K_2 = [T^{2-}]\,[H^+]/[HT^-] = 3.77} \qquad \mathbf{[18]}$$

At increasing pH, the equilibrium copper-tartrate complex formation can be expressed as [39]:

$$\mathbf{Cu^{2+} + 2\,OH^- + 2\,T^{2-} \rightleftarrows CuT_2(OH)_2^{4-}} \qquad \mathbf{[19]}$$

At pH 2.7 to 3.5, the predominate copper complex will be CuT. From pH 3.5 to 5.7, the predominate copper complex will be CuT_2^{2-} and above pH 5.7, the predominate species will be $CuT_2(OH)_2^{4-}$ [39].

2.8 Electrodeposition of Copper onto Titanium

Chang et al. [41] studied electrodeposition of copper onto a titanium substrate with different oxide thicknesses in a cupric sulfate-sulfuric acid solution at under-galvanostatic conditions. The oxide layer of TiO_2 on the titanium substrate studied was thin and relatively defect free, and the copper nucleation density was low. However, thicker TiO_2 films, having a larger defect density, showed nucleation of a large density of copper nuclei. Rosario et al. [42] demonstrated a possible under-potential deposition of copper onto TiO_2 using a copper-sulfuric acid electrolyte.

CHAPTER 3: OBJECTIVES AND SCOPE

The objectives of this thesis work are to:

- Prepare vertically oriented and ordered nanotubular arrays of TiO_2 by electrochemical anodization of titanium substrates.
- Synthesize hybrid nanotubular/nanoporous oxide layers onto titanium and titanium-manganese by a two-step anodization process.
- Develop an electrochemical method to electrodeposit metal nanowires (specifically copper nanowires) into the TiO_2 nanotubular arrays to form core-shell nanostructures.
- Investigate the electrochemical energy storage characteristics of the nanotubular/nanoporous anodic oxides of titanium and titanium-manganese substrates for super-capacitor applications as a function of annealing conditions (defect concentration).
- Anodize commercial purity titanium substrates and Ti-(8 wt%)Mn alloy substrates
- Anodize both pure titanium and Ti-(8 wt%)Mn alloy in one aqueous electrolyte (0.5 *M* H_3PO_4 +0.14 *M* NaF) and in one non-aqueous electrolyte (ethylene glycol) containing NH_4F and a small amount of water (max 5 vol%)
- Anodize at potentials in the range of 20-60 volts and times up to 4 hours.
- Anneal at a temperature of 450 ˚C for 2 hours in air, nitrogen and oxygen.
- Study the electrochemical energy storage properties by conducting cyclic voltammetry at different pH conditions (pH 0-14) in (1 *M* H_2SO_4, 0.1 *M* LiCl, 0.1 *M* LiCl + 0.1 *M* HCl, 0.1 *M* NaCl) at different scan rates.

- Electrodeposit copper onto TiO_2 nanotubes in both an electrolyte based on those used in the Damascene process and in an alkaline electrolyte with a tartrate complex
- Use a scanning electron microscope to evaluate the morphology of the oxide nanotubes and copper nanostructures

The following are beyond the scope of this work:

- Understanding nucleation and growth of copper onto TiO_2
- Understanding structural evolution at the TiO_2-copper interface
- Understanding the kinetics of electrolyte concentration within the oxide nanotubes

CHAPTER 4: EXPERIMENTAL

4.1 Growth of TiO_2

The first step in the experimental portion of the project was to anodize the titanium foils. This experiment required a solution containing 0.5 *M* phosphoric acid (H_3PO_4), 0.14 *M* sodium fluoride (NaF) and ultra-high purity water in the 18 MΩ-cm purity range. Generally, a 1 L solution was used, which equated to 34.1 mL of H_3PO_4 and 5.94 grams of NaF. Because mixing water and acid produces an exothermic reaction, the order was also important. First the 1 L beaker was filled a little more than half way with 18 MΩ-cm water, then the acid was added in slowly, next the NaF was added in, and finally the beaker was filled to the 1 L mark with 18 MΩ-cm water.

Titanium foil (0.25mm, 99.7% purity, Sigma Aldrich) was used as both the anode and the cathode for the anodization process. Because the project required working on a nanoscale, the titanium surface smoothness of the anode was also important. The titanium foil was cut into approximately a 4-5 cm^2 piece with a tag cut from one side for gripping with the alligator clip. A common problem with solution chemistry is accidentally getting the clip to close to the surface of the solution which can cause a short circuit in the system. Once the titanium was cut, one of its faces was sequentially sanded with 800, 1000, 1500, and 2000 grit sandpaper. Between each sanding, the titanium foil and the sanding stone were washed with 18 MΩ-cm water and dried with a kimwipe. This was to avoid any larger sand grit from contaminating the next finer grit. The titanium was finally washed with 18 MΩ-cm water and dried with a kimwipe. The unsanded side was then taped with electroplater's masking tape to avoid any TiO_2 growth on the backside of the titanium foil.

A cathode of similar size is needed to balance the anode. Both the anode and the cathode were submerged into the solution described above with the positive lead connecting to the sanded

and taped anode, which the TiO_2 was to grow on, and the negative lead attached to the cathode. The leads were hooked up to a Sorensen XPF 60-20 DC Power Supply. Using a typical 2 electrode system the power supply was turned on at 20 V for 40 minutes. Another important point was the timing and setup for the power supply. The solution is highly corrosive to titanium, and it was desired to minimize the time in solution before the power was supplied to the system. This was accomplished by setting the 1 L solution on a lab jack stand and placing the anode and cathode at the correct height above the solution so that the jack could be lifted quickly to a height at which the anode and cathode would be submerged at the same time. The power supply was then quickly turned on. The lab jack stand procedure should take less than 5 seconds.

After the 40-minute procedure was up, the power supply was turned off and the lab jack was lowered to ensure that the anode would not be left in the corrosive solution. The anodized TiO_2 was then released from the clamp and quickly washed in 18 MΩ-cm water and dried in an air stream.

The second method for growth of TiO_2 was similar to the first, but used an organic electrolyte to grow nanotubes which would then be removed. Briefly, this anodization was done because it produced a much cleaner, smoother walled nanotube array than the aqueous method did. The down side was that it created a carbon doped nanotube which had a higher conductivity, which made electrodeposition of copper difficult. The hope was to combine the two different methods of anodization to get the advantages of both. The second step of this method directly correlates to the previous method with the exception that the titanium foil used was not sanded in preparation but simply anodized once the oxide layer was removed. The first step used an organic solution which contained 4 wt% 18 MΩ-cm water and 0.14 *M* NH_4F dissolved in ethylene glycol (EG). Typically, a 1 L beaker was used which contained 11.7 mL of NH_4F and 33 mL of 18 MΩ-cm

water. It should be noted that 4% of 1 L is 40 mL. However, the missing 7 mL of water can be accounted for in the 11.7 mL of NH_4F, which is only 40% pure. This means that 60% of it is water.

The same titanium foil was used for this anodization with a few minor preparation changes. The size of the anode was much smaller, around 1x1.5 cm^2. The sample was sanded in the way described in the previous anodization method, but it was painted with enamel paint instead of taped because the electroplater's masking tape tended to come off in the organic solution. The paint required about 24 hours drying time, or it could be placed under a heat gun for 2-3 hours.

Once the solution was made and the foil prepped, the same Sorensen XPF 60-20 DC Power Supply was employed to anodize the titanium foil at 60 V for 3-4 hours. The sample was removed from the solution at this time and washed in 18 MΩ-cm water, then dried in an air stream. The oxide layer was peeled off using electroplater's masking tape, which revealed a smooth nano-indented surface which was to be used as a pattern in the next anodization.

4.2 Electrochemical Deposition of Copper

4.2.1 Electrolyte Solution Preparation

There were a total of 51 solutions used in the experiments. Most of these solutions were used to understand the kinetics of the various additives commonly used in the electronic industries' Damascene process for low aspect ratio trench filling. These additives included inhibitors, which are large molecules used to block copper deposition, such as: polyethylene glycol (PEG)(88 μM), polyethyleneimine (PEI)(0.1 μM) and ethylene glycol (EG)(88 μM). There were also accelerator additives including: bis(sulfopropyl)disulfide ([SPS], $Na_2[S(CH_2)_3SO_3]_2$)(50 μM) sodium chloride (NaCl)(2 mM) and sodium fluoride (NaF)(2 mM). The first solution, referred to as the base solution contained 0.16 M $CuSO_4$, 1.8 M H_2SO_4 and 18 MΩ-cm H_2O. Solutions 2-7 contained an extra individual inhibitor or accelerator additive. Solutions 8-13 were used to investigate the effects of

mixing two of these additives together, while solutions 28-34 were used to investigate mixing three or more additives together. Solutions 14-27 were used to understand the effects of additive concentration changes. In order to accomplish this, the original concentration of each additive was halved and then doubled. Solution 35-38 investigated changes in the copper concentration. In solutions 39 and 40, methanol was added to reduce the surface tension in the solution. Solutions 41-51 were used to understand changes in pH (0.5 to 12.7) and the effects of the complexing agents, citric acid and tartaric acid with concentrations ranging from 0.015 *M* to 0.06 *M*.

Solutions 1-34 were each made by preparing 250 mL of base solution containing 0.16 *M* $CuSO_4$ (10.2 g), 1.8 *M* H_2SO_4 (24.9 mL) and the remainder 18 MΩ-cm water in a 250 mL volumetric flask. The procedure, once again, required the addition of about half the water first then the extra slow addition of the acid, followed by the addition of $CuSO_4$ and finally the rest of the water. The reaction between the acid and water was quite strong. The solution was usually split up into two, 125 mL storage beakers for later addition of inhibitor/accelerative additives.

Each of the inhibitor/accelerator additives required special attention to be paid to the amounts added because the amounts were so small. SPS, PEG, NaF and NaCl were solids, PEG required a large enough weight that it could be measured on a scale while SPS, NaF and NaCl required a solution to be made and then diluted. PEI and EG were both liquids and also required so little weight that dilutions had to be made. PEI, EG, SPS ,NaF, and NaCl were all added to the base solution using a micropipette. Only PEG was added in the solid form.

Solutions 35-38 were similar to the base solution but with different concentrations of $CuSO_4$ and H_2SO_4. Solutions 39 and 40 required much care when adding methanol. About half of the water was added first, then the H_2SO_4 was added, and finally the methanol was added extremely slowly. The reaction was vigorous, causing a large formation of bubbles. Solutions 41-51 were made

with a lower concentration (0.03 *M*) of $CuSO_4$ and varying amounts of citric acid or tartaric acid, ranging from 0.015 *M* to 0.06 *M*.

4.2.2 Use of Gamry Interface 1000 for Electrodeposition

Once an electrolyte had been chosen and prepared, the Gamry Interface 1000 was employed to deposit copper into the TiO_2 nanotubes. Figure 4.1 shows an example of a typical setup of the electrolyte with: working, counter and reference electrodes.

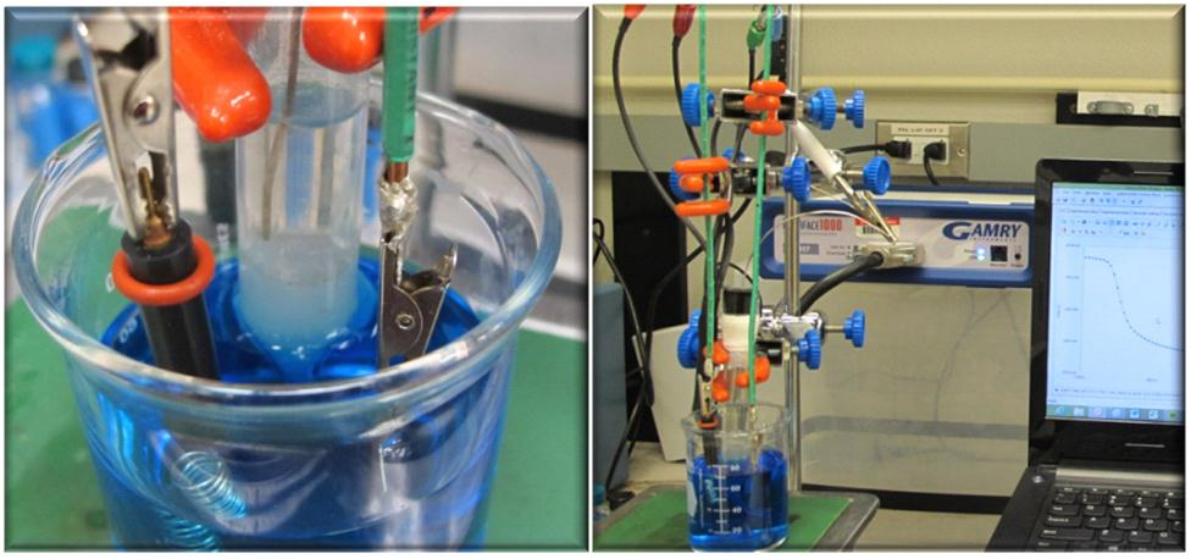

Figure 4.1: Typical setup for electrodeposition using Gamry Interface 1000

The counter electrode was a spiral platinum electrode and was clipped with the red and orange alligator clips, the working electrode was the anodized TiO_2 foil and was clipped with the blue and green alligator clips, and the reference electrode was an Ag/AgCl reference electrode and was clipped with the white alligator clip. The Gamry unit was turned on and the Gamry Framework software was started. Once the software was able to communicate with the unit, the desired electrodeposition technique was selected.

There were five main techniques used for copper deposition as well as two custom techniques written by a Gamry specialist specifically for these experiments. The five main tests

were accessed through Gamry Framework's menu bar Experiment tab. They were called Potentiostatic (C, B), Galvanostatic (C, 8), Potentiostatic Generic Pulse (F, B), Galvanostatic Generic Pulse (F, C), and Cyclic Voltammetry (E, 5). The two custom techniques were variations on the two pulsing techniques which included a third resting step and were obtained by contacting a Gamry representative. Thousands of tests were performed using these seven techniques at various voltage ranges, current ranges, step times, etc.

4.2.3 Use of the Gamry Interface 1000 for Electrochemical Characterization

In addition to electrodeposition, the Gamry Interface 1000 was also used for electrochemical characterization of samples as well as for measuring some solution kinetics through cyclic voltammetry.

Cyclic voltammetry was used to examine the changes in solution kinetics that occurred with the addition of inhibitors and accelerators at different concentrations as discussed in the results section.

Four test electrolyte solutions were made for these electrochemical characterization tests. Lithium chloride (LiCl) and sodium hydroxide (NaOH) were both solids while hydrochloric acid (HCl) and sulfuric acid (H_2SO_4) were liquids. The first electrolyte contained 0.1 *M* of LiCl and the remainder was 18 MΩ-cm water. In a 250 mL beaker, this was equal to 1.07 g of LiCl. The second electrolyte contained 0.1 *M* of NaOH, and the remainder was 18 MΩ-cm water. In a 250 mL beaker, this was equal to 1.03 g of NaOH. The third electrolyte contained 0.1 *M* of LiCl, 0.1 *M* HCl, and the remainder was 18 MΩ-cm water. In a 250 mL beaker, this was equal to 1.07 g of LiCl and 2.11 mL of HCl. The second electrolyte contained 1 *M* of H_2SO_4, and the remainder was 18 MΩ-cm water. In a 250 mL beaker, this was equal to 13.83 mL of H_2SO_4.

4.3 Creating an Ag/AgCl Reference Electrode

Fresh Ag/AgCl reference electrodes are important for gathering consistent and accurate data and results with electrochemical tests. Fresh electrodes were made in plastic disposable pipettes. Agar was used to keep the KCl solution from leaking out while still maintaining conductivity. The first step was to check and see if there was any saturated KCl in the lab. If there was not, a solution was made by adding 75 grams of KCl in 200 mL of 18 MΩ-cm water. Once this solution was made, it was placed in a well labeled plastic bottle. The second step was to take 20 mL of the KCl solution and heat it to about 80 ˚C. It was important not to let the solution boil. Once the solution was hot, 1 gram of agar was added. The solution was then mixed over heat until it became thick enough to be used. The solution should be as thick as possible, while still allowing the pipette to smoothly suck up the solution. Once the agar was in the pipette, it was quickly moved under cold water to cool and solidify the agar into place. Once the pipette was sufficiently cooled, it was placed in a beaker for later use.

The next part of creating an Ag/AgCl reference electrode was to anodize silver wire in KCl for 15 minutes at 5 V. The saturated KCl worked as the electrolyte, a silver wire approximately five inches in length served as the working electrode and a platinum counter electrode was employed. Only about one inch of the wire was placed in the solution for anodization.

Once that process was complete, the top part of the pipette was cut off. The silver wire was wrapped at one point with enough parafilm to create a stopper. The top portion of the pipette was then filled about half way with KCl. The silver wire was then seated into the pipette to create a complete Ag/AgCl reference electrode.

4.4 Reducing TiO_2 Nanotube Bottoms

Reducing the nanotubes was a process very similar to depositing copper on the TiO_2. There were two main differences: the electrolyte was different and the time scale was much more important during the reduction process. The reduction process was carried out in a 1 *M* ammonium sulfate solution by applying a cathodic potential for a few seconds. The reduction process actually began prior to any applied voltage. This was especially important as leaving the sample in the solution while preparing the parameters would almost ensure over reduction. The correct procedure was to set up the experiment with a reference electrode, counter electrode and working electrode, while having the ammonium sulfate electrolyte on a lab jack stand ready to raise up to the correct level. The computer portion of the process was completely set up and ready to go prior to raising the lab jack. Once the electrolyte was raised to the correct height, the test was started.

4.5 Oxidizing Ti-Mn Samples

The Ti-Mn foil samples had a much higher volatility when a voltage was applied. It should be noted that while the process for creating an oxide layer on Ti-Mn is similar to regular titanium foils, a much smaller sample is needed as well as a large volume of electrolyte. Large samples would eventually boil the electrolyte solution, potentially creating a toxic environment and work place. It is recommended not to work with Ti-Mn samples larger than 4 cm^2.

Another important point is to make sure that the DC power supply is capable of handling the larger current that Ti-Mn is subject to. It is not uncommon to find DC power supplies that are only rated to 0.5 A, whereas even a small sample of Ti-Mn commonly produces well over 1 A of current at 60 V.

CHAPTER 5: RESULTS AND DISSCUSSION

5.1 Cyclic Voltammetry on Platinum

5.1.1 Study of Solution Behavior on Platinum with No Additives

Figure 5.1 shows the cyclic voltammograms (CVs) carried out in the electrolyte with different additives using a platinum substrate at a scan rate of 10 mV/s. The focus is on the higher cathodic potentials where the copper deposition takes place.

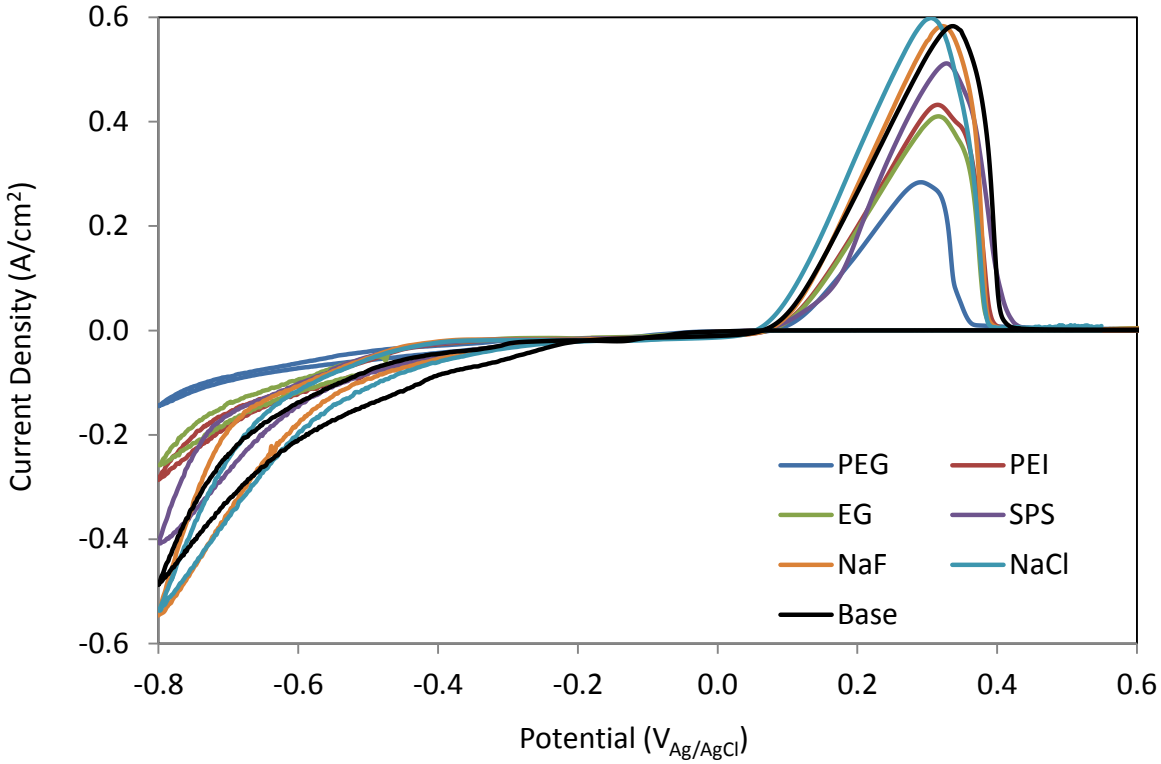

Figure 5.1: CVs of inhibitor and accelerator additives on Pt. electrode at 10 mV/s. The base solution contained 0.16 *M* $CuSO_4$ + 1.8 *M* H_2SO_4

During the cathodic potential sweep from open circuit potential to -0.8 $V_{Ag/AgCl}$, one of the reactions occurring on the platinum surface is [25]:

$$Cu^{2+}(H_2O)_x(SO_4^{2-})_y + e^- \rightarrow Cu^{+}(H_2O)_z(SO_4^{2-})_n + (x\text{-}z)\,H_2O + (y\text{-}n)\,SO_4^{2-} \quad [1]$$

This reaction is almost equivalent to:

$$Cu^{2+} + e^- \rightleftarrows Cu^+ \qquad E^\circ = -0.047\ V_{Ag/AgCl} \qquad [20]$$

The cathodic current wave that starts at around -60 $mV_{Ag/AgCl}$ is attributed to the reduction of cupric ions to cuprous ions. The slopes of the cathodic current profile change at -0.285 $V_{Ag/AgCl}$, -0.45 $V_{Ag/AgCl}$ and -0.66 $V_{Ag/AgCl}$. The constant current density observed from -60 $mV_{Ag/AgCl}$ to -285 $mV_{Ag/AgCl}$ could be attributed to the diffusion limited reduction of cupric to cuprous ions. The activation controlled current profile at the potential region -285 $mV_{Ag/AgCl}$ to -450 $mV_{Ag/AgCl}$ could be attributed to the reduction of cuprous ions to copper given by the reaction:

$$Cu^+(H_2O)_2(SO_4^{2-})_n + e^- \rightarrow Cu^0 + 2\,H_2O + n\,SO_4^{2-} \qquad [21]$$

At cathodic potentials up to -450 $mV_{Ag/AgCl}$, the cupric ions could be directly reduced to Cu^0 following the basic reaction:

$$Cu^{2+} + 2\,e^- \rightleftarrows Cu^0 \qquad E^\circ = 0.337 + 0.0285 \log [Cu^{2+}]\ V_{SHE} \qquad [5]$$

Considering a mean activity of 0.15,[43], [44] the redox potential for this electrolyte can be calculated as:

$$E^\circ = 0.337 + (0.059/2)\log(0.15*0.16) = 0.289\ V_{SHE} = 0.092\ V_{Ag/AgCl} \qquad [22]$$

If we consider the concentration of 0.16 *M* Cu^{2+} and 1.96 *M* SO_4^{2-}, then the activity coefficient becomes 0.04. In this case, the redox potential will be:

$$E^\circ = 0.337 + (0.059/2)\log(0.04*0.16) = 0.272\ V_{SHE} = 0.075\ V_{Ag/AgCl} \qquad [23]$$

The anodic peak could be attributed to the oxidation of Cu^0 to Cu^{2+}. Even though the cupric ion is more noble than the cuprous ion, a direct reduction of cupric ions to copper requires a large over-potential. In addition to the reduction of cupric and cuprous ions, hydrogen ions are also reduced at potentials more negative than -0.2 $V_{Ag/AgCl}$ at this pH condition. This equation is given below:

$$2\,H^+ + 2\,e^- \rightarrow H_2 \qquad E^\circ = -0.197\ V_{Ag/AgCl} \qquad [24]$$

5.1.2 Study of Solution Behavior on Platinum with Inhibitor Additives

Figure 5.2 shows a simplified version of Figure 5.1 with only the base and inhibitor CVs. The addition of PEG (88 μM) shifted the reduction potential of equation 23 to a more negative potential by 38 mV. The cathodic current density with PEG addition was similar to that of the base solution until a potential of -280 $mV_{Ag/AgCl}$, the potential at which hydrogen evolution initiates. At potentials more negative than -80 $mV_{Ag/AgCl}$, the current density was much lower in the electrolyte containing PEG than the electrolyte without PEG. When the platinum was polarized at -0.8 $V_{Ag/AgCl}$, the cathodic current density was -480 mA/cm^2 in the base solution, whereas under similar conditions, the PEG addition showed a current density of 143 mA/cm^2. The reduction in the current could be attributed to the adsorption of PEG to the platinum surface, which may be blocking the reduction of both copper ions and hydrogen ions.

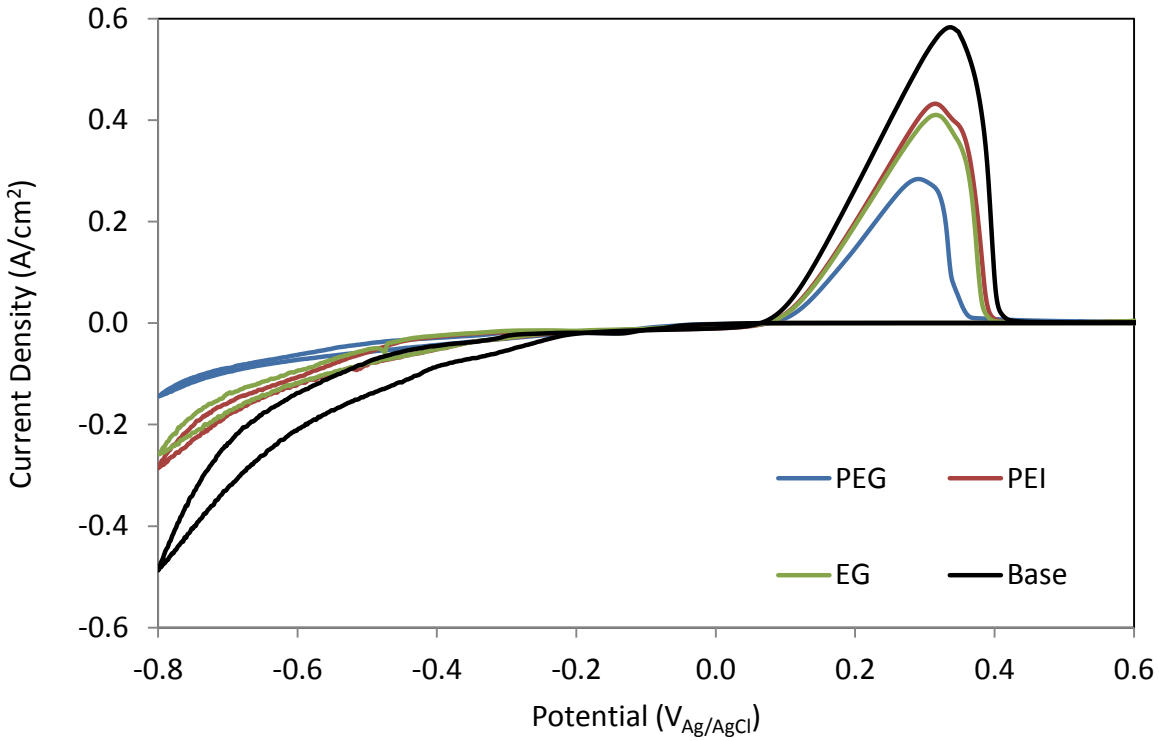

Figure 5.2: CVs of base solution compared with inhibitor additives only, at 10 mV/s, Pt. electrode

During anodic potential sweeping in the PEG additive solution, a strong oxidation peak was observed at 280 $mV_{Ag/AgCl}$, about 45 mV more negative than the peak potential of the base solution. The faint shoulder peak which is observed at around 314 $mV_{Ag/AgCl}$, could be attributed to the oxidation of Cu^{+} in the form of $Cu^{+}(H_2O)_z(SO_4^{2-})_n$ to Cu^{2+} as $Cu^{2+}(H_20)_x(SO_4^{2-})_y$ with a standard redox potential of 324 $mV_{Ag/AgCl}$. Since the anodic current wave of the base solution initiated at 78 $mV_{Ag/AgCl}$, the oxidation reaction could be attributed to the oxidation portion of the reaction in equation 5. The oxidation current peak of the PEG containing solution was also smaller than that of the base solution. It should be noted that the solution did not contain a chloride additive. In spite of the absence of chlorides, the addition of PEG showed inhibiting effects on the platinum surface for the copper electroplating. The sulfate anions could be anchoring sites for the adsorption of the PEG species.

Addition of 0.1 μM PEI to the base solution without any other additives showed inhibiting behaviors similar to the behaviors observed with the 88 μM of PEG. Since the molar concentration of PEI was about three orders of magnitude smaller than that of PEG, the inhibiting effects were smaller. Even with this micromolar addition, PEI, because of its branched configuration and nitrogen with lone electron pairs, showed strong adsorption on the platinum surface and decreased the current density to -280 mA/cm^2. The addition of 88 μM of EG showed almost the same polarization and inhibiting behaviors as that of the 0.1 μM of PEI.

5.1.3 Study of Solution Behavior on Platinum with Accelerator Additives

Figure 5.3 shows the cyclic voltammograms of 0.16 *M* $CuSO_4$ + 1.8 *M* H_2SO_4 with individual additions of SPS, NaCl and NaF compared with the base solution. The addition of 50 μM of SPS showed an increase in the cathodic polarization. Since there was no chloride addition, the presence of SO_4^{2-} as the anion did not help reveal the accelerating behavior of SPS for copper

electrodeposition. Addition of 2 *mM* NaCl to the base solution moderately increased the current density when the potentials were more negative than -0.7 V. Similar behavior was observed with the addition of 2 *mM* of NaF.

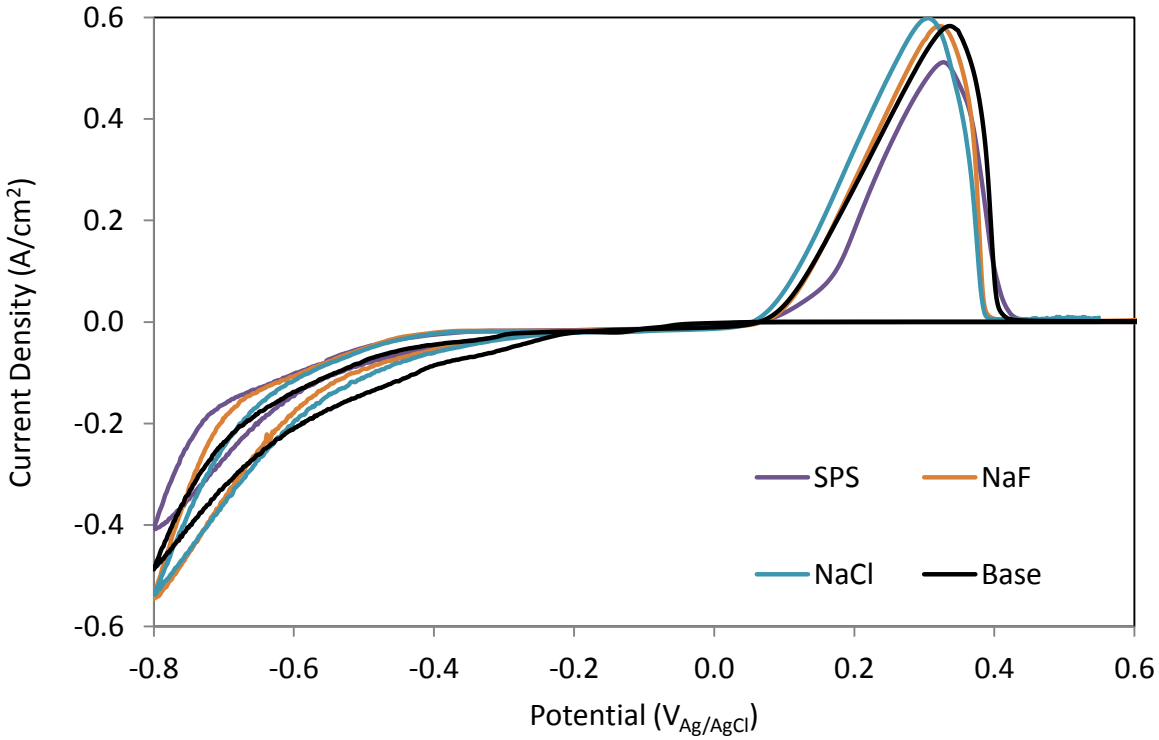

Figure 5.3: CVs of base solution compared with accelerator additives only, at 10 mV/s, Pt. electrode

When 88 *µM* of PEG was added along with 2 *mM* NaCl, the polarization effect of PEG increased. The current density also decreased to -50 mA from -67 mA once the 2 *mM* of NaCl was added to the 88 *µM* of PEG.

Addition of 50 *µM* SPS, 2 *mM* of NaCl and 88 *µM* of PEG together increase the polarization in the cathodic direction. The diffusion limited current density was observed until -425 $mV_{Ag/AgCl}$. The final cathodic current density at -0.8 $V_{Ag/AgCl}$ was about -300 mA/cm^2 which was around 70% of the current density without any additives.

When chloride is added, the redox reaction could be given as:

$$Cu^{2+} + Cl^-_{ads} + e^- \rightleftarrows CuCl_{ads} \qquad E^\circ = 0.383\ V_{Ag/AgCl} \qquad [25]$$

$$CuCl_{ads} + e^- \rightleftarrows Cu^0 + Cl^- \qquad E^\circ = -0.047\ V_{Ag/AgCl} \qquad [26]$$

Figure 5.4 shows the cyclic voltammetry results of different electrolytes using platinum as the substrate. The LHS-y-axis current density values belong to solutions 8, 14 and 28. The RHS-y-axis belongs to electrolytes 50 and 51 with a pH of 5.25.

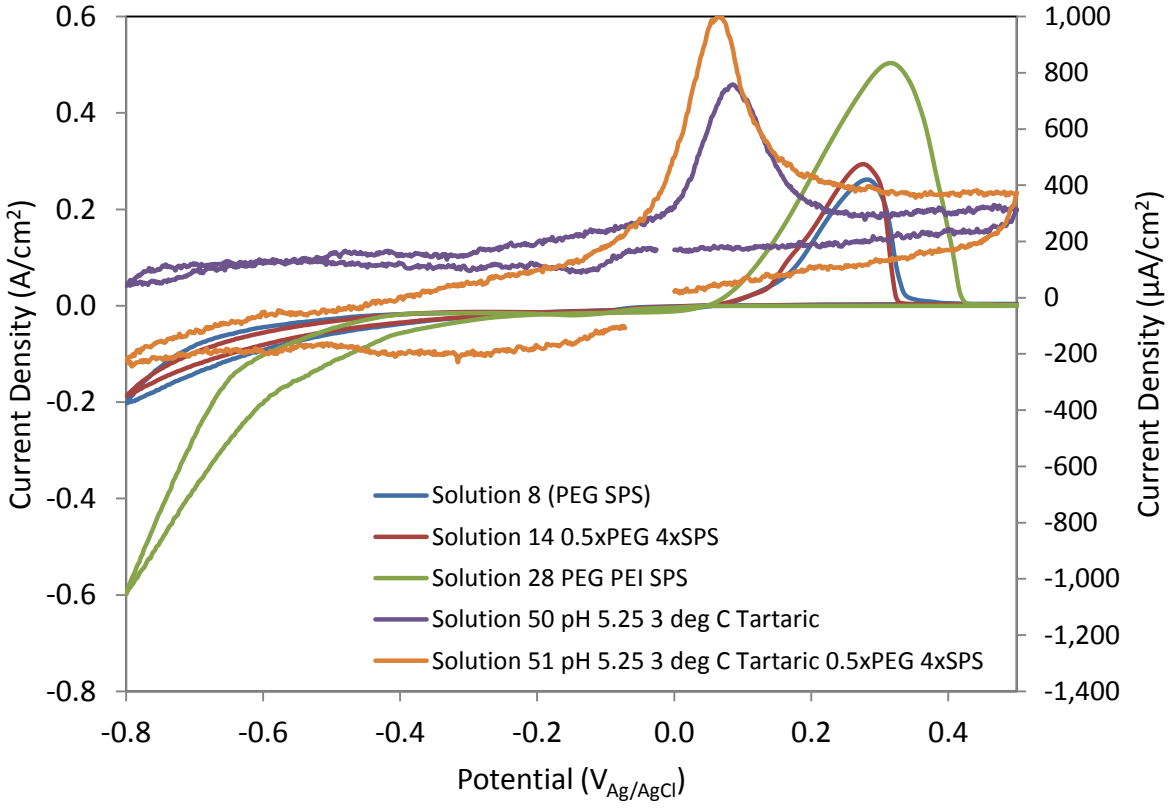

Figure 5.4: CVs of 5 best copper-depositing solutions at 10 mV/s, Pt. electrode. Solution 50 and 51 are on the right hand axis. Solution 8, 14 and 28 are on the left hand axis

The combination of additives in solution 28, 0.1 *µM* PEI, 22 *µM* EG, and 12.5 *µM* SPS showed the highest current density at -0.8 $V_{Ag/AgCl}$ among all the electrolytes considered in this figure. Furthermore, this electrolyte showed the lowest cathodic polarization (about 150 mV more positive than electrolytes 8 and 14). However, the take-off potentials for the anodic peak current was almost the same for all the acid electrolytes (Solutions 8, 14, and 28). The highest anodic peak current density and largest charge accumulations for the oxidation reaction were both observed in Solution 28. The cathodic and anodic current densities were similar for the electrolytes 8 and 14.

When tartaric acid was added and when the electrolyte composition was changed to be more neutral by the addition of NaOH, the reduction and oxidation reaction rates of Cu^{2+}/Cu^{0} systems were drastically different from that of the acidic solutions. Overall, the current density decreased by almost three orders of magnitude in the basic solution as compared to the acid solutions. Solution 50 and 51 did not show clear cathodic reduction waves. In solution 51, cathodic current density was observed at potentials more cathodic than -0.7 $V_{Ag/AgCl}$. Ballesteros et al. [39] attributed the cathodic current density occurring at this potential to the reactions listed here:

$$\mathbf{Cu^{2+} + 2\,OH^{-} + 2\,T^{2-} \rightleftarrows Cu^{2+}(T)_2(OH^{-})_2 \quad where\ T = (C_4H_4O_6)} \qquad \mathbf{[27]}$$

$$\mathbf{CuT_2(OH)_2^{4-} + 2\,e^{-} \rightleftarrows Cu^{0} + 2\,T^{2-} + 2\,OH^{-}} \qquad \mathbf{[28]}$$

During the reverse scan, anodic current was observed at potentials more positive than -0.4 $V_{Ag/AgCl}$.

5.2 Cyclic Voltammetry on TiO_2

5.2.1 Study of Solution Behavior on TiO_2 with No Additives

Figure 5.5 shows the results of CVs carried out on Solutions 1-7. Solution 1 has been referred to as the "base" solution with 0.16 *M* $CuSO_4$ + 1.8 *M* H_2SO_4, and solution 2-7 contain the base plus a single additive of PEG, SPS, NaCl, NaF, PEI or EG.

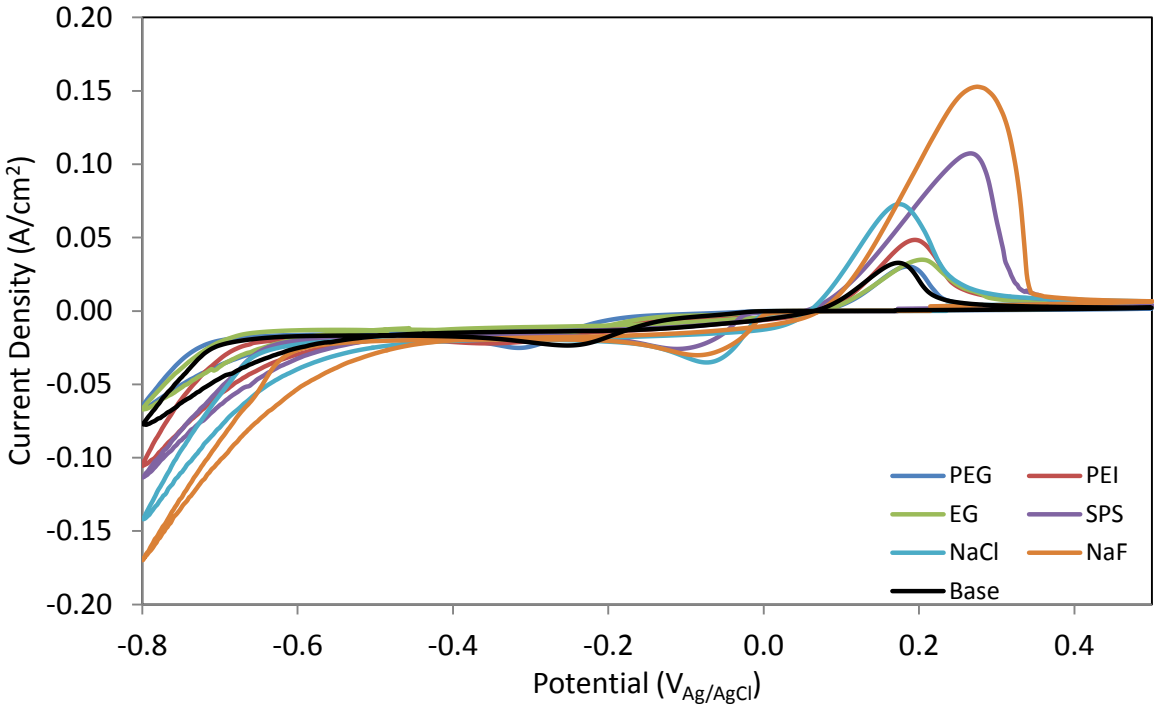

Figure 5.5: CVs using TiO_2 substrate with a base solution of 0.16 *M* $CuSO_4$ + 1.8 *M* H_2SO_4 with different additives at 10 mV/s

The base solution showed an initiation of cathodic current density at -25 $mV_{Ag/AgCl}$ and a first cathodic peak current of 35 mA/cm^2 at -240 $mV_{Ag/AgCl.}$ At potentials more negative than -240 $mV_{Ag/AgCl}$, the current density decreased to about -25 mA/cm^2, showing a concentration polarization behavior until -685 $mV_{Ag/AgCl}$. An activation polarization behavior was observed at cathodic potentials up to -686 $mV_{Ag/AgCl}$, leading to a final current density of -116 mA/cm^2. Compared to the platinum substrate, the deposition of copper onto TiO_2 was observed to be different. The first difference was that the onset of a cathodic current wave was less negative by 35 $mV_{Ag/AgCl}$ on TiO_2 (-25 $mV_{Ag/AgCl}$) when compared to the platinum substrate (-60 $mV_{Ag/AgCl}$). Secondly, there was a district cathodic current peak at -245 $mV_{Ag/AgCl}$ on the TiO_2. The third difference was that there was a strong barrier for activation polarization up to -685 $mV_{Ag/AgCl}$ on the TiO_2. Lastly, there was an absence of a shoulder peak on TiO_2 during oxidation that was typically observed at potentials more positive than 300 $mV_{Ag/AgCl}$ on the platinum electrode.

Considering the TiO_2 electrode, the anodic wave plateaued at about 235 $mV_{Ag/AgCl}$. The redox potentials of the Cu^{2+}/Cu^{+} system under standard conditions is -0.47 $V_{Ag/AgCl}$. Taking the concentration of Cu^{2+} as 0.16 *M*, the activity coefficient as 0.15 and the activity of Cu^{+} as $3x10^{-4}$ *M*, the redox potential, E°, could be estimated as:

$$E^{\circ} = 0.047 + 0.059\log[Cu^{2+}]/[Cu^{+}]$$
$$= 0.047 + 0.059\log[0.15x0.16]/[3x10^{-4}] = 0.064\ V_{Ag/AgCl} \quad [29]$$

The concentration of Cu^{+} was estimated from the equilibrium constant of the reaction [28]:

$$Cu^{2+} + Cu^{0} \rightleftarrows 2\,Cu^{+} \qquad K_{Eq*Cu} = [Cu^{+}]^2/[Cu^{2+}] = 6.0x10^{-7}M \quad [30]$$

However, it is noted that the reaction combination proportion reaction listed in equation 30 is not possible without a copper substrate. The onset of the cathodic current on the TiO_2 substrate could therefore be attributed to the possible underpotential deposition of copper. Rosario et al. [42] observed underpotential deposition of copper onto TiO_2 electrodes.

5.2.2 Study of Solution Behavior on TiO_2 with Inhibitor Additives

Figure 5.6 shows the CVs of only the inhibitors compared with the base. The addition of 88 μM PEG to the base solution did not alter the shape of the CV curve of the TiO_2 nanotubular substrate. However, the placement of the cathodic peak current was shifted to a more cathodic potential by almost 60 mV (-303 $mV_{Ag/AgCl}$ vs. -245 $mV_{Ag/AgCl}$). There was also a marginal increase in the current density (about 7% higher than that of the base solution. The cathodic shift in the potentials of reduction current by addition of PEG could be attributed to the adsorption of PEG on the TiO_2 surface. The inhibiting effect of PEG on TiO_2 resulted in a decrease in the current density at higher cathode potentials. The final current density at -0.8 $V_{Ag/AgCl}$ in the PEG additive electrolyte was -65 mA/cm^2 vs. -77.3 mA/cm^2 without any additives. Similarly, the anodic peal current density was also decreased with the addition of PEG. When compared to the platinum surface, the effect of PEG adsorption onto the TiO_2 surface was not significant. For example, the current density of the

platinum at -0.8 $V_{Ag/AgCl}$ was reduced by almost 3.5 times upon addition of PEG. On the other hand, the current density of the TiO_2 is only observed to be reduced by about 16%.

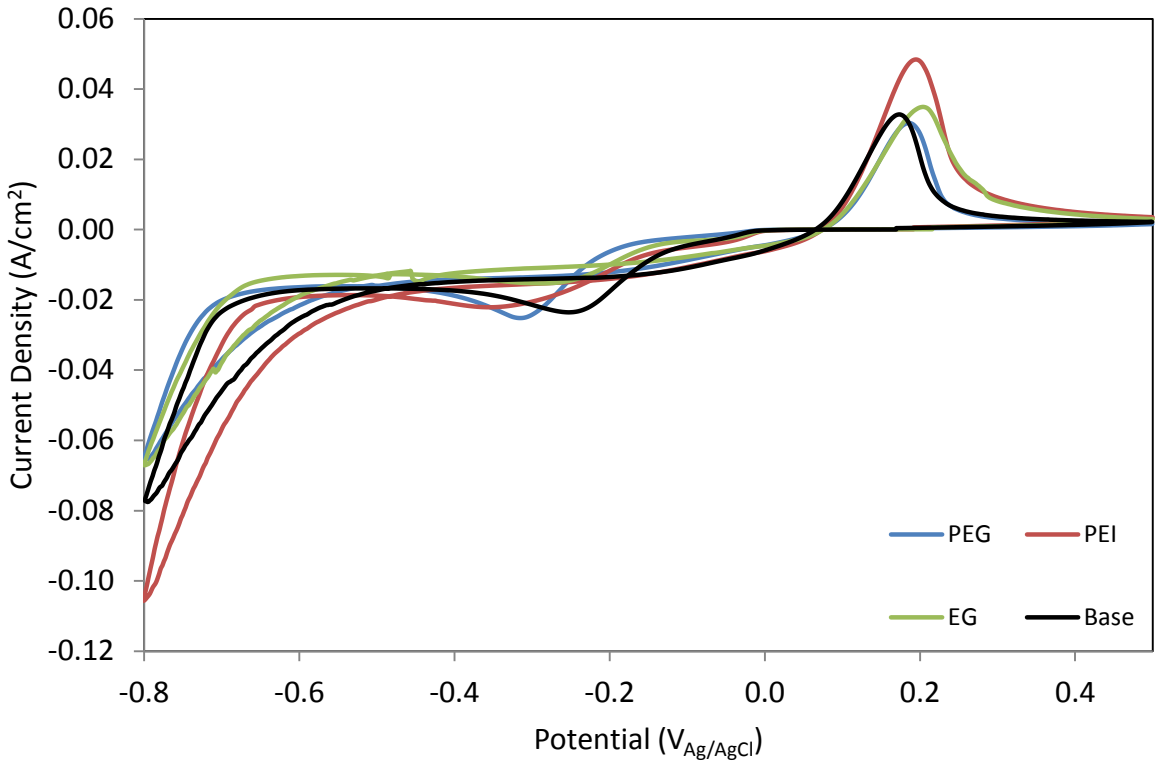

Figure 5.6: CVs of base solution compared with inhibitor additives only, at 10 mV/s, TiO_2 electrode

Interestingly, PEI addition showed increasing effects on the TiO_2 electrode in contrast to the effects observed on the platinum electrode. The addition of PEI shifted the potential of the first cathodic peak current to a more negative potential, the effects were similar to that of PEG addition. However, the current density was about 7% lower than that of the base solution. At more negative potentials, the effects of PEI were reversed. The second cathodic wave (after a diffusion limited current segment) was initiated at about -0.64 $V_{Ag/AgCl}$, 40 mV more positive than the corresponding potential of the base solution. The final current density at -0.8 $V_{Ag/AgCl}$ was -105 mA/cm^2 with the PEI additive vs. -77 mA/cm^2 for the base solution. Similarly, the oxidation current density of the PEI additive solution was also higher than that of the base solution. These observations clearly indicate

that the PEI acted as an accelerator for copper deposition onto the TiO_2 electrode. From Figure 4.4, it can be seen that the addition of 88 μM EG acted as a weak inhibitor.

5.2.3 Study of Solution Behavior on TiO_2 with Accelerator Additives

Figure 5.7 shows the CVs of only the accelerators compared with the base. The results of the addition of SPS were very similar to that reported by Chiu and Dow [45] using a gold electrode. A very distinct cathodic peak at -0.09 $V_{Ag/AgCl}$, characteristic of organosulfide accelerated copper deposition, could be observed. Chui and Dow called this the α-peak and attributed the peak to the formation of copper nanoparticles on the additive-modified electrode surface. Adsorption of SPS onto TiO_2 was found to facilitate electron transfer for the reduction of Cu^{2+}. The onset of cathodic current was observed even as -0.013 $V_{Ag/AgCl}$, and the onset of the second cathodic current wave was also shifted anodically by about 70 mV. As seen from the CV curve in Figure 5.7, the anodic shift in the potential of activation-controlled, second-cathodic current wave showed an increased current density by about 60% when compared to the base solution with no SPS additive. The increased reduction of current density is manifested into a larger oxidation /stripping current density upon anodic polarization.

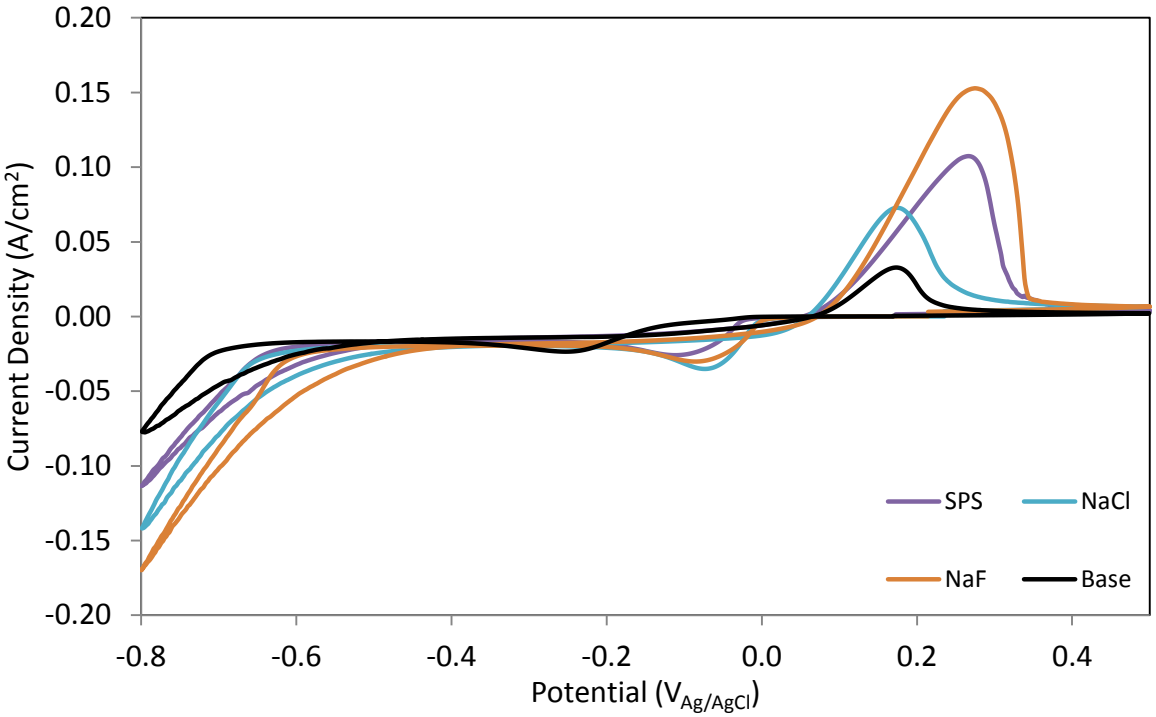

Figure 5.7: CVs of base solution compared with accelerator additives only, at 10 mV/s, TiO_2 electrode

Individual additions of 2 *mM* NaCl and 2 *mM* NaF resulted in accelerated copper electrodeposition conditions. It is well documented that a combination of Cl^- and SPS helps to increase the electron transfer for the reduction of cupric ions [46], [47]. In this case, individual additions of NaCl, SPS and NaF exhibited accelerated copper plating behaviors. Among these additives, NaF showed the highest accelerating effect by shifting the potential of the second cathodic wave to -0.6 $V_{Ag/AgCl}$ and increasing the current density to -141 mA/cm^2, almost twice the value of the base solution.

5.2.4 Study of Solution Behavior on TiO_2 with Mixed Additives

Figure 5.8 shows the results of CVs carried out on TiO_2 with electrolytes having different combinations of additives. The combination of SPS and PEG showed a strong inhibiting effect on the TiO_2. The first cathodic current peak was shifted to a more negative potential, and the second peak was not observed until -0.8 $V_{Ag/AgCl}$.

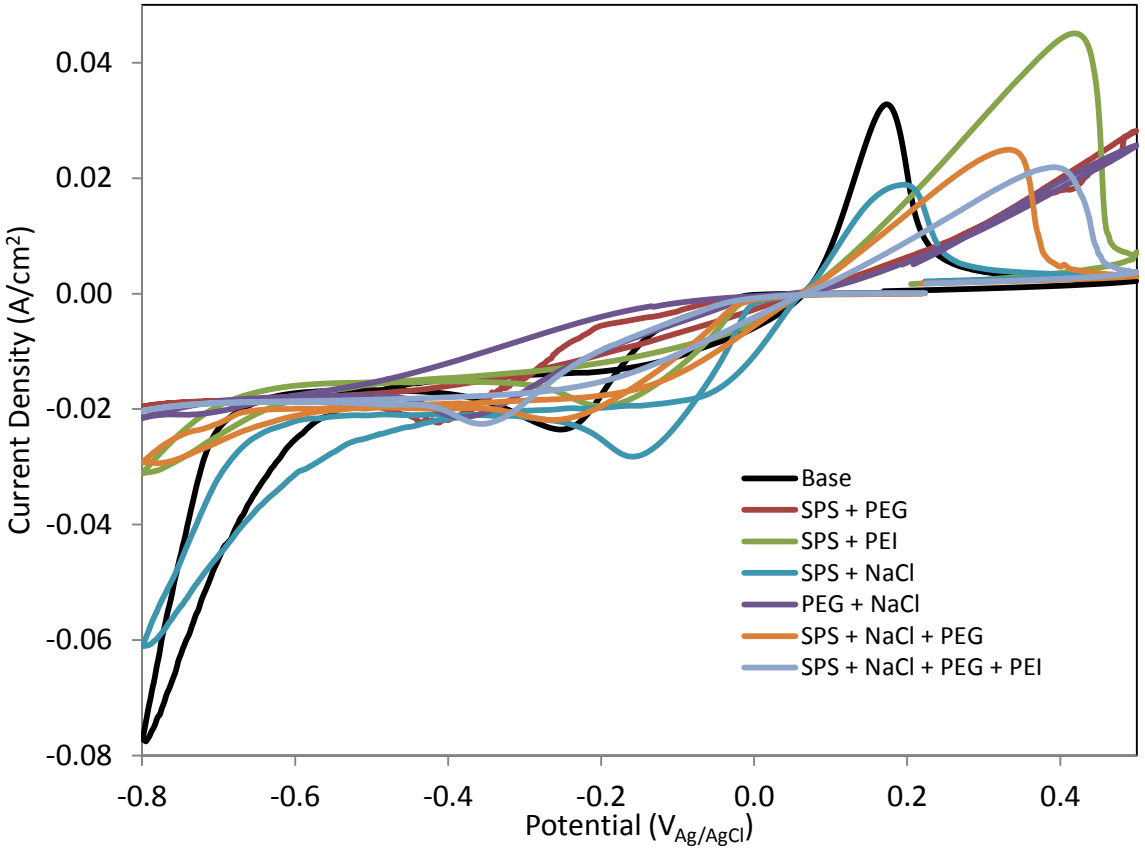

Figure 5.8: CVs of various mixed additives on TiO_2 substrate

Addition of both SPS and PEI showed a moderate inhibiting effect. In this case, the onset potential of the first cathodic current was shifted in the anodic direction by almost 60 mV (-181 $mV_{Ag/AgCl}$ vs. -240 $mV_{Ag/AgCl}$ for the base solution). However, the current density of the first cathodic peak with SPS and PEI was only 80% of that of the base solution. The final current density of the second cathodic wave at -0.8 $V_{Ag/AgCl}$ of the SPS and PEI solution was about 40% of the base solution. It should be noted that, when individually added, both SPS and PEI showed accelerating effects.

The combination of PEG and NaCl showed a strong inhibiting effect. This behavior was similar to that observed on platinum or copper electrodes. The combination of SPS and NaCl did not show a significant change in the cathodic current magnitudes when compared to the current densities of the base solution. Overall, a moderate inhibiting effect is noted in contrast to the

accelerating effects of SPS and Cl^- observed on the regular copper/standard copper process electrodes. Combinations of SPS, NaCl and PEG as well as SPS, NaCl, PEG and PEI also showed overall inhibiting effects on the TiO_2 electrode.

5.3 Super Honeycomb

5.3.1 Morphology

The creation of the final structure was accomplished through three major steps. The first step was to anodize in ethylene glycol at 60 V for 4 hours. Figure 5.9 (Right) shows the morphology of the oxide layer after this step. The TiO_2 nanotubes shown have a diameter of 90-120 nm. The tube length will continue to grow until the anodization process is stopped or the Ti foil is completely oxidized.

The second step in the creation of the Super Honeycomb structure was to remove the oxide layer and examine the nano-indented structure as can be seen in Figure 5.9 (Left). The nanoindentations had roughly the same diameter as the initial TiO_2 nanotubes that were removed. This surface became the template for the anodization in step three.

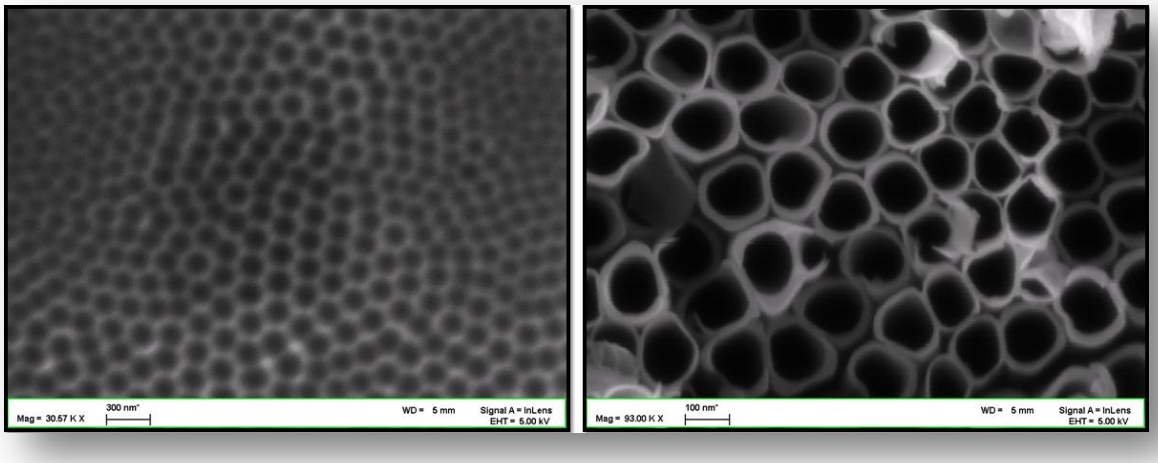

Figure 5.9: (Left) Nanoindentations after 1st oxide layer is removed. (Right) TiO_2 nanotube structure after 1st anodization in EG

Step three involved re-anodizing the nanoindented foil in an aqueous fluoride solution at 20 V for 40 minutes. This step created the final Super Honeycomb structure seen in Figure 5.10. This structure has a large format honeycomb structure with honeycomb wells of 110-130 nm in diameter. Each honeycomb well is dotted with 15-20 nanotubes ranging in diameter from 15-40 nm. The surface oxide layer is about 350 nm at its highest points and about 150 nm at the bottom of the honeycomb wells. An SEM Micrograph of both the top and side views is shown in Figure 5.10.

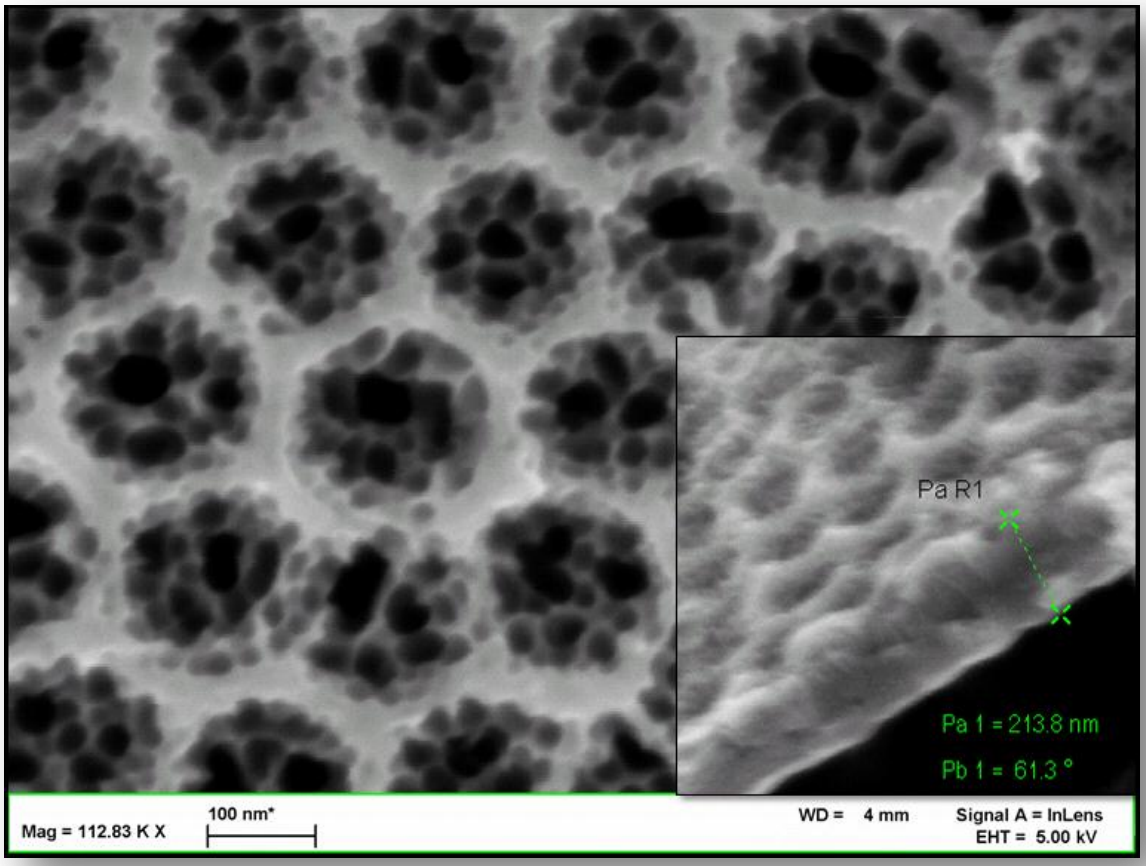

Figure 5.10: Top view of Super Honeycomb TiO_2 morphology, inset is a side view

5.3.2 Electrochemical Characterization

Figure 5.11 shows the cyclic voltammograms used for calculating the capacitance of the TiO_2 Super Honeycomb morphology in a 1 *M* H_2SO_4 electrolyte when N_2 annealed. The top of the three curves shows the anodic oxidation of the test samples where they lose an electron by oxidizing from Ti^{3+} to Ti^{4+}. This reaction is the foundation of where titanium gets its capacitive energy storage ability. A reaction is given on the top of the graph which shows the participation of hydrogen ions in the reduction and oxidation reactions involved in energy storage. Although the curve at 1000 mV/s has a bigger cycle, it is actually the 100 mV/s cycle that has the highest capacitance because capacitance is time dependent, a variable which is not represented well in a CV. Figure 5.12 shows another set of CVs on O_2 annealed TiO_2 Super Honeycomb samples for comparison.

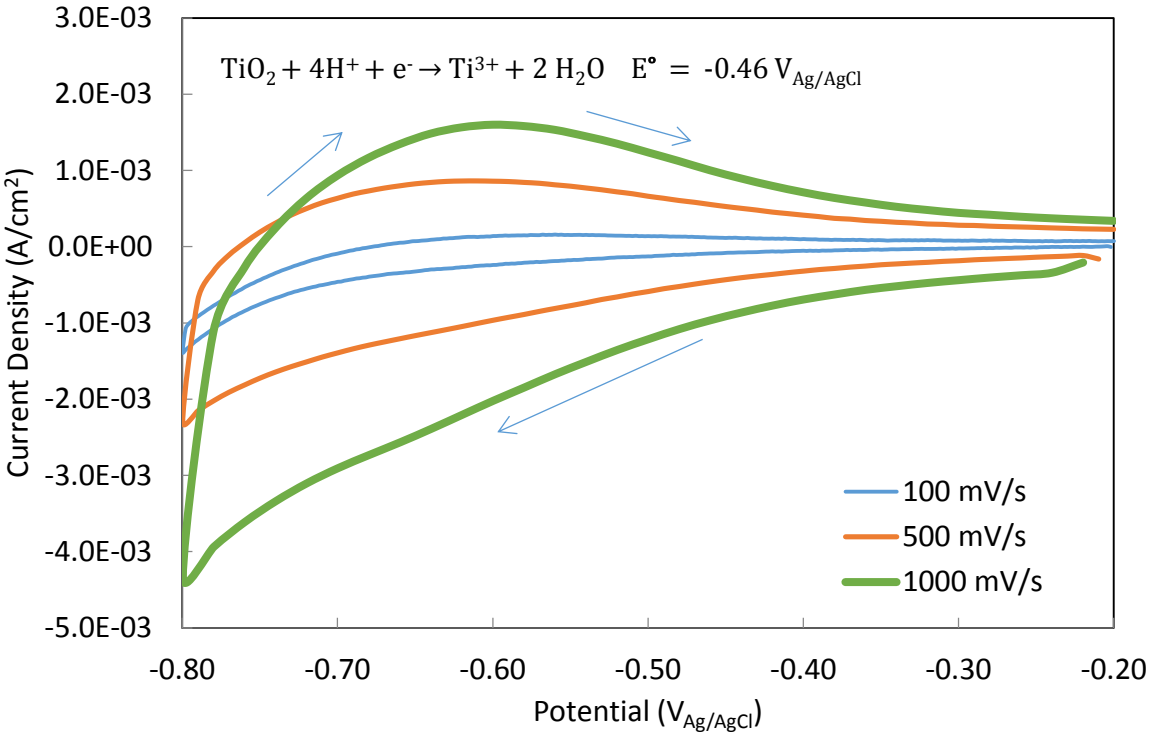

Figure 5.11: CVs on Super Honeycomb EG/NaF, 1 *M* H_2SO_4, N_2 annealed 100, 500 and 1000 mV/s

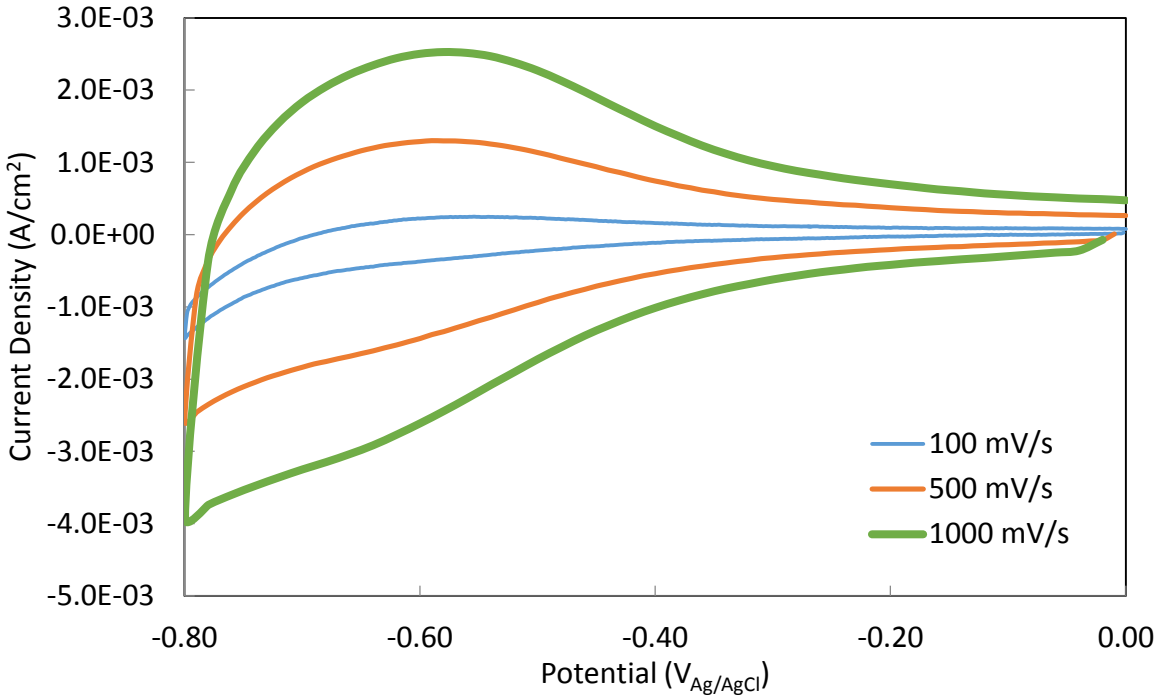

Figure 5.12: CVs on Super Honeycomb EG/NaF, 1 *M* H_2SO_4, O_2 annealed 100, 500 and 1000 mV/s

Figure 5.13 shows the capacitance CVs in a 0.1 *M* LiCl electrolyte. The main difference to note is the lack of hydrogen participating in the energy storage reaction. The reaction given on the top of the graph represents the lithium's participation in energy storage for this electrolyte system. Figure 5.14 is also given for the same system with oxygen annealed sample tests. It should be expected to have higher capacitance values on the samples that have been annealed in nitrogen due to the annihilation of oxygen vacancies. The more oxygen vacancies a material has the better its capacitance should be. By removing oxygen from the annealing atmosphere, the vacancies cannot dissipate as quickly.

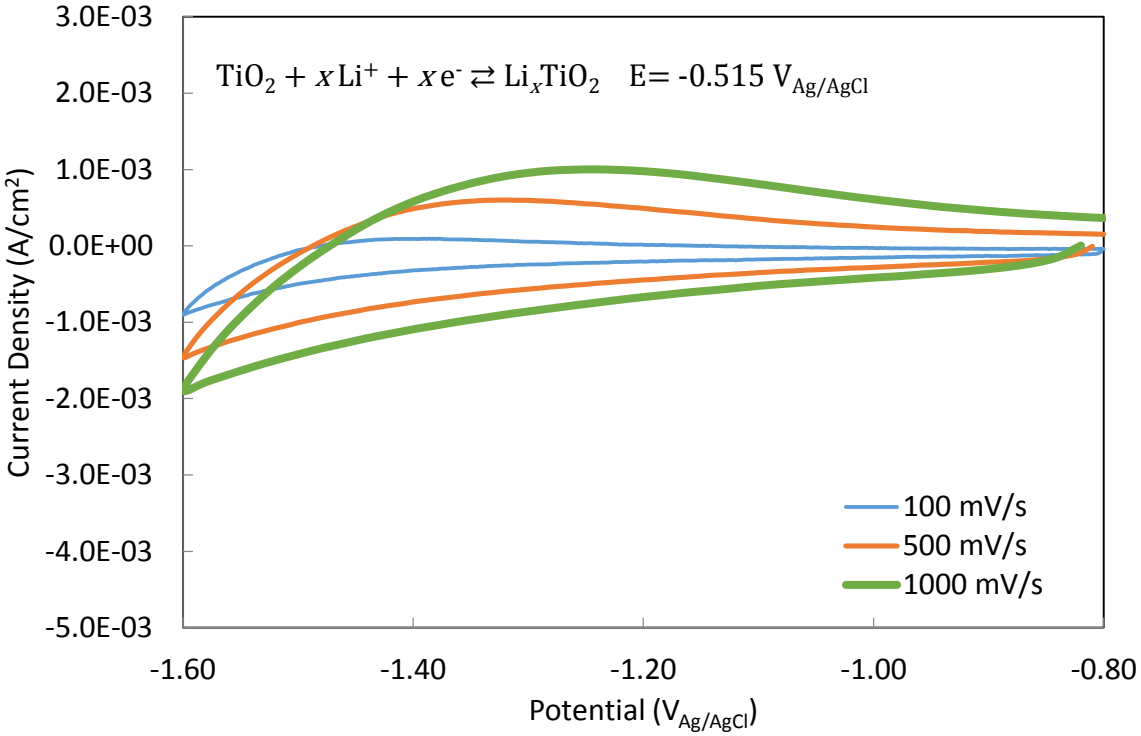

Figure 5.13: CVs on Super Honeycomb EG/NaF, 0.1 *M* LiCl, N_2 annealed 100, 500 and 1000 mV/s

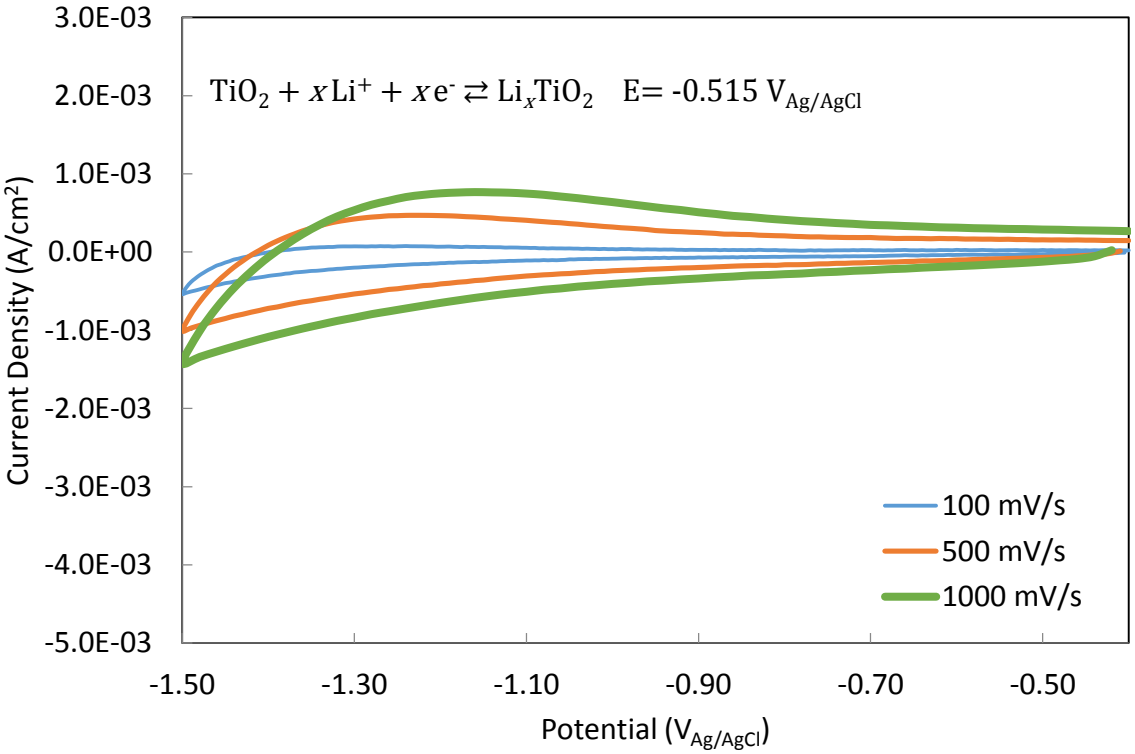

Figure 5.14: CVs on Super Honeycomb EG/NaF, 0.1 *M* LiCl, O_2 annealed 100, 500 and 1000 mV/s

It was assumed that a higher capacitance value could be achieved by obtaining both of the reactions from the top of Figure 5.11 and 5.13. An electrolyte containing both hydrogen ions and lithium ions was used, and a condensed version of the capacitance results can be found in Figure 5.15. Figure 5.15 was calculated from the CVs on Super Honeycomb TiO_2 in a 0.1 *M* LiCl + 0.1 *M* HCl electrolyte. As expected, the nitrogen annealed samples did much better than the oxygen annealed samples, giving a capacitance value of 19.6 mF/cm^2 as the highest value obtained. A regular titanium nanotube sample, created through previously mentioned anodization methods in an aqueous electrolyte, is also included in the graph for comparison. Figure 5.16 shows the capacitance results for an electrolyte containing 0.1 *M* NaOH. Although the capacitance is not as good for this graph, it is important to note that the same trends follow in both electrolytes.

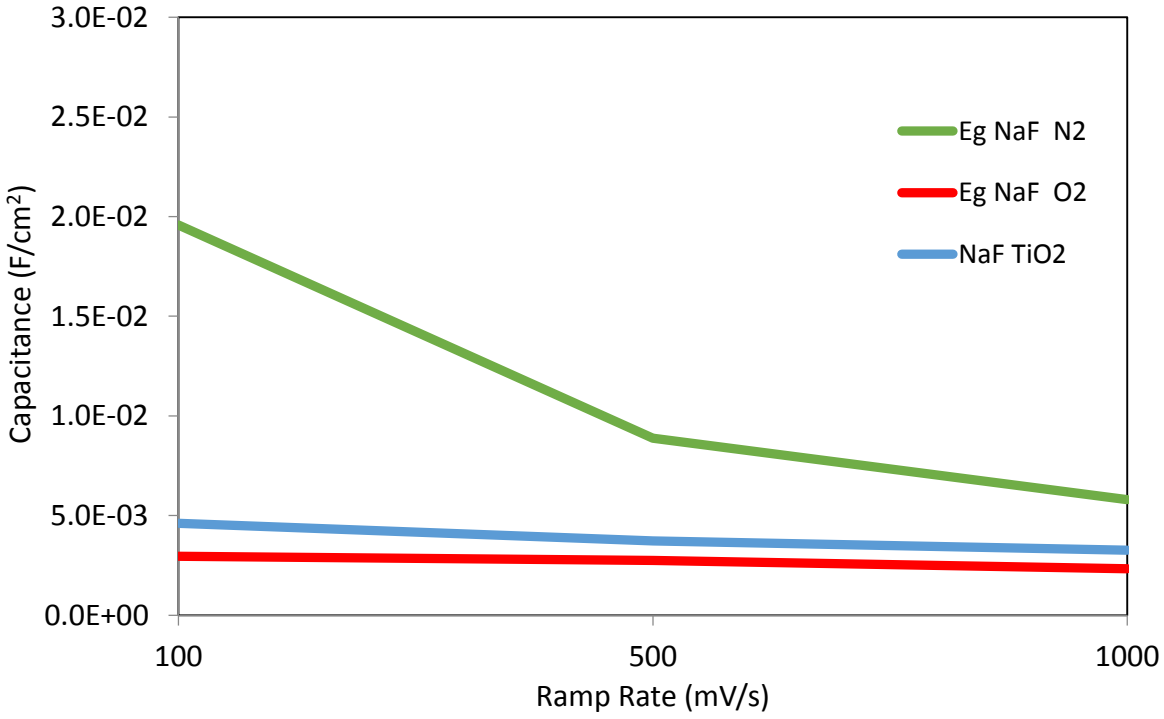

Figure 5.15: Average capacitance 0.1 *M* LiCl + 0.1 *M* HCl, EG/NaF anodized

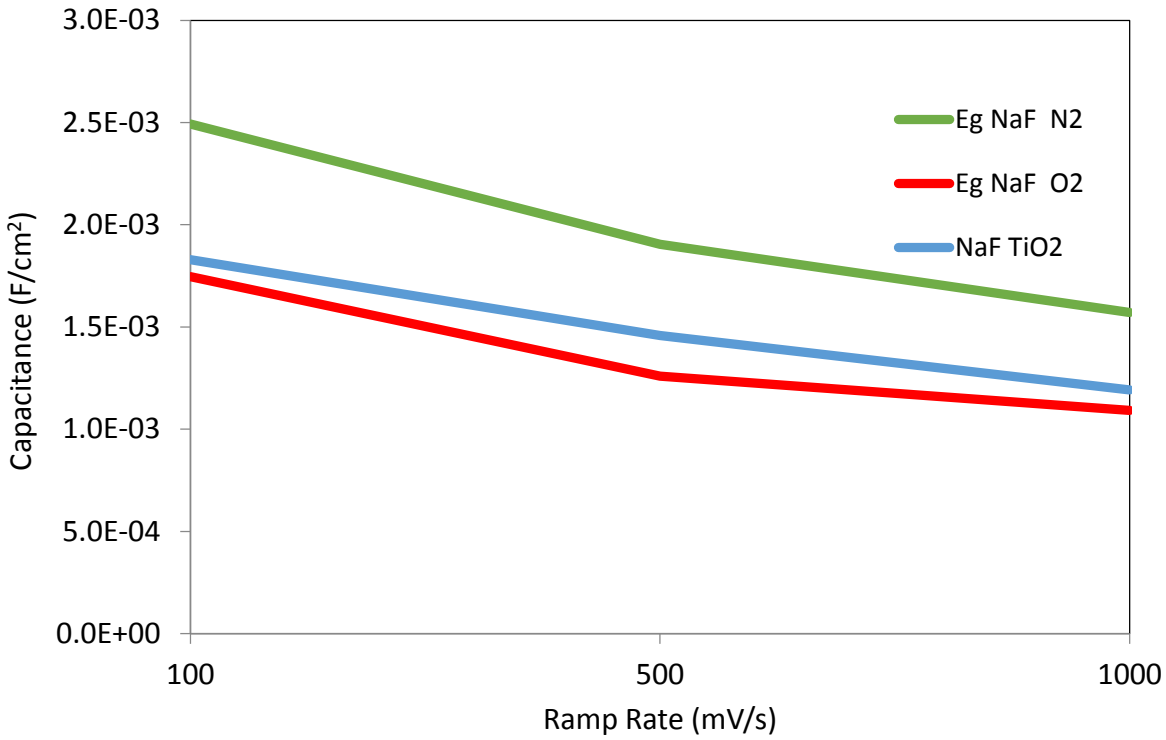

Figure 5.16: Average capacitance 0.1 *M* NaOH, EG/NaF anodized

Figure 5.17 shows the bode plots from two of the electrolytes used in the electrochemical characterization tests. Bode plots are helpful in showing the resistance of the material. It is expected that the O_2 annealed samples should have a higher resistance or modulus of impedance. For each electrolyte, a trend can be seen where the oxygen annealed samples show a higher resistance by an average of about 20% in NaOH and by 8% in LiCl. It should be taken into account when viewing Figure 5.17 that the y-axis in particular is in decades. Even though the data appears similar, it is in fact not as close as it appears.

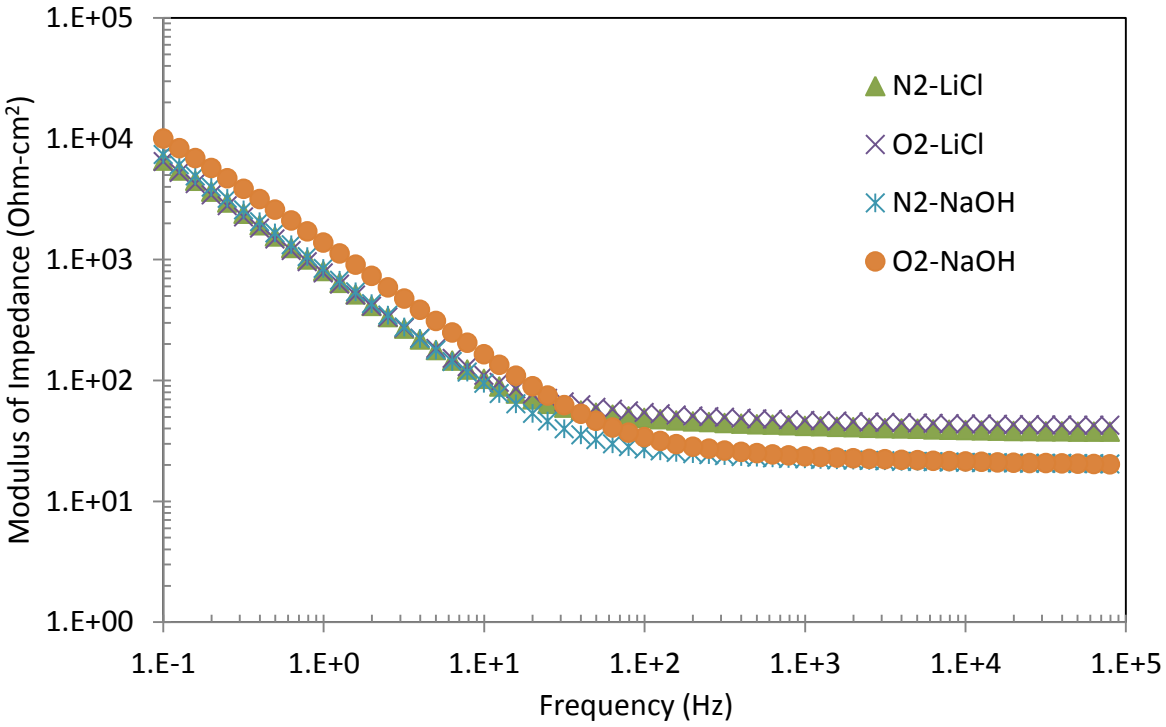

Figure 5.17: Bode plots from both 0.1 *M* LiCl and 0.1 *M* NaOH electrolytes, Super Honeycomb, EG/NaF anodized

5.4 Titanium-Manganese Applications of Super Honeycomb

5.4.1 Morphology

TiO_2 Super Honeycomb morphology showed promising results. Manganese, when oxidized to MnO_2, however, is known to have very high capacitance and energy storage properties. It was thought that reproducing the super honeycomb morphology on a titanium-manganese (Ti-Mn) alloy might reveal interesting electrochemical properties. Figure 5.18 shows the morphology of the oxide layer obtained after anodizing a Ti-Mn alloy (8 wt% Mn) foil of similar size with the same procedures and conditions used to obtain the TiO_2 Super Honeycomb. The microstructure obtained was not the expected Super Honeycomb morphology. Figure 5.19, however, reveals that the second anodization in an aqueous electrolyte did create nanotubular structures on each of the pieces shown in Figure 5.18. The average size of the nanotubes was around 20 nm.

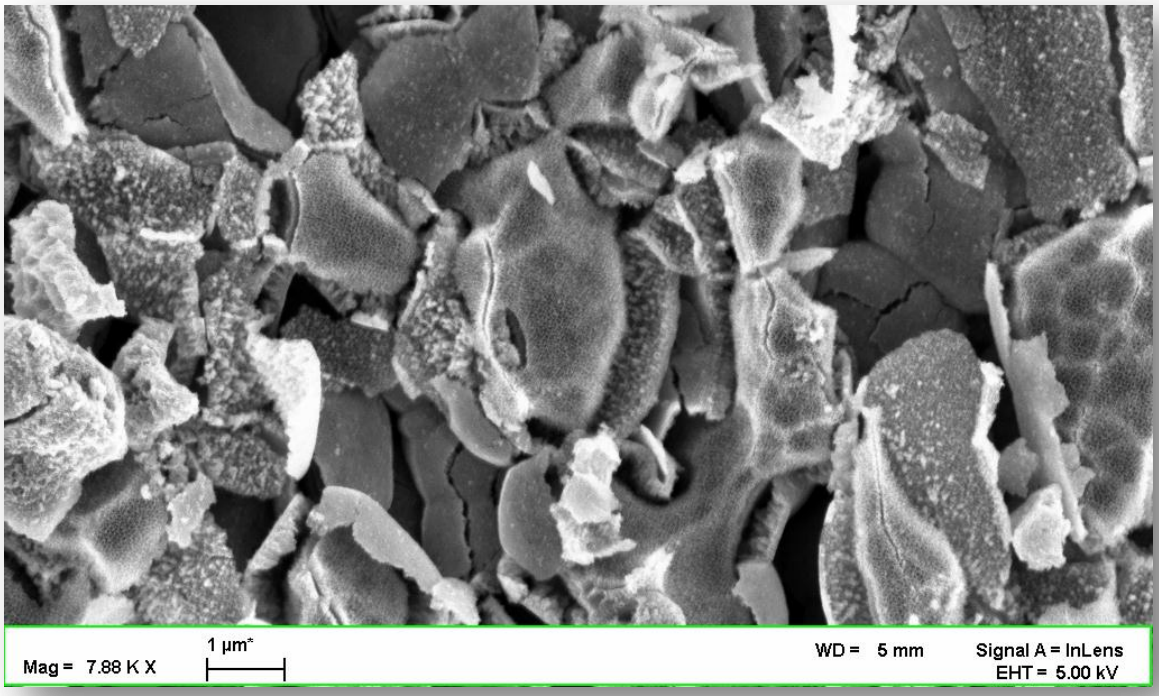

Figure 5.18: Ti-Mn alloy oxide layer microstructure, EG/NaF anodized

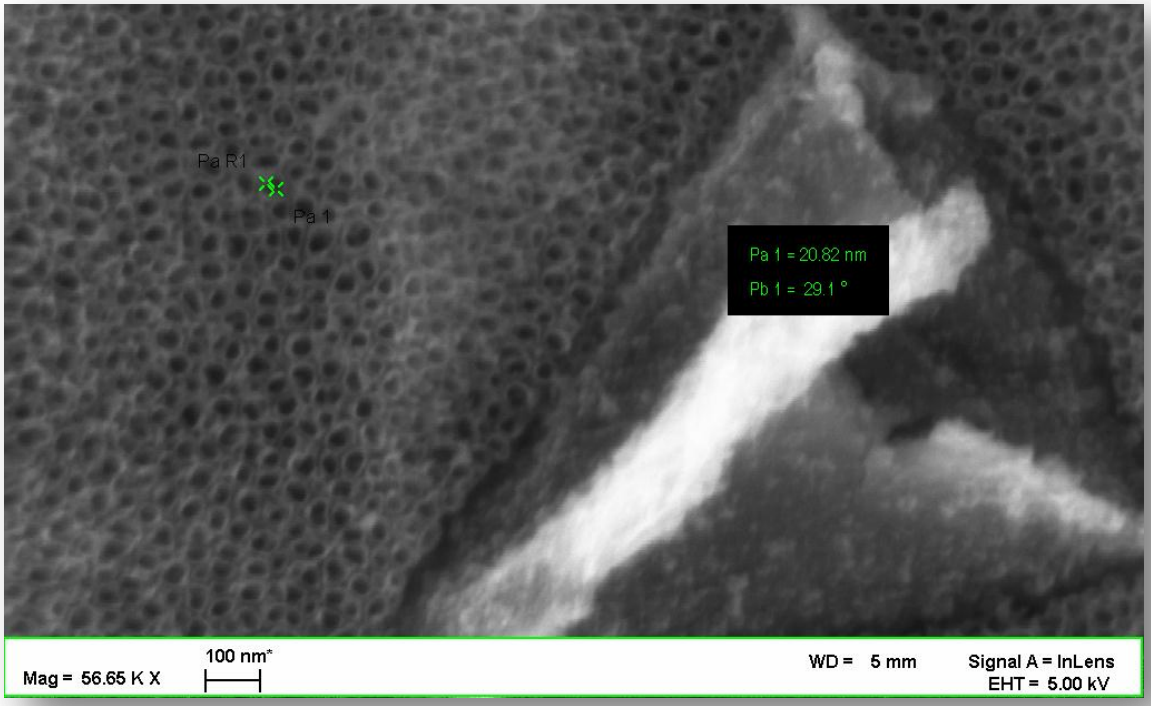

Figure 5.19: Ti-Mn alloy oxide layer morphology high magnification, EG/NaF anodized

5.4.2 Electrochemical Characterization

Section 5.3 presented capacitance data from cyclic voltammograms, in this section cyclic charge/discharge (CDC) graphs will be used to present capacitance in a more comprehensive way in order to get a more complete understanding of the mechanisms involved. Figures 5.20, 5.21 and 5.22 all show Ti-Mn samples in the as-anodized condition in a 1 *M* sulfuric acid electrolyte. Figure 5.20 has the slowest charge/discharge rate at ±1 mA/s. Figure 5.21 has a faster charge/discharge rate of ±10 mA/s, and Figure 5.22 has the fastest charge/discharge rate shown at ±20 mA/s.

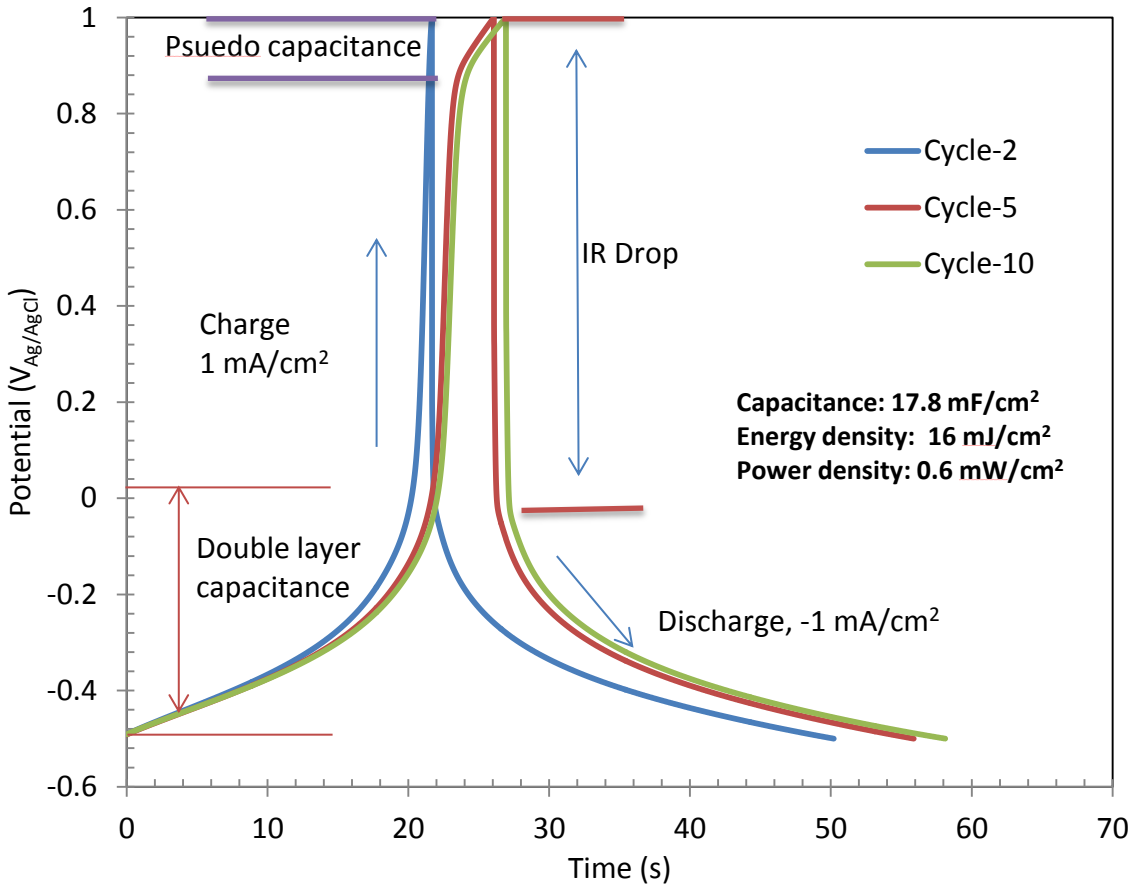

Figure 5.20: Charge/discharge (±1 mA/cm^2) Ti-Mn, unannealed, 1 *M* H_2SO_4

Figure 5.20 shows three cycles. Cycle 2, which is the first complete cycle in the test, has a much lower capacitance than cycles 5 and 10. This is actually quite common with capacitors. They do not reach their potential right away, but actually need some charge/discharge use in order to be

conditioned to their fullest potential. This effect is amplified with a slow CDC rate. The first portion of Figure 5.20, between -0.5 V and ~0 V can be attributed to electric double layer capacitance. At approximately 20 seconds the sample is instantaneously charged to about 0.9 V. From 0.9 V to 1 V, the samples showed pseudo capacitance behavior. At approximately 28 seconds, a large IR drop can be noted. This should be minimized as much as possible as it represents an instantaneous potential loss. There are three main trends that should be tracked as these three CDC graphs are followed. The first trend is that the capacitance does not decrease very much as the CDC rate is increased. The second trend is that the energy density also does not decrease very much as the CDC rate is increased. The final trend is that the power density does significantly increase as the CDC rate is increased. There is also an increase in the IR drop, which can somewhat justify the loss in capacitance as the CDC rate is increased as expected.

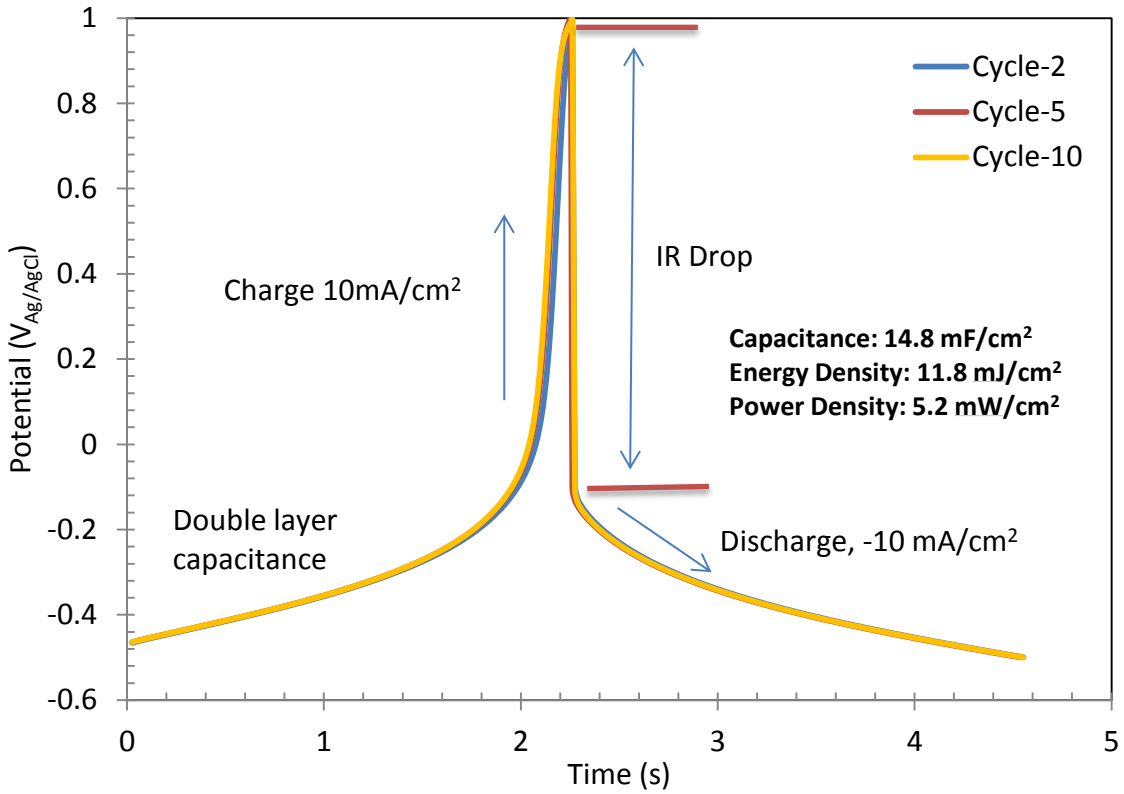

Figure 5.21: Charge/discharge (±10 mA/cm^2) Ti-Mn, unannealed, 1 *M* H_2SO_4

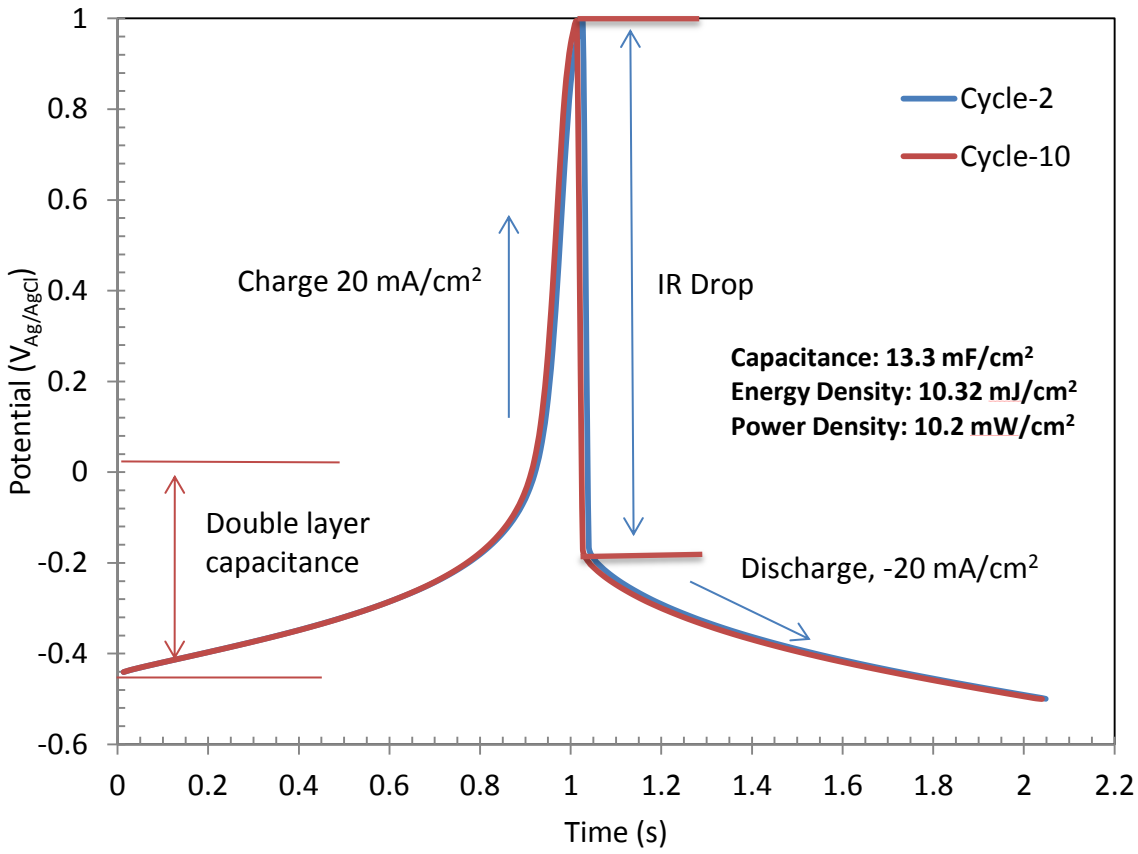

Figure 5.22: Charge/discharge (±20 mA/cm^2) Ti-Mn, unannealed, 1 *M* H_2SO_4

Figure 5.23 is a Ragone plot which tracked the change in the energy density vs. power density over the three Figures 5.20, 5.21 and 5.22. These three tests were performed in 1 *M* H_2SO_4 in the as-anodized condition. A horizontal trend on the Ragone plot is ideal. Commonly, materials will have an almost vertical trend.

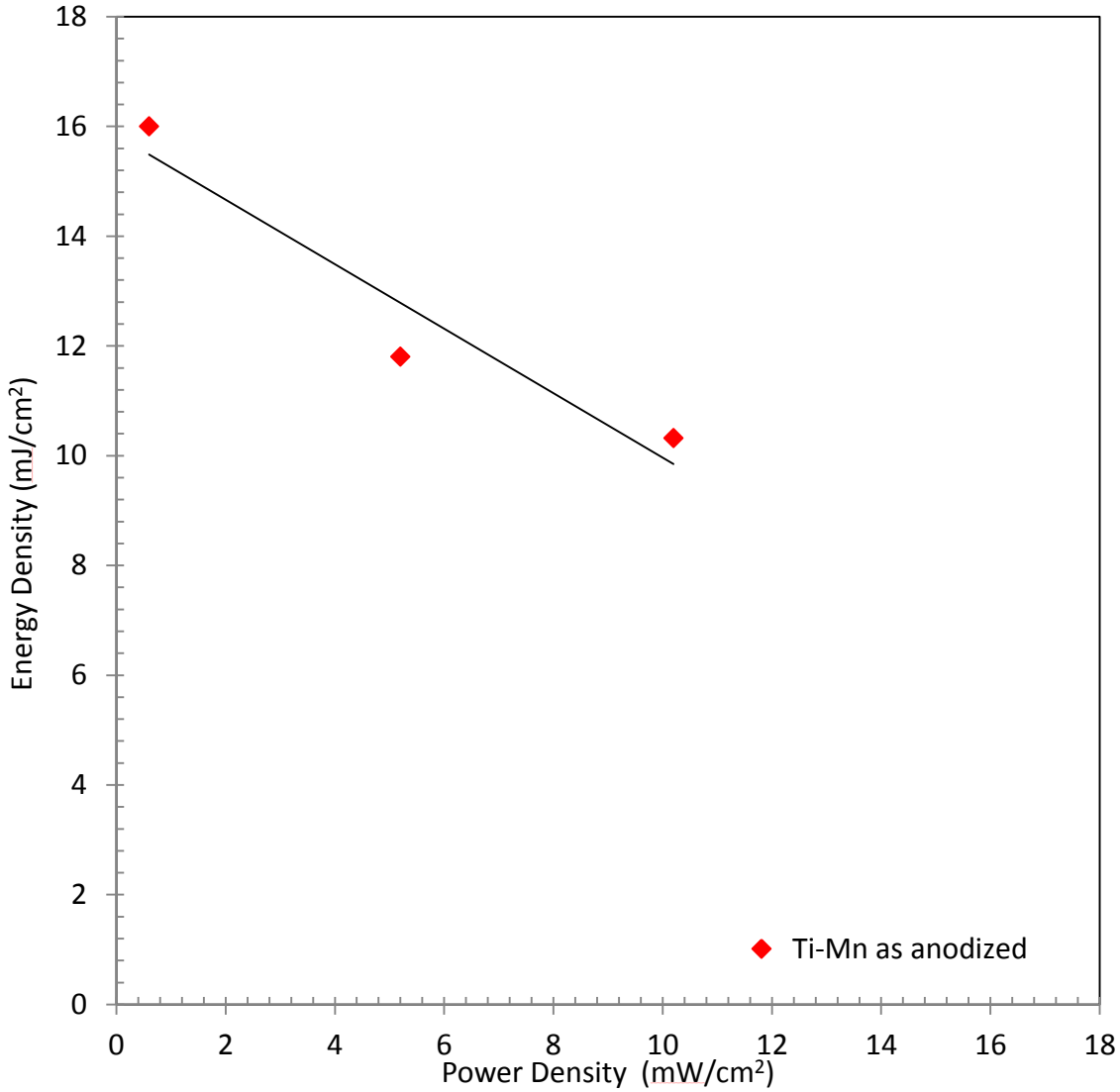

Figure 5.23: Ragone plot 1 *M* H_2SO_4, tracked changes in power density vs. energy density of Figures 5.20, 5.21 and 5.22

Figure 5.24 shows the graph of CDC tests performed in sulfuric acid at two different CDC rates on a Ti-Mn alloy sample annealed in a nitrogen atmosphere. It was expected that there would be an increase in capacitance due to the increase in oxygen vacancies. Although the IR drop did seem to improve with annealing the sample, it did not increase the capacitance. Under the conditions tested in Figure 5.24, the highest capacitance found was only 7.2 mF/cm^2. More tests need to be performed to understand exactly why the material did not act as expected.

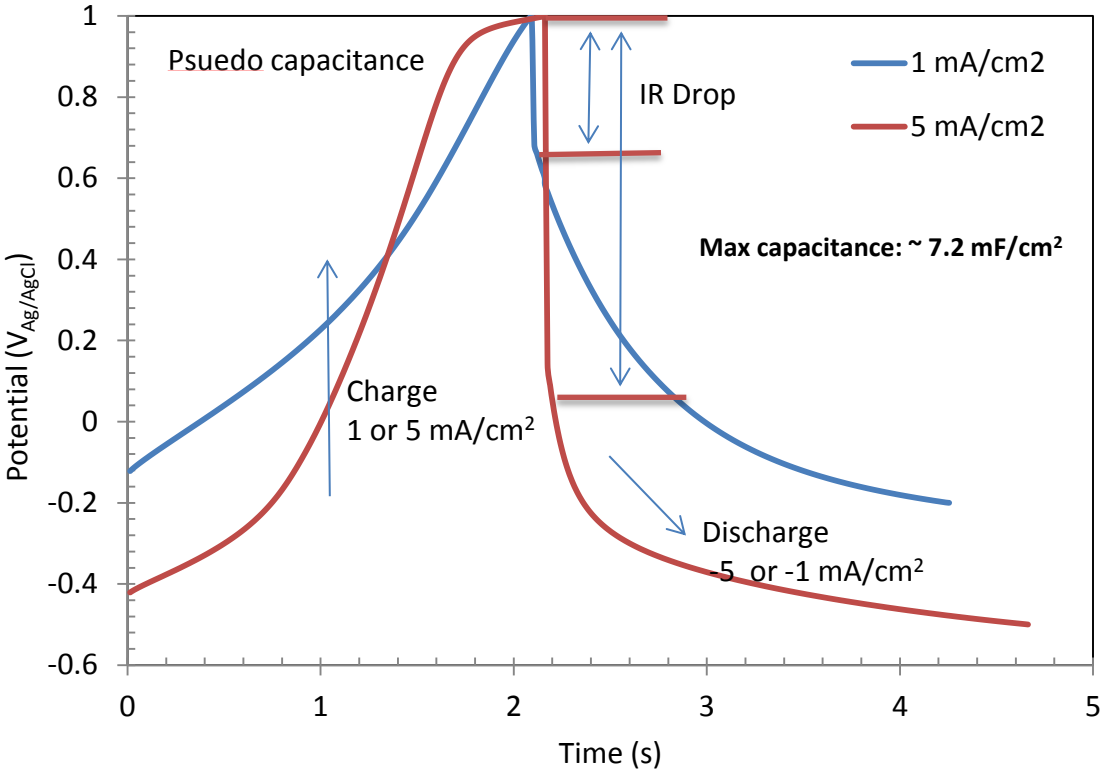

Figure 5.24: Charge/discharge Ti-Mn, N_2 annealed, 1 *M* H_2SO_4

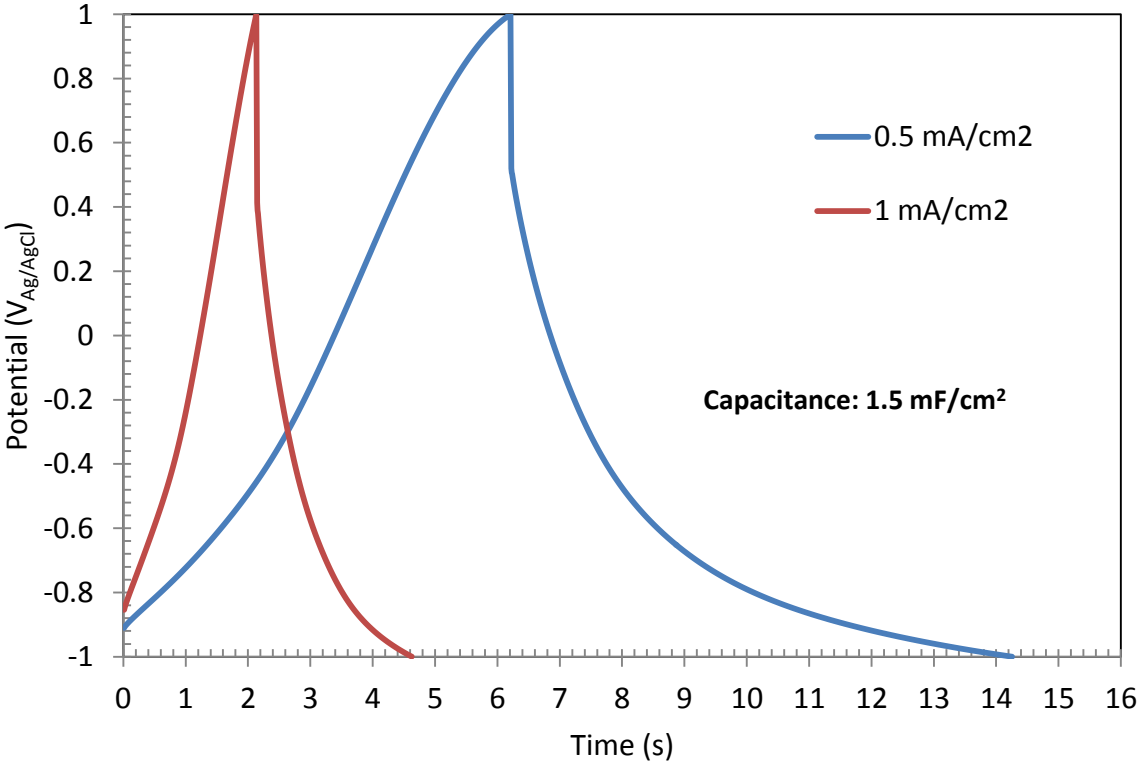

Figure 5.25: Charge/discharge Ti-Mn, N_2 annealed, 0.1 *M* LiCl

Figures 5.25 and 5.26 show the same unexpected drop in capacitance when the tests were performed in a 0.1 *M* LiCl electrolyte. Figure 5.25 shows another nitrogen annealed sample, in a different electrolyte, which should slightly increase the oxygen vacancies and therefore the capacitance. Figure 5.26 shows an air annealed sample for comparison. The same unexpected trends are followed.

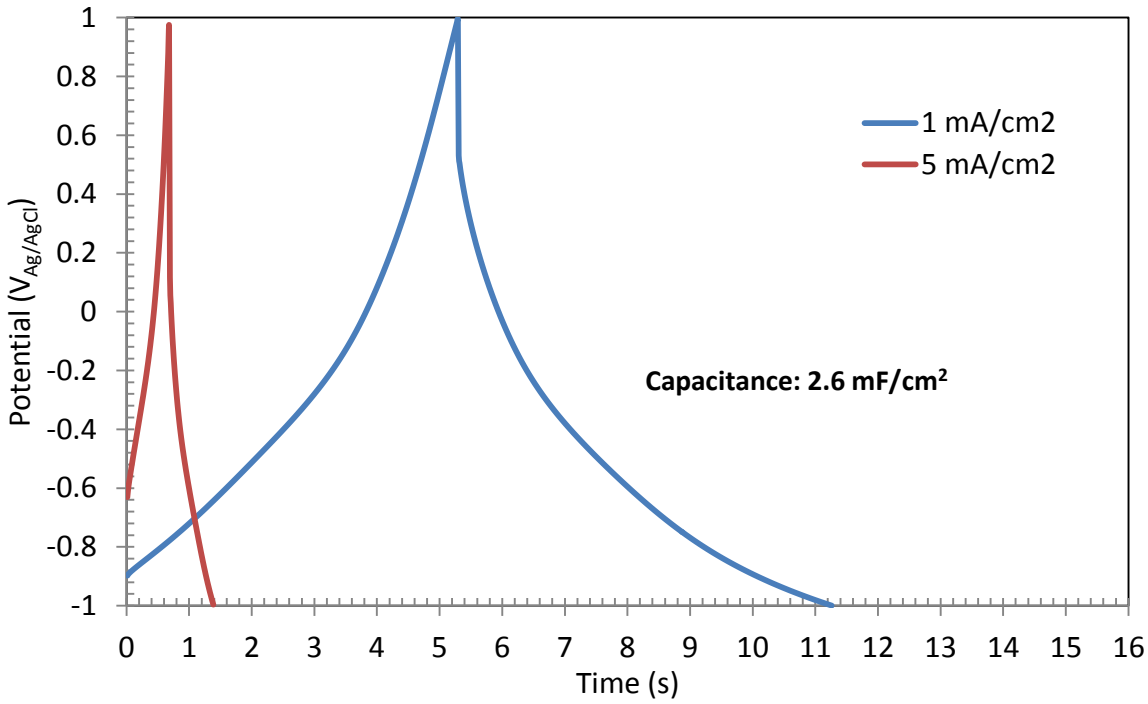

Figure 5.26: Charge/discharge Ti-Mn, air annealed, 0.1 *M* LiCl

Figure 5.27 is a Nyquist plot of Ti-Mn samples both nitrogen annealed and as-anodized compared with regular TiO_2 nanotubes created by anodization in an aqueous electrolyte through the previously mentioned method. When Nyquist plots have a low imaginary impedance, it is a good indicator that the material is an excellent capacitor. Nyquist plots are created at open circuit potential, however, and this means that they can only measure the space charge layer capacitance. Because only the oxide layer is being measured, the nitrogen annealed sample does give the expected better results. When compared with all the other data previously mentioned about the

unexpected decrease in measurable capacitance, it can be deduced that the majority of the capacitance does not come from space charge layer capacitance for this material.

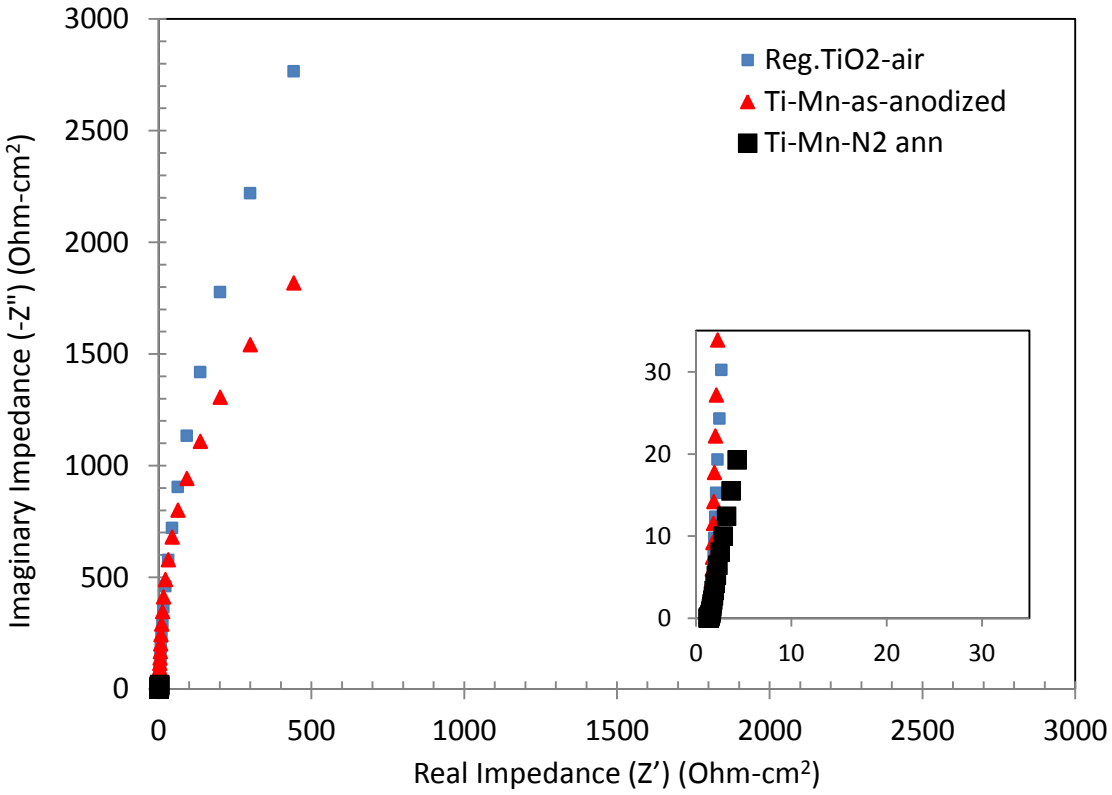

Figure 5.27: Nyquist plot, 1 *M* H_2SO_4 comparing Ti-Mn N_2 annealed, Ti-Mn unannealed and regular TiO_2

Figure 5.28 is another Bode plot which again shows the resistance of the material. It was expected that the nitrogen annealed sample would have less resistance. In fact, it had two orders of magnitude less resistance. This should indicate that it will give much better capacitance. This, as stated, was not the case, which again proves that more tests need to be performed to understand exactly how much and what type of capacitance this alloy material is capable of achieving.

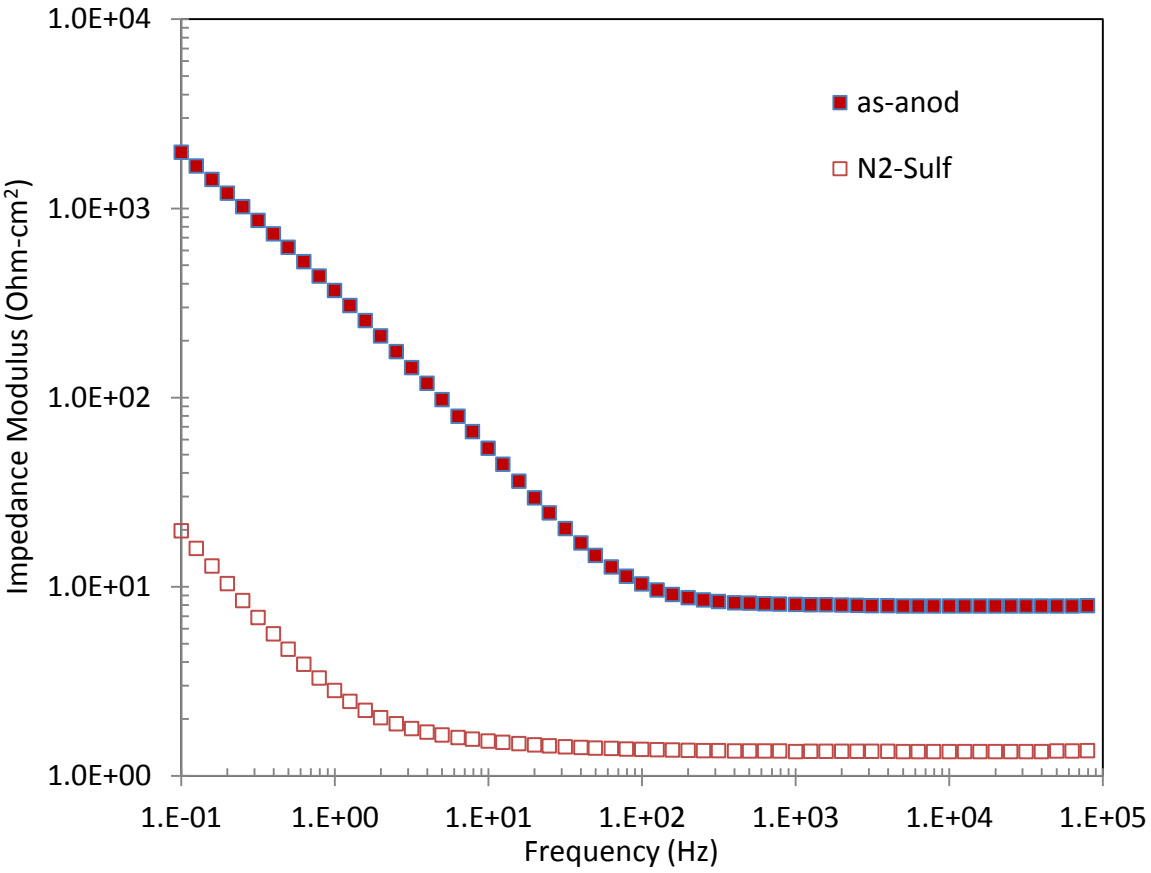

Figure 5.28: Bode plot Ti-Mn, 1 *M* H_2SO_4 comparing N_2 annealed with unannealed samples

CHAPTER 6: CONCLUSIONS AND FUTURE WORK

The inhibitor and accelerator additives did not work well in producing a bottom-up deposition. Ultrasonication did make some morphological changes to the copper deposited crystals but did not help to achieve a bottom-up deposition. The addition of methanol, which was thought to lower the surface tension of the electrolyte, unfortunately did not help to increase the wettability.

The pH study also gave interesting results, all pH changes were made with NaOH. Both high and low pHs did not work well, but pH around pH 6 did work much better. This is likely due to the fact that the isoelectric point of TiO_2 is right at 5.8. High copper concentrations resulted in extreme surface blockage, while very low concentrations worked much better. The addition of tartaric acid as a complexing agent worked well to improve the copper deposition. Citric acid did not work well as it tended to precipitate out of solution rather than complex with copper. Changing to low temperature deposition showed the most notable improvement in copper deposition inside of the nanotubes.

The best filling of the nanotubes that was achieved was under potentiostatic 2-step pulsing at 0 $mA_{Ag/AgCl}$ for 5 sec and -0.5 $mA_{Ag/AgCl}$ for 5 sec for 100 cycles. The pH of the solution was 5.25, the temperature was 1-3˚C and the solution contained 0.03 *M* tantric acid and $CuSO_4$. Although filling the nanotubes with a complete nanowire was not achieved, significant progress was made in understanding the electrolyte system and its deposition effects on TiO_2 nanotubes. Figures 6.1 and 6.2 show the results of filling these nanotubes with copper nanoparticles.

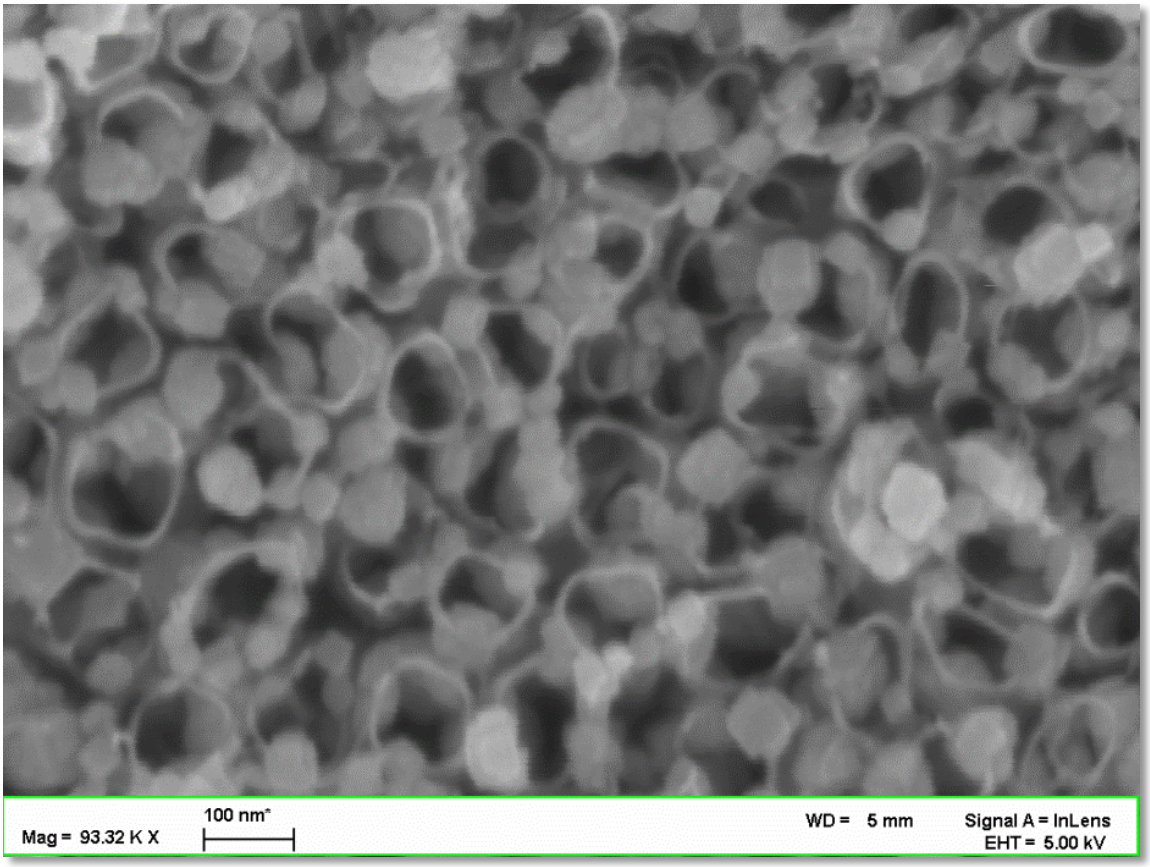

Figure 6.1: Top view of TiO_2 nanotubes filled with copper particles

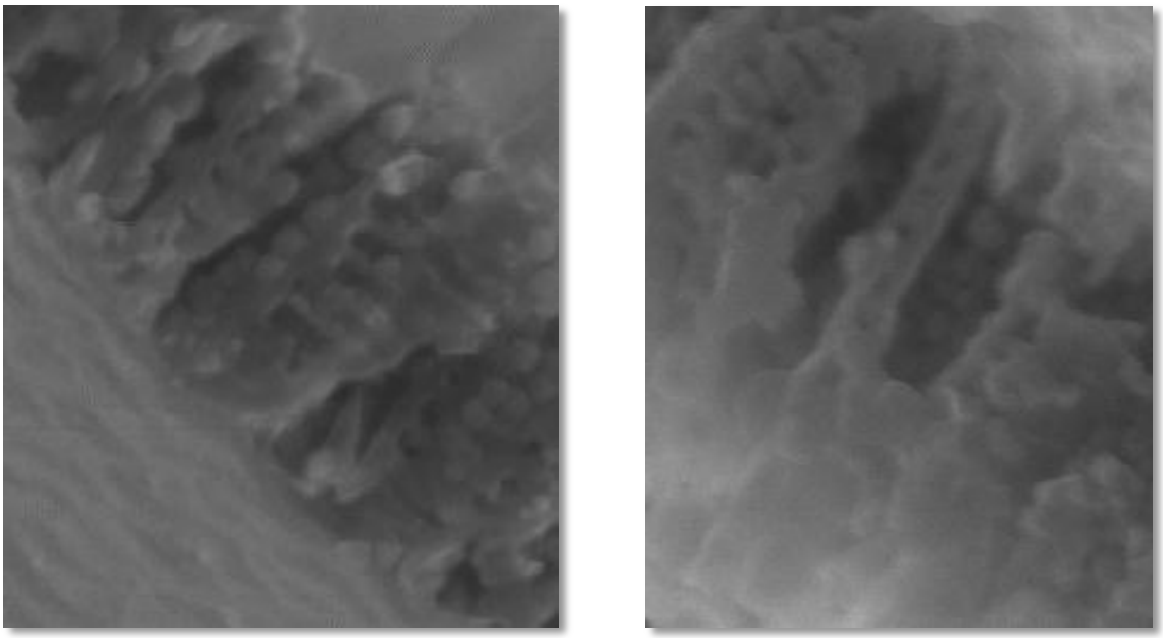

Figure 6.2: Side view (2 images) of TiO_2 nanotubes filled with copper particles

TiO_2 Super Honeycomb was successfully fabricated. Many tests were performed to understand the electrochemical characteristics of the new morphology. Capacitance values were obtained through these tests as high as 19.6 mF/cm^2.

A Ti-Mn alloy oxide layer was successfully made; though it did not have the Super Honeycomb structure, it was still nanotubular in nature. Electrochemical characterization tests were also performed on this substrate. The power density and capacitance were found to be superior to those found in literature with values for power density as high as 10.2 mW/cm^2 and values for capacitance as high as 17.8 mF/cm^2 at a 20mA/cm^2 charge/discharge rate [48].

There is much future work that needs to be done to understand these three systems. The Super Honeycomb structure needs to be tested more thoroughly for capacitance, especially through charge/discharge tests. The applications of this new TiO_2 morphology need to be explored and the mechanisms for creating and fine-tune the shape of the honeycomb need to be researched.

The Ti-Mn alloy oxide layer produced some good results as well as some results that did not seem to fit. More research is needed to understand why annealing this sample series resulted in lower capacitance. More research is also needed on how to improve the capacitance while minimizing the IR drop on the charge discharge test for capacitance.

More work is also needed to fine-tune the deposition of copper into TiO_2. Specifically, more research is needed on the interfacial region between the TiO_2 and the electrolyte, the goal being to turn the Volmer-Weber cluster islands that were deposited in the TiO_2 into continuous nanowires.

CHAPTER 7: ELECTROCHEMICAL GROWTH OF COPPER NANOWIRES INSIDE OF SEMICONDUCTING TIO_2 NANOTUBES

7.1 Abstract

Growth of metal/oxide nanowires inside of semiconducting nanotubes has several applications for energy storage and energy conversion. In this study, the bottom-up growth of copper nanowires through electrodeposition techniques was studied as a method to fill TiO_2 nanotube arrays. Specifically, emphasis was placed on the study of copper containing electrolyte solution kinetics through inhibitor and accelerator additives commonly used in the Damascene process. It was observed that the electrical conductivity and wetting characteristics of the TiO_2 nanotubes played significant roles in the bottom-up growth of copper nanowire deposition. The electrolytes commonly used in the Damascene process were found not to be useful for direct copper deposition inside of the TiO_2 nanotubes. Higher pH solution of $CuSO_4$ with tartaric acid as a complexing agent and pulsed deposition conditions showed promising results for copper deposition within the TiO_2 nanotubes.

7.2 Introduction

7.2.1 Background

The growth of metal/oxide nanowires in nanotubes to create a core/shell structure has been widely studied. One of the most studied structures is anodic aluminum oxide (AAO) as the shell with many different cores [49]–[53]. Electrochemical growth of nanowires using AAO as a template is straight forward because AAO is an insulator and the applied electric field is only available through the back contact of a thin sputtered layer of copper or gold which aids in the bottom-up growth of nanowires by filling the AAO nanoporous structure. However, in the case of

TiO_2 nanotubes, the bottom-up electrodeposition is hindered by the semiconducting nature of the material. Because it has a higher electrical conductivity than AAO, nucleation of copper deposits do not preferentially occur at the bottom of the nanotubes to aid in the bottom-up growth process.

The bottom-up process is hindered when the sidewalls become more conductive and the tube bottoms become less conductive, as is the case in the creation of a TiO_2 nanotube array template. It is also difficult to create a double open ended nanotube structure with titanium because of its superior corrosion resistance and since TiO_2 is an n-type semiconductor rather than an insulator, it is problematic to start the copper deposition at the bottom of the nanotubes in preference over the sidewalls of the nanotubes.

In this investigation, copper was chosen as a core nanowire material for two reasons. The first reason is that the electrochemistry of copper deposition inside narrow trenches is well understood, specifically with reference to the Damascene process. Secondly, copper nanowires in the elemental or oxidized forms as the core of a semiconducting shell can be used in several applications such as: solar cells [54]–[56], water splitting to harvest hydrogen which is possibly the fuel of the future, energy storage and sensors [57], [58].

In order to achieve bottom-up growth of copper nanowires through electrodeposition in the TiO_2 nanotubes, the conductivity of the nanotube walls was modified by both annealing the samples in oxygen and by a reduction process. The TiO_2 nanotubes in the as-anodized condition have a large concentration of oxygen vacancies [59]. When annealed in an oxygen atmosphere, the defect concentration decreases because of the annihilation of oxygen vacancies. Therefore the electrical resistivity increases. Following the oxygen annealing process with a reducing cathodic potential made the bottom of the nanotubes more conductive because of the presence of Ti^{3+} [60]. This produces a nanotube with a conductivity gradient having a top and walls with higher resistivity and a bottom with lower resistivity.

In order to improve the wettability of the electrolyte so that the nanotubes would be completely filled with the electrolyte, the chemistry of the electrolyte was modified with different types of additives. A number of experiments were undertaken to understand the kinetics of inhibitor and accelerator additives which are commonly used by the electronic industry in the Damascene process for low aspect ratio trench filling [61]–[63]. The temperature of electrodeposition was experimented with from near the solution freezing point to ~70 ˚C. It is noted that the surface energy of TiO_2 can be increased by decreasing the temperature. High surface energy of TiO_2 will result in better wettability. The solution pH was experimented with from pH 0.5 to 12.7. The effects of the addition of two complexing agents, citric acid and tartaric acid, were studied. Agitating the solution through ultrasonication was experimented with during electrodeposition. The copper concentration was changed from 0.03 *M* to 0.9 *M*.

7.3 Experimental

7.3.1 Anodization of Titanium Foil

The first phase in starting the experimental process was to grow titania nanotubes. This was done through anodization of titanium foil. Figure 7.1 shows a picture of the experimental setup. The anode and the cathode were consistently titanium for this process. Two types of electrolyte solutions were used. The first was an organic electrolyte with a base of ethylene glycol. This electrolyte also contained 3-4 vol% 18 MΩ-cm water and 0.14 *M* to 0.18 *M* NH_4F. The second electrolyte solution was an aqueous electrolyte with a base of 18 MΩ-cm water. This electrolyte solution contained 0.5 *M* phosphoric acid and 0.14 *M* NaF. The anodization process for the organic electrolyte typically lasted anywhere from 3-4 hours at a potential of 60 V. The aqueous electrolyte was much more conductive and required both less time and a smaller potential. Typical experiments lasted 40 minutes at a potential of 20 V.

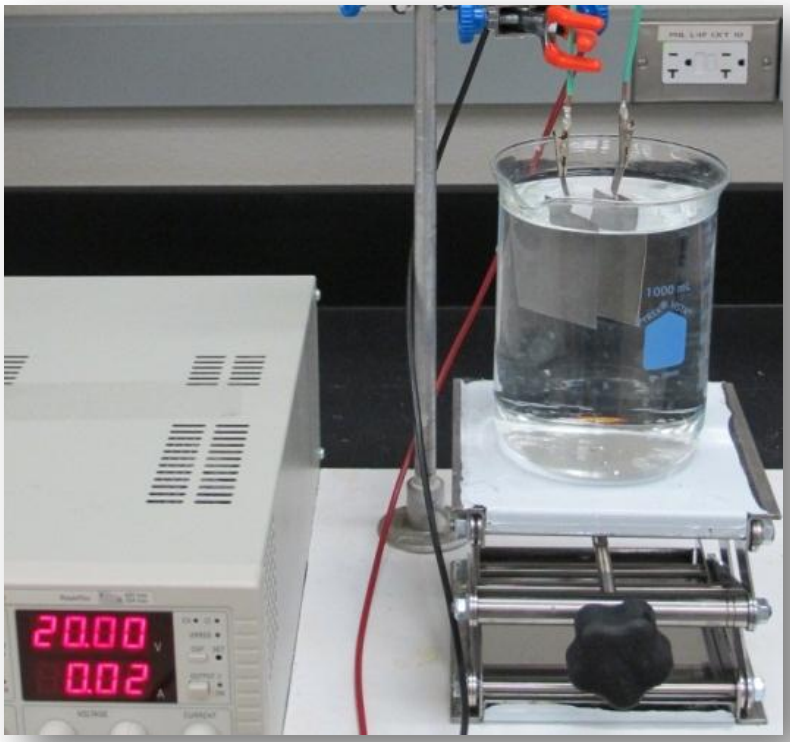

Figure 7.1: Typical anodization setup for making TiO_2 nanotubes

The characteristics of each type of solution have advantages and disadvantages. The aqueous electrolyte was quick and produced self-ordering nanotubes with a low doped carbon content, but also with inherent point defects in the TiO_2 lattice [64]. The organic electrolyte, on the other hand, had a higher electrical resistance, required a higher voltage, and resulted in nanotubes with a higher doped carbon content and lower resistivity [65]. An experiment was devised to combine these two processes. Titanium foil was anodized in the organic solution to create well-defined nanotubes. These nanotubes were then removed using both ultrasonication and electroplater's masking tape. Once the nanotubular oxide layer was removed, the nano-indented titanium foil was re-anodized in the aqueous solution. This was done assuming that the well-defined pattern etched in the titanium would be followed but with the low carbon doped nanotubes.

7.3.2 Electrodeposition of Copper

A variety of electrodeposition techniques were employed during the deposition of copper into TiO_2 nanotubes such as: galvanostatic, potentiostatic, pulsed electrodeposition and cyclic polarization. A Gamry Interface 1000 with Gamry Framework software was used for all electrodeposition techniques. 2-step and 3-step pulsing electrodeposition was used to pulse either current or potential.

The experimental setup can be seen in Figure 7.2. A spiral platinum counter electrode, as well as a Ag/AgCl reference electrode were always used. The working electrode was a 1*1.5 cm^2 piece of anodized titanium foil containing nanotubes approximately 800 nm in length and 80 nm in diameter. The electrolyte used in electrodeposition always contained $CuSO_4$ and 18 MΩ-cm water and depending on the solution may have also contained citric acid, tartaric acid, sulfuric acid, methanol, or small quantities of inhibitors and/or accelerators. The base solution had a composition of 0.16 *M* $CuSO_4$ + 1.8 *M* H_2SO_4. Additives were dissolved in this 'base' solution as individual components or as combinations of multiple additives to evaluate their effects on the copper nanowire growth.

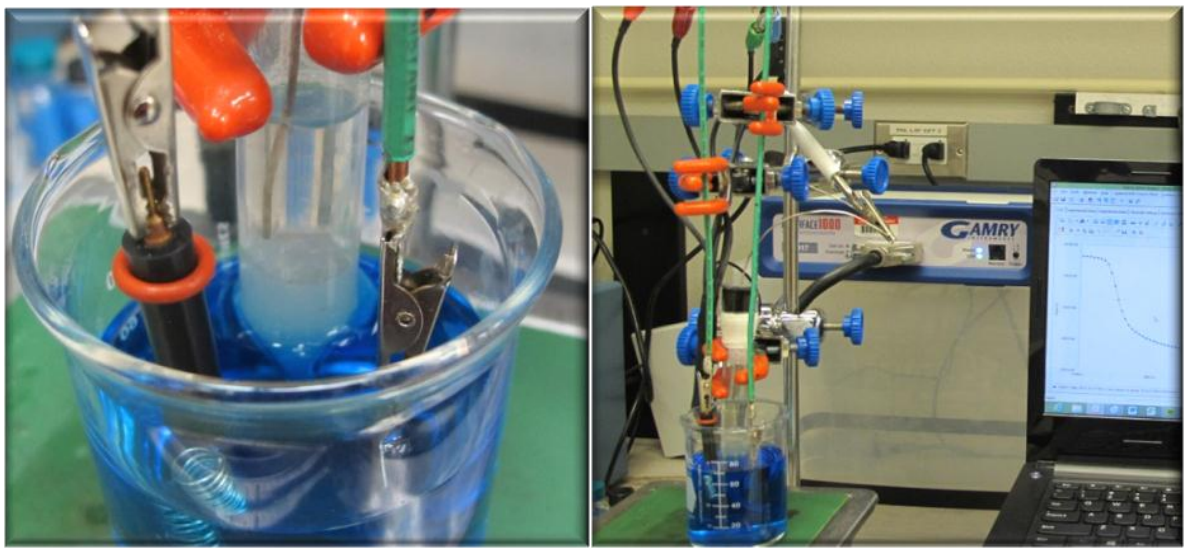

Figure 7.2: Typical setup using platinum counter electrode and Ag/AgCl reference electrode

There were a total of 51 solutions used in the experiments. Most of these solutions were used to understand the kinetics of the various additives commonly used in the electronic industry for low aspect ratio trench filling. These additives included inhibitors, which are large molecules used to block copper deposition, such as: polyethylene glycol (PEG)(88 μM), polyethyleneimine (PEI)(0.1 μM) and ethylene glycol (EG)(88 μM). Accelerator additives were also used, including: bis(sulfopropyl)disulfide ([SPS], $Na_2[S(CH_2)_3SO_3]_2$)(50 μM), sodium chloride (NaCl)(2 mM) and sodium fluoride (NaF)(2 mM). The first solution, referred to as the base solution, contained 0.16 M $CuSO_4$, 1.8 M H_2SO_4 and 18 MΩ-cm water. Solutions 2-7 contained an individual inhibitor or accelerator additive. Solutions 8-13 were used to investigate the effects of mixing two of these additives together, while solutions 28-34 were used to investigate mixing three or more additives together. Solutions 14-27 were used to understand the effects of additive concentration changes. In order to accomplish this, the original concentration of each additive was halved and then doubled. Solution 35-38 investigated changes in the copper concentration. In solutions 39 and 40, methanol was added to reduce the surface tension in the solution. Solutions 41-50 were used to understand changes in pH (0.5 to 12.7) and the effects of the complexing agents, citric acid and tartaric acid with concentrations ranging from 0.015 M to 0.06 M.

7.4 Results and Discussion

7.4.1 Anodization of Titanium Foil

Figure 7.3 shows two SEM micrographs comparing the nanotubes from the aqueous and the organic electrolytes used for anodization of titanium foil.

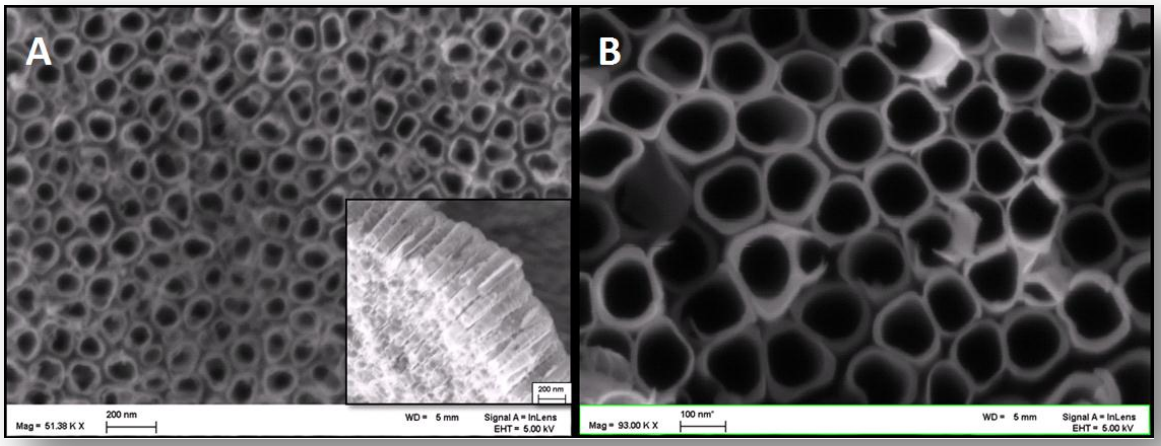

Figure 7.3: (A) The morphology of the TiO_2 nanotubes prepared in the aqueous electrolyte, the inset shows the side view of the nanotubes. (B) The top view of the nanotubes synthesized in the organic electrolyte

As can be seen in Figure 7.3(A), the top view clearly shows that the aqueous electrolyte created nanotubes that are less well defined than the nanotubes created in the organic electrolyte shown in Figure 7.3(B). The nanotubes had an aspect ratio of 10-12 with inside diameters of 60-70 nm and a wall thickness of about 5-10 nm. The tube length was approximately 700 to a 1000 nm. Figure 7.4 shows the top and side view of the new morphology of the nanoporous structure after a double anodization procedure. The first anodization was carried out in an ethylene glycol solution at 60 V. The oxide layer was then removed prior to carrying out a second anodization in the aqueous acid-fluoride solution at 20 V. The new morphology is deemed: Super Honeycomb TiO_2. Figure 7.4 is a good example of what the entire surface of the oxide layer looked like. The larger honeycomb wells averaged between 110-130 nm with wall thicknesses between 15-20 nm. The oxide layer thickness was between 300-700 nm at the tallest point while the bottoms of the honeycomb wells were between 150-500 nm thick. The smaller nanopores inside of the honeycomb wells ranged from 15-40 nm in diameter.

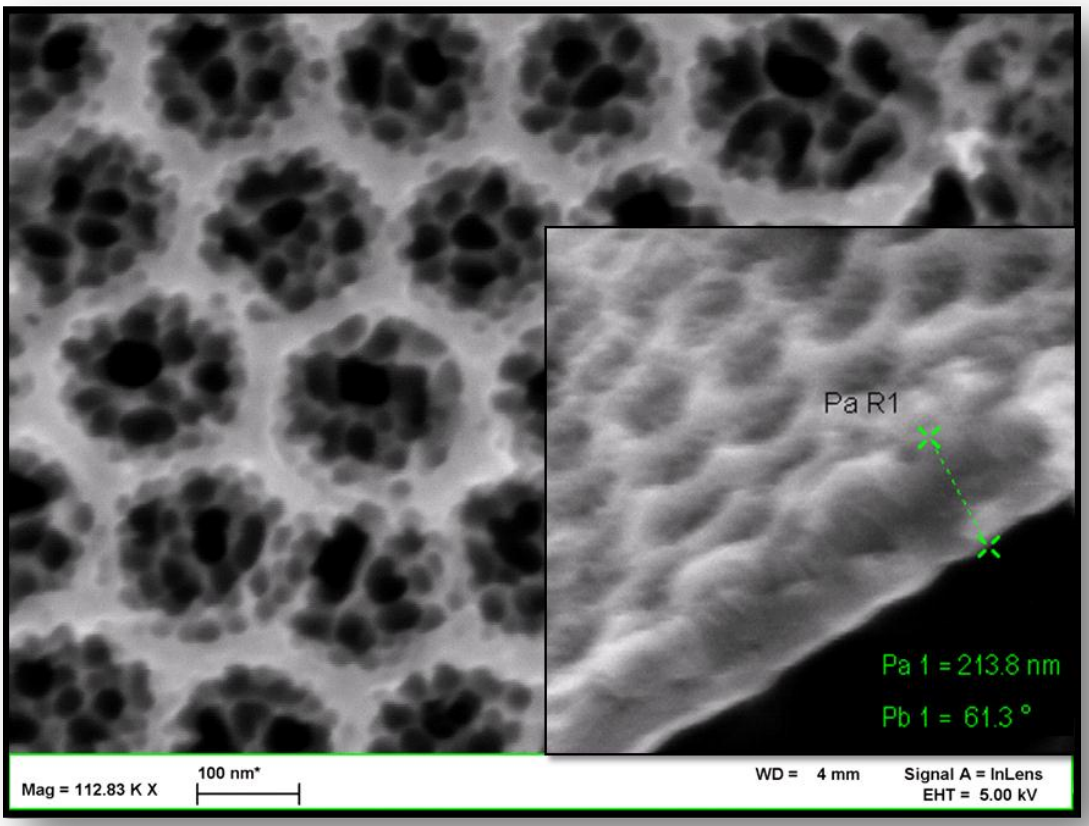

Figure 7.4: Micrograph of new Super Honeycomb TiO_2 morphology.

7.4.2 Cyclic Voltammograms of Inhibitor and Accelerator Additives on a Pt. Substrate

Figure 7.5 shows the cyclic voltammograms (CVs) carried out in the electrolyte with different additives using a platinum substrate at a scan rate of 10 mV/s. The focus is on the higher cathodic potentials where the copper deposition takes place.

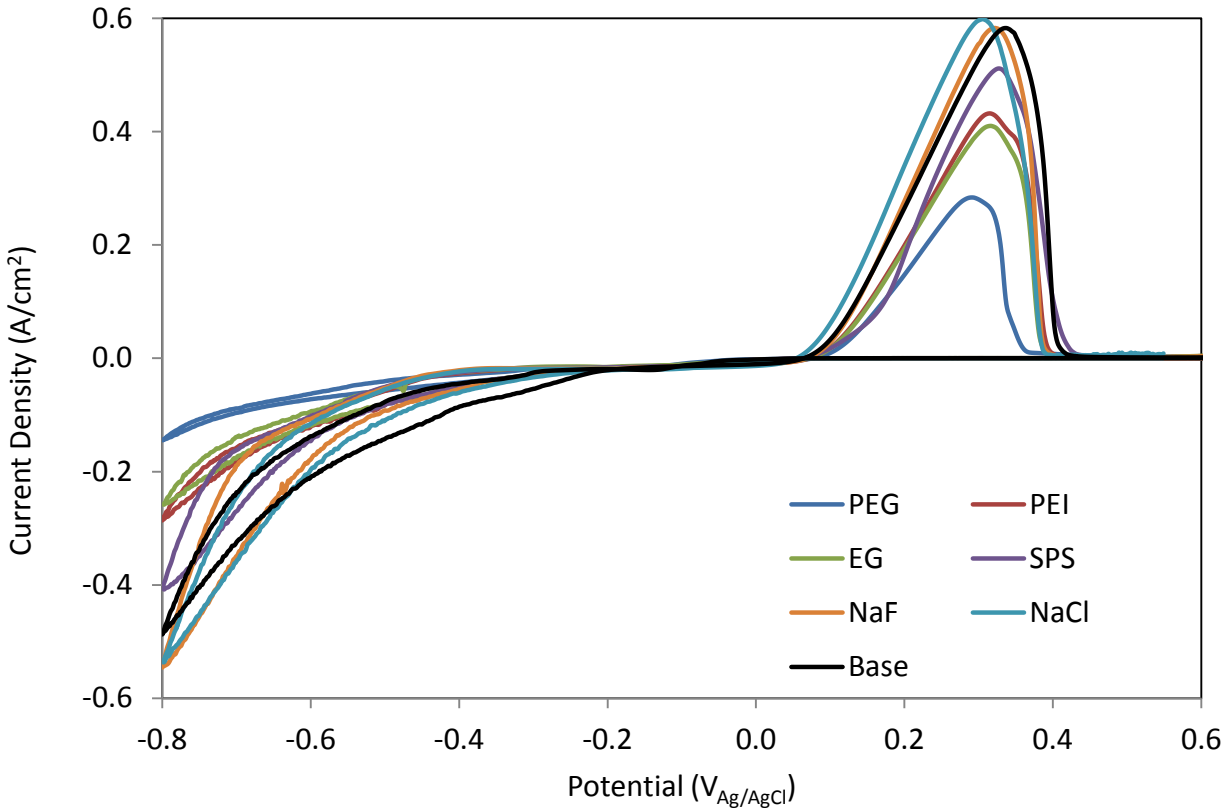

Figure 7.5: CVs of inhibitor and accelerator additives on Pt. electrode. The base solution contained 0.16 *M* $CuSO_4$ + 1.8 *M* H_2SO_4

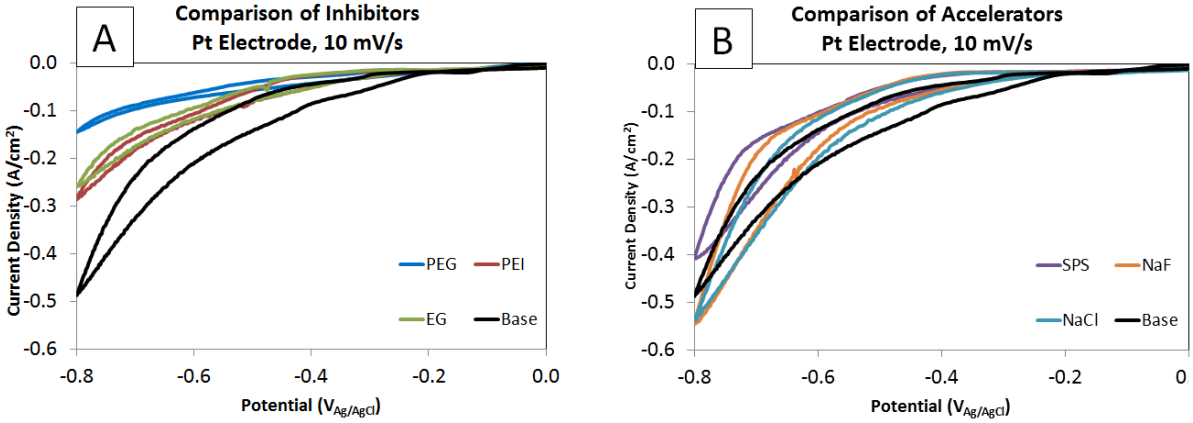

Figure 7.6: (A) Shows the CVs for the inhibitors. (B) Shows the CVs for the accelerators

During the cathodic potential sweep from open circuit potential to -0.8 $V_{Ag/AgCl}$, one of the reactions occurring on the platinum surface is [66]:

$$Cu^{2+}(H_2O)_x(SO_4^{2-})_y + e^- \rightarrow Cu^{+}(H_2O)_z(SO_4^{2-})_n + (x\text{-}z)H_2O + (y\text{-}n)SO_4^{2-} \quad [1]$$

The cathodic current wave starting at around -60 $mV_{Ag/AgCl}$ is attributed to the reduction of cupric ions to cuprous ions. The slopes of the cathodic current profile change at -0.285 $V_{Ag/AgCl}$, -0.45 $V_{Ag/AgCl}$ and -0.66 $V_{Ag/AgCl}$. The constant current density observed from -60 $mV_{Ag/AgCl}$ to -285 $mV_{Ag/AgCl}$ could be attributed to the diffusion limited reduction of cupric to cuprous ions. The activation controlled current profile at the potential region -285 $mV_{Ag/AgCl}$ to -450 $mV_{Ag/AgCl}$ could be attributed to the reduction of cuprous ions to copper given by the reaction:

$$Cu^{+}(H_2O)_2(SO_4^{2-})_n + e^- \rightarrow Cu^0 + 2\,H_2O + n\,(SO_4^{2-}) \quad [2]$$

At cathodic potentials up to -450 $mV_{Ag/AgCl}$, the cupric ions could be directly reduced to Cu^0 following the reaction:

$$Cu^{2+} + 2e^- \rightleftarrows Cu^0 \qquad E^\circ = 0.337 + 0.0285 \log [Cu^{2+}]\ V_{SHE} \quad [3]$$

When chloride is added, the redox reaction could be given as [28]:

$$Cu^{2+} + Cl^-_{ads} + e^- \rightleftarrows CuCl_{ads} \qquad E^\circ = 0.383\ V_{Ag/AgCl} \quad [6]$$

$$CuCl_{ads} + e^- \rightleftarrows Cu^0 + Cl^- \qquad E^\circ = -0.047\ V_{Ag/AgCl} \quad [7]$$

The suppressor/accelerator competitive adsorption process is given by Vereecken et al. as follows [16]. The reaction for the suppressor adsorption is:

$$n\,CuCl_{ads} + HO[(CH_2)_xO]_yH \rightleftarrows \{HO[(CH_2)_xOCuCl]_n[(CH_2)_xO]_{y-n}H\}_{ads} \quad [10]$$

The equation that describes the disruption of the suppressor adsorption by the accelerator is:

$$\{HO[(CH_2)_xOCuCl]_n[(CH_2)_xO]_{y-n}H\}_{ads} + n\,MPS \rightleftarrows HO[(CH_2)_xO]_yH + n\,Cl^- + n\,Cu^{+}(Thiolate)_{ad} \quad [12]$$

Figure 7.6(A) shows an enlarged CV of this potential region, which shows the base solution compared only with the inhibitor solutions. The addition of PEG (88 μM) shifted the reduction potential to a more negative potential by 38 mV. The cathodic current density with the addition of PEG was similar to that of the base solution until a potential of -280 $mV_{Ag/AgCl}$, which is the potential at which hydrogen evolution initiates. At potentials more negative than -80 $mV_{Ag/AgCl}$, the current

density was much lower in the electrolyte containing PEG than the electrolyte without PEG. When the platinum was polarized at -0.8 $V_{Ag/AgCl}$, the cathodic current density was -480 mA/cm^2 in the base solution, whereas under similar conditions, the solution with the PEG additive had a current density of -134 mA/cm^2. The reduction in the current could be attributed to the adsorption of PEG to the platinum surface, which may be blocking the reduction of both copper ions and hydrogen ions. The PEI and EG additives also showed an inhibiting effect for Cu^{2+} reduction on the platinum substrate. However, the inhibiting effect of PEG was stronger than that of PEI and EG.

Figure 7.6(B) shows the same section of the curve, comparing the accelerator additives to the base instead of the inhibitors. The addition of 50 *μM* of SPS showed an increase in the cathodic polarization. Since there was no chloride addition, the presence of SO_4^{2-} as the anion did not help reveal the accelerating behavior of SPS for copper electrodeposition. Once the SPS was used in conjunction with NaCl (Solution 11, not shown), the current density was moderately increased as expected. The addition of 2 *mM* of NaCl to the base solution moderately increase the current density when the potentials were more negative than -0.7 V. Similar behavior was observed with the addition of 2 *mM* of NaF.

Figure 7.7 shows the cyclic voltammetry results of multiple additives in the electrolytes using platinum as the substrate. The LHS-y-axis current density values belong to solutions 8, 14 and 28. The RHS-y-axis belongs to electrolytes 50 and 51 with a pH of 5.25 and tartaric acid as a complexing agent.

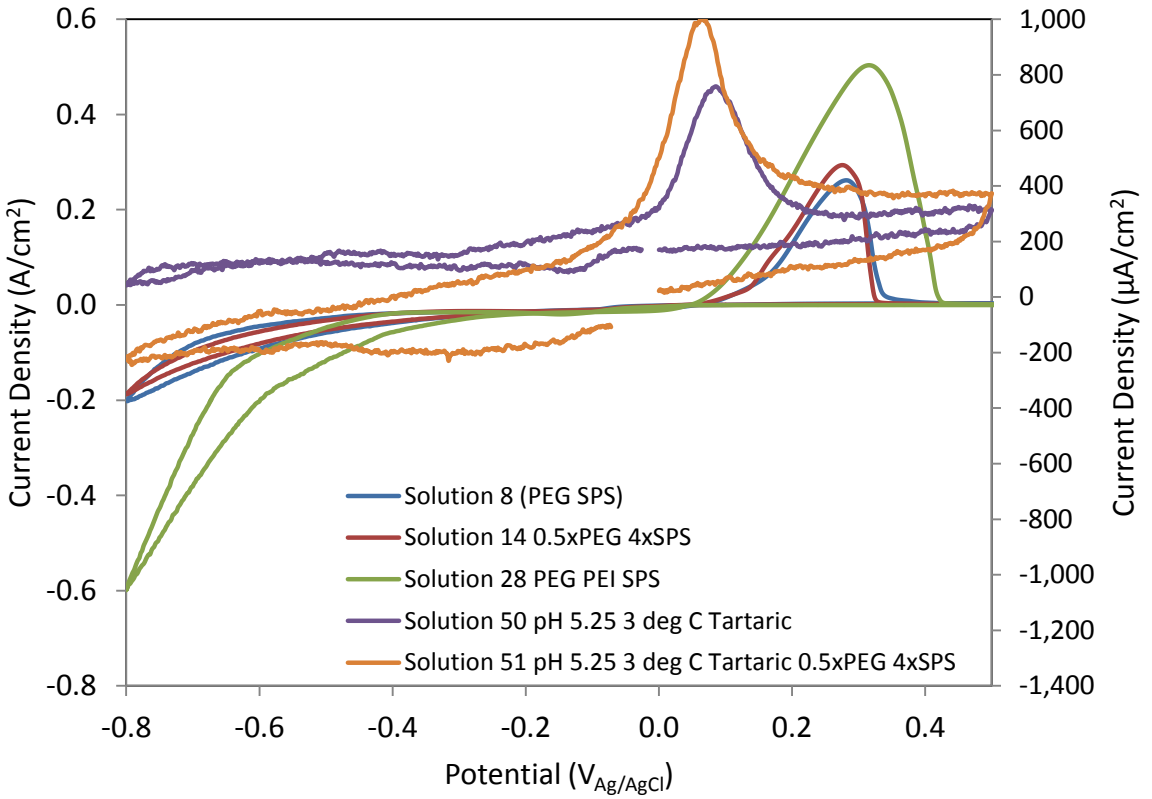

Figure 7.7: CVs of 5 best copper-depositing solutions at 10 mV/s, Pt. electrode. Solution 50 and 51 are on the right hand axis. Solution 8, 14 and 28 are on the left hand axis

The composition of solution 8 was: the base solution + 88 *µM* PEG *+ 50 µM* SPS. The composition of solution 14 was: the base solution + 44 *µM* PEG + 200 *µM* SPS. The combination of additives in solution 28, which included 0.1 *µM* PEI, 22 *µM* EG, and 12.5 *µM* SPS, showed the highest current density at 0.8 $V_{Ag/AgCl}$ among all the electrolytes considered in this figure. Furthermore, this electrolyte showed the lowest cathodic polarization (about 150 mV more positive than solutions 8 and 14). However, the take-off potentials for the anodic peak current were almost the same for all the acid electrolytes (solutions 8, 14, and 28). The highest anodic peak current density and largest charge accumulations for the oxidation reaction were both observed in solution 28. The cathodic and anodic current densities were essentially equal for solutions 8 and 14.

When the electrolyte composition was changed by adding tartaric acid and by adding NaOH in order to increase the pH to make a more neutral solution, the reduction and oxidation reaction

rates of Cu^{2+}/Cu^{0} systems were drastically different from that of the acidic solutions. Overall, the current density decreased by almost three orders of magnitude in the more basic solution as compared to the acid solutions. Solutions 50 and 51 did not show clear cathodic reduction waves. In solution 51, cathodic current density was observed at potentials more cathodic than -0.7 $V_{Ag/AgCl}$. Ballesteros et al. attributed the cathodic current density occurring at this potential to the reactions listed here [39]:

$$Cu^{2+} + 2\,OH^{-} + 2\,T^{2-} \rightleftarrows Cu^{2+}(T)_2(OH^{-})_2^{6-} \qquad \text{where } T = (C_6H_4O_6) \qquad [27]$$

$$CuT_2(OH)_2^{4-} + 2\,e^{-} \rightleftarrows Cu^{0} + 2\,T^{2-} + 2\,OH^{-} \qquad [28]$$

During the reverse scan, the anodic current was observed at potentials more positive than -0.4 $V_{Ag/AgCl}$. It should be noted that tartrate ion is considered an oxygen donor ligand, which does not stabilize the Cu^{+}. Therefore, the concentration of Cu^{+} will be smaller in the presence of tartrate [67].

Among all the inhibitor and accelerator additives, combinations of SPS, PEG and PEI showed the most promise during electrodeposition of copper within TiO_2 nanotubes. The addition of tartaric acid in a neutral pH solution also proved to be an excellent additive. It should be noted that solution 51 is merely solution 50 with solution 14's additives.

7.4.3 Cyclic Voltammograms of Inhibitor and Accelerator Additives on a TiO_2 Substrate

Figure 7.8 shows the results of CVs carried out on TiO_2 substrates in solutions 1-7. Solution 1 has been referred to as the "base" solution with 0.16 *M* $CuSO_4$ + 1.8 *M* H_2SO_4, and solutions 2-7 contain the base plus a single additive of PEG, SPS, NaCl, NaF, PEI or EG.

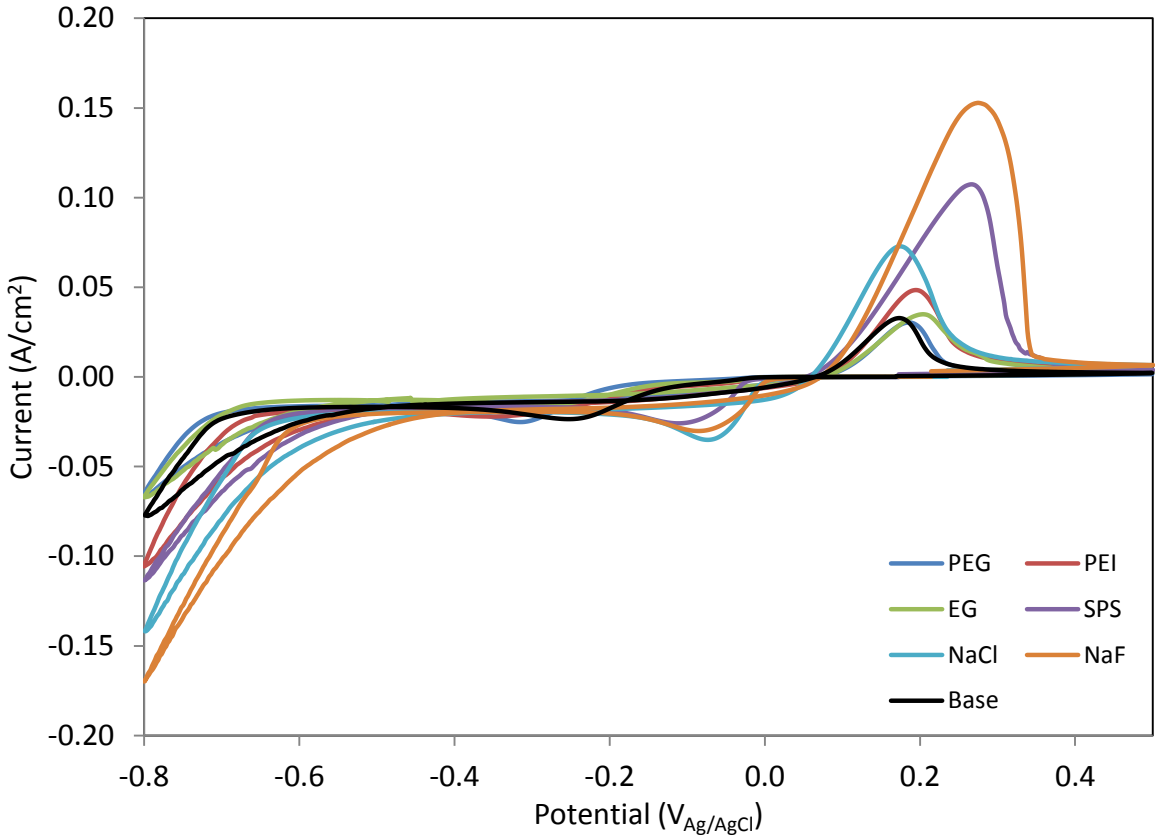

Figure 7.8: CVs using TiO_2 substrate using a base solution of 0.16 *M* $CuSO_4$ + 1.8 *M* H_2SO_4 with different additives at 10 mV/s.

The base solution showed an initiation of cathodic current density at -25 $mV_{Ag/AgCl}$ and a first cathodic peak current of 35 mA/cm^2 at -240 $mV_{Ag/AgCl.}$ At potentials more negative than -240 $mV_{Ag/AgCl}$, the current density decreased to about -25 mA/cm^2, showing a concentration polarization behavior until -685 $mV_{Ag/AgCl}$. An activation polarization behavior was observed at cathodic potentials up to -686 $mV_{Ag/AgCl}$, leading to a final current density of -116 mA/cm^2. Compared to the platinum substrate, the deposition of copper onto TiO_2 was observed to be different. The first difference was that the onset of a cathodic current wave occurred at a higher potential by 35 mV on TiO_2 (-25 $mV_{Ag/AgCl}$ vs. -60 $mV_{Ag/AgCl}$ for the platinum). Secondly, there is a district cathodic current peak at -245 $mV_{Ag/AgCl}$ on the TiO_2. The third difference was the occurrence of a strong barrier for activation polarization up to -685 $mV_{Ag/AgCl}$. Lastly, there was an absence of a shoulder peak on TiO_2

during oxidation, which was typically observed at potentials more positive than 300 $mV_{Ag/AgCl}$ on the platinum electrode.

Considering the TiO_2 electrode, the anodic wave plateaued at about 235 $mV_{Ag/AgCl}$. The redox potential of the Cu^{2+}/Cu^{+} system under standard conditions is -0.47 $V_{Ag/AgCl}$. Taking the concentration of Cu^{2+} as 0.16 *M*, the activity coefficient as 0.15 and the activity of Cu^{+} as $3x10^{-4}$ *M*, the redox potential, E˚, could be estimated as:

$$\mathbf{E^{\circ} = 0.047 + 0.059\log[Cu^{2+}]/[Cu^{+}] = 0.047 + 0.059\log[0.15*0.16]/[3*10^{-4}] = 0.064\ V_{Ag/AgCl}} \quad \mathbf{[29]}$$

The concentration of Cu^{+} could be estimated from the equilibrium constant of the following reaction [28]:

$$\mathbf{Cu^{2+} + Cu^{0} \rightleftarrows 2\ Cu^{+} \qquad K_{Eq*Cu} = [Cu^{+}]^2/[Cu^{2+}] = 6.0*10^{-7}\ M} \quad \mathbf{[30]}$$

However, it is noted that the reaction combination proportion reaction listed in equation 30 is not possible without a copper substrate or copper nuclei. The onset of the cathodic current on the TiO_2 substrate, therefore, could be attributed to the possible underpotential deposition of copper. Rosario et al. observed underpotential deposition of copper onto TiO_2 electrodes [42].

7.4.4 Electrodeposition of Copper Inside of TiO_2 Nanotubes Using Low pH $CuSO_4$ Solutions

The TiO_2 samples were annealed in an oxygen atmosphere at 450 ˚C for two hours after anodization. This annealing process resulted in an increase in the resistivity of the nanotubes because of the decrease in concentration of the oxygen as compared to the as-anodized condition. The oxygen annealed nanotubular templates were given a localized reduction process in order to selectively increase the electrical conductivity at the bottom of the nanotubes. The reduction process was carried out in a 1 *M* ammonium sulfate solution by applying a cathodic pulse of -1.5 V for three seconds. The goal was to reduce the tube bottoms from Ti^{4+} to Ti^{3+} and then stop the

process before it could move to reduce the tube walls as well. It was thought that the preferential reduction occurring at the bottom of the nanotubes would aid copper nucleation and adsorption of accelerator species such as Cl^- and SPS and that this would, in turn, promote a bottom-up growth of copper nanowires within the TiO_2 nanotubes.

Effects of Inhibitor and Accelerator Additives. The additives commonly used in the electronic industry did not work well to cause a bottom-up deposition of copper inside of the TiO_2 nanotubes. Figure 7.9 shows the copper deposit morphology using 250 *μM* NaCl, 12.5 *μM* SPS and 44 *μM* PEG additives (solution 33), by potentiostatic pulsing from 0 V for 1 second to -0.5 V for 0.1 seconds for 100 cycles. A possible reason for not achieving the bottom-up growth is as follows: the additives used in this investigation were originally designed for depositing copper onto a copper seed layer. The presence of a copper seed layer results in the formation of Cu^+ ions with proportion reactions such as $Cu^{2+} + Cu^0 \rightleftarrows 2\ Cu^+$. The cuprous ions easily complexed with the additives, revealing conformal or super filling effects [16], [18], [20], [33], [61], [63]. In the absence of such a copper seed layer, the additives were not effective. It was anticipated that copper nucleation would initially occur at the bottom of the nanotubes, which would be followed by adsorption/segregation of the Cl^- and SPS on the top surface of the copper nuclei to promote a bottom-up growth. However, copper deposition was observed only on the top surface of the template as shown in Figure 7.9. This behavior was attributed to inadequate wetting of the electrolyte. Therefore, several trials were carried out to promote complete filling of the nanotubes by the electrolytes. The following section describes the effect of ultrasonication and the addition of methanol to improve the wetting. Furthermore, the concentration of the $CuSO_4$ was also varied to minimize deposition of copper on the top openings of the nanotubes.

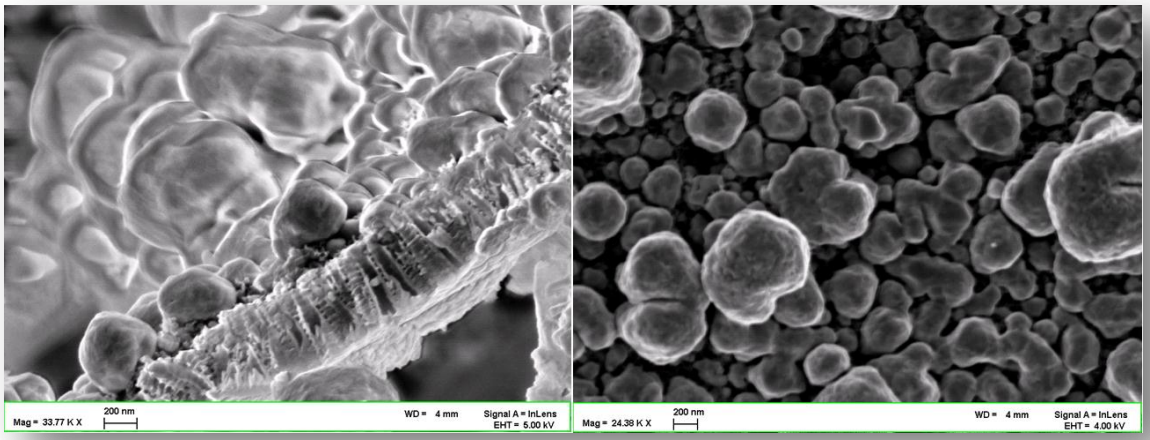

Figure 7.9: (Left) Side view and top view (Right) of copper deposition into TiO_2 nanotubes in an electrolyte containing 250 μM NaCl, 12.5 μM SPS and 44 μM PEG (solution 33) by potentiostatic pulsing from 0 V for 1 second to -0.5 V for 0.1 seconds for 100 cycles

Deposition under Ultrasonication. Ultrasonicating the solution during the deposition process resulted in smaller copper crystals being deposited on the surface of the TiO_2 nanotubes. There was some promise to this method, and it should be researched further, but under the experimental conditions studied, ultrasonication was unable to aid in solving the surface blockage and wettability problems. Examples of surface blockage problems (Left) and wettability problems (Right) are shown in Figure 7.10. The surface blockage micrograph shows a copper layer lifted off of the TiO_2 substrate. The fingers of copper that were attempting a top-down deposition can be seen. The wettability micrograph shows that there are still open nanotubes, but the interface of the TiO_2 surface and the electrolyte would not allow the electrolyte to wet the inside of the nanotubes.

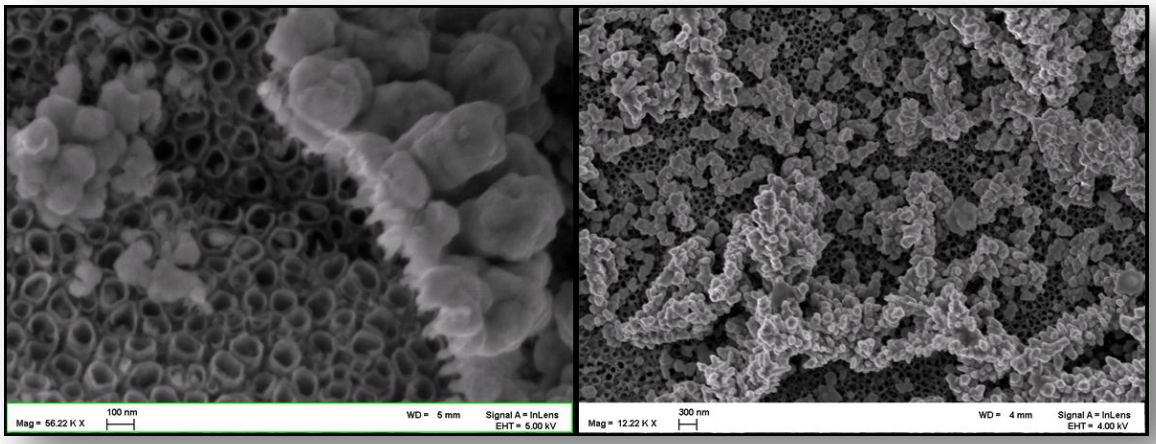

Figure 7.10: (Left) Typical surface blockage problem on TiO_2. Example from solution 5, containing 50 M SPS under ultrasonication by cyclic voltemetry from OCP to -0.8 V to 0.5 V. (Right) Typical wettability problem on TiO_2. Example from solution 13, containing 200 μM NaCl, 0.1 μM PEI, 88 μM PEG and 50 μM SPS potentiostatic pulsing from -1 V for 2 seconds to 0.5 V for 1 second for 100 cycles

Methanol Addition. It was thought that the addition of methanol would lower the surface tension of the electrolyte enough that it would wet the inside of the nanotubes. In practice, however, this did not help to achieve a bottom-up deposition or seem to help in increasing the wettability. Another closely related process that was experimented with was soaking the TiO_2 samples in pure methanol. Once the methanol had sufficient time to wet the TiO_2, the sample was removed from the methanol and immediately placed in the copper electrolyte. It was believed that this process would pull the copper electrolyte solution into the nanotubes as the methanol, which theoretically was able to wet the inside of the nanotubes, evaporated. However, no encouraging results were observed after potentiostatic pulsing from -0.4 V for 0.08 seconds to +0.25 V for 0.16 seconds for 100 cycles in solution 31, containing 0.1 μM PEI and 12.5 μM SPS.

Copper Concentration. High concentrations of copper caused severe surface blockage of copper under all types of electrodeposition testing. Medium concentrations worked better, but still frequently exhibited surface blockage problems. Low concentrations around 0.03 M $CuSO_4$ worked best in depositing copper.

Changes in pH Level. All pH changes were made with the addition of NaOH. Changes in the pH made a noticeable difference in the copper deposition. Interestingly, both pH's >12 and pH's < 5 did not work well in the experiments. At pHs around 6, the copper deposition showed a marked improvement. This is likely because the isoelectric point of TiO_2 is at 5.8. It seemed that a variation too far from this point would result in either to many positive ions or too many negative ions in the solution for the TiO_2 surface/electrolyte interface to interact properly. Solution 50, which enabled the most effective copper deposition, had a pH of 5.25.

Complexing Agents. Citric acid did not work well as a complexing agent and would often precipitate out of solution. Tartaric acid, on the other hand, worked well and showed improvement in copper deposition.

7.4.5 Copper Deposition Using Tartaric Complex

Using solution 50 as the electrolyte, which contained 0.03 *M* $CuSO_4$ and 0.03 *M* tartaric acid, a filling of the nanotubes array was achieved. Though it was not a complete core filling of the nanotube array, it was a consistent filling with nanoparticles as can be seen in Figure 7.11. The solution was modified to a pH of 5.25 with addition of NaOH and was cooled to ~2 ˚C. The electrodeposition process was a 2-step galvanostatic pulsing for five seconds each from 0 to -0.5 $mA_{Ag/AgCl}$ for 1000 cycles. It is key to point out that the entire surface was evenly filled with little to no over-deposition. The side view, shown in Figure 7.11, reveals that the nanoparticles did in fact fill the nanotubes all the way to the bottom.

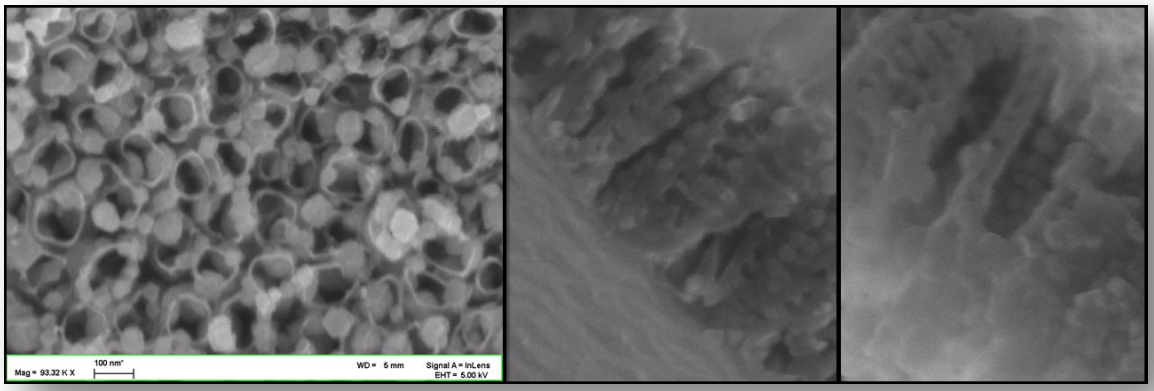

Figure 7.11: (Left) Top view of successfully filled TiO_2 nanotubes with copper by galvanostatic pulsing deposition from 0 mA to -0.5 mA for 5 seconds each for 1000 cycles. (Center and Right) side views of successfully filled TiO_2 nanotubes with copper. The solution contained 0.03 *M* $CuSO_4$ + 0.03 *M* Tartaric acid, pH: 5.25, T: 2 ˚C

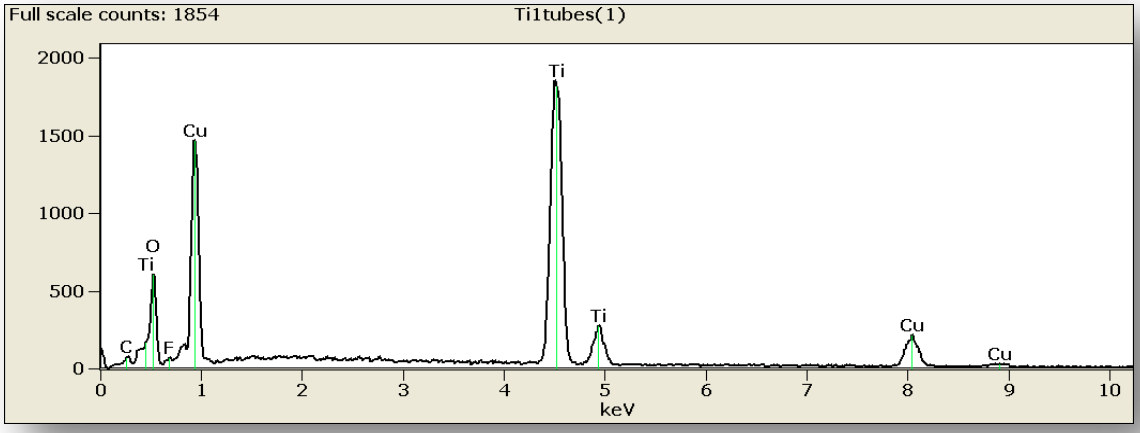

Figure 7.12: EDS of copper-filled TiO_2 substrate area

Figure 7.12 shows an EDS of an area of the substrate approximately 1.8 μm^2. Copper, titanium and oxygen are expected, fluorine and carbon are also expected but only in the nanotube substrate. This is due to the slight doping effect when anodizing the nanotubes. A comparison EDS of a single point on one of the nanoparticles, shown in Figure 7.13, reveals that the fluorine and carbon are, in fact, only found in the nanotubes. This gives some evidence that the nanoparticles are copper. Also, if the nanoparticles were copper oxide, they should have easily filled the

nanotubes due to copper oxide's ability to wet TiO_2. Therefore, due to the morphology and the EDS evidence, the nanoparticles are considered to be copper.

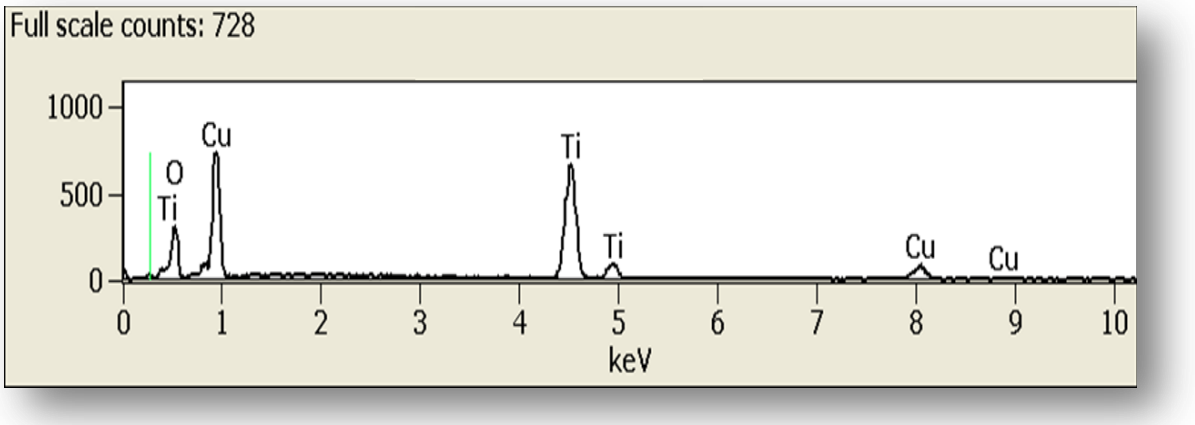

Figure 7.13: EDS of a single point on a copper particle

Copper metallization of through-silicon vias (TSV) using alkaline copper plating chemistry has been reported by Armini [35]. The deposition of copper nanoparticles inside the TiO_2 nanotubes could be attributed to the following factors: a) copper-tartrate complex, even in the octahedral coordination, has been found to adsorb on the TiO_2 surface significantly [68]; b) the formation of the complex with tartaric acid reduced the activity of the Cu^{2+} and shifted its reduction potential to more negative values, which hindered deposition of a blocking copper layer on the top surface; c) the pH of the electrolyte was closer to the isoelectric pH of the TiO_2 (5.8). Therefore, the adsorption/reduction of the Cu/tartrate complex ions on the TiO_2 nanotube walls was not affected by the adsorption and reduction of hydrogen ions; and d) low temperature deposition condition resulted in favorable surface energy for the TiO_2 and slower electrochemical kinetics that helped electrodeposition of copper nanoparticles within the nanotubes. The growth of copper into TiO_2 nanotubes could be considered cluster growth (Volmer-Weber growth) [69]. This could possibly be attributed to the interfacial surface energy of TiO_2/Cu being higher than the difference in the surface energies of TiO_2 (0.35 J/m^2) and copper (1.49 J/m^2) (($\gamma_{interface} > \gamma_{TiO_2} - \gamma_{Cu}$). The ridges in the

TiO_2 nanotube walls may also have acted as preferential nucleation sites for the copper. In the absence of clear experimental evidence, it is anticipated that TiO_2 (110) planes are the preferred planes for copper nucleation with (111) orientation [69].

7.5 Conclusions

In conclusion, it was observed that the electronic industry standard additives for trench filling did not work well to fill high aspect ratio TiO_2 nanotubes. Low temperature deposition showed a clear improvement, likely due to the increase in surface energy and therefore better wettability. The tartaric acid complexing agent helped to slow the copper deposition, thereby, avoiding surface blockage. A neutral pH, close to the isoelectric point of TiO_2 worked better than high or low pH's. While the method for completely filling the nanotubes with a solid core are still being fine-tuned, it is believed that with further research, a simple electrodeposition method can be developed to completely fill TiO_2 nanotubes with no seed layer.

CHAPTER 8: SUPER HONEYCOMB: A NEW HIGHLY ORDERED MORPHOLOGY OF TIO_2

8.1 Abstract

This chapter reports the discovery of a new highly ordered morphology of TiO_2 nanostructure and compares its capacitance when annealed in O_2 and N_2 at 450˚C for two hours to reported values of TiO_2 nanotubes in two electrolyte solutions. The new Super Honeycomb TiO_2 morphology resembles a large format honeycomb structure with 15-20 nanotubes with diameters ranging from 15-40 nm inside of each honeycomb structure. The large format honeycomb structures are 110-130 nm in diameter with inter-wall thicknesses of ~20 nm. Because the oxide layer is naturally thin (150-300 nm) and yet contains ordered porosity on two levels, it was believed that the viable surface area would lead to high capacitance values when compared to previously reported values of capacitance for typical TiO_2 nanotube oxide layers. The current study shows some better results for capacitance, the best result being 500% better than the highest reported capacitance value known by the authors per cm^2 of surface area. Nitrogen annealed samples consistently had higher capacitance than typical TiO_2 nanotubes. The morphology was created by using a previously anodized titanium foil in order to make use of the nanoindented surface.

8.2 Introduction

Since the unveiling of TiO_2 nanotubes in 1996 by Hoyer, et al.[70], much attention has been given to the fabrication of one-dimensional titania nanotubes. Although Hoyer did not discover the most interesting feature of TiO_2, the self-ordering nature by electrochemical oxidation, that was shortly afterwards discovered by Zwilling and colleagues in 1999 [71]. There is no indication, however, that they realized the importance of their discovery, and it was not until 2001 when

Gong, et al. [72] published their first work on anodic oxidation to create self-aligning TiO_2 nanotubes that the research world realized how important this structure could be. Since that time, an explosion of research has been done on nearly every aspect of titania, including applications for dye-sensitized solar cells [54]–[56], [73]–[77], rechargeable batteries [78], gas sensors [14], supercapacitance [79]–[82], photovoltaics [83], biomedical devices [84], as well as other applications [85]–[88].

There are various methods used for the creation of TiO_2 nanotubes, such as: template assisted, electrochemical, sol-gel methods, atomic layer deposition, hydro/solvothermal, and anodic oxidation of titanium foils. This last method might be the most important because it is cost effective and gives self-ordered TiO_2 nanotubes with tunable dimensionality. Another area of TiO_2 study that gained popularity was the various formations and morphologies. Many different self-ordering morphologies of TiO_2 have been reported such as, smooth wall nanotube [89], the onion ring nanotube or bamboo nanotube [90], [91], double walled nanotubes [92], Y- branched nanotubes [93] and nanolace [91]. Some more advanced structures with double walls have also been reported by Schmuki et al. [94] For excellent discussions on the electrochemical synthesis and application of TiO_2 nanotubes and structures please see both of these reviews [65], [94].

In recent years, there has been a drive to use supercapacitor material to make better energy storage devices. Usually, a higher potential for capacitance exists with increased surface area. In addition to high surface area, a supercapacitor should have the ability to retain its natural structure over time. Many oxide layers have no ordered structure and breakdown quickly. Theoretically with more order comes more structural stability, and this leads to a longer lasting capacitor. That is why nanostructured materials have received a lot of attention. In addition, there are many other features which make nanostructured materials attractive for use as supercapacitors such as: small size, low production cost, good reversibility and high cycle life. Of the many oxides

studied for this use, TiO_2 is one of the most promising due to its abundance, low cost, and environmental friendliness.

Conventional dielectric capacitors (non-supercapacitors) operate in pulse mode, and the pulse width is on the nanosecond scale [95]. However, these capacitors have capacitances in the range of $10^{-12} – 10^{-9}$ F/cm^2. On the other hand, electrochemical supercapacitors have capacitance in the 10^{-3} F/cm^2 range, but store and deliver charge in the time scale of a few seconds. The development of applications of "asymmetric" supercapacitors, possessing higher specific energy in comparison with a well-known carbon-carbon "symmetric" supercapacitor, has intensified over the last few years. Asymmetric supercapacitors are being studied as an alternative technology to improve energy density for supercapacitors, which can also provide a wider operating potential window compared to symmetric capacitors. Pseudocapacitance based capacitors use both planar and porous electrode systems. Hydrated ruthenium oxide is considered to be the most effective material for supercapacitor application with a capacitance of 720 F/g [96]. Even though $RuO_2 \bullet xH_2O$ shows very high capacitance, the high cost, limited availability and issues with toxicity restricts its commercial usage.

It is for these reasons that TiO_2 has become one of the more promising materials for capacitance. Wang et al. [97] have reported TiO_2-B as having a capacitance of 17.7 F/g (scan rate of 20 mV/s). Although their TiO_2 was made by solvothermal methods in a powder, it is still worth comparing. Salari et al. [82] reported their anodized TiO_2 nanotubes to have a capacitance of 911 μF/cm^2 (scan rate of 1 mV/s). They do not report the longevity of their supercapacitors but do suggest that their values are "several times higher than those of conventional double layer capacitors" (page 5041). Lu et al. [48] reported their hydrogenated TiO_2 nanotubes to have a capacitance of 3.24 mF/cm^2 (scan rate of 100 mV/s). Even though this is the highest value known by the authors to have been reported to date, the most exciting part of their research was that the

decrease in capacitance after 10,000 cycles was only 3.1%. Salari et al. [80] reported their rutile TiO_2 nanotubes to have a capacitance of 2.6 mF/cm ^{2} (scan rate of 1 mV/s). It is important to understand the role that crystallinity and defects in the crystal lattice play in the change/discharge cycle. Ramadoss et al. [81] reported rutile TiO_2 nanorods to have a capacitance of 85 μF/cm^2 (scan rate of 5 mV/s). It is important to point out that these were nanorods not nanotubes used for capacitance testing. They were able to get 80% retention of the capacitance after 1000 cycles. Endut et al. [98] reported that TiO_2 nanotubes anodized for only 1800 seconds at 45 V achieved a capacitance of 49.9 μF/cm^2 (scan rate of 5 mV/s).

8.3 Experimental

Prior to electrochemical anodization the samples were cut into 1 cm x 1.5 cm rectangular pieces from titanium foil (.25mm, 99.7% purity, Sigma Aldrich). The back sides of the foils were painted with a Rust-oleum oil-based protective enamel paint to prevent anodization on the reverse side. The working faces of the titanium foils were sanded to a mirror finish sequentially using 800, 1000, 1500, 2000 and 3000 grit silicon-carbide paper. They were then cleaned by sonicating with acetone for 5 minutes, rinsing in 18 MΩ-cm water and drying in an air stream.

For electrochemical anodization, a typical two electrode system using a Sorensen XPF 60-20 DC Power Supply was employed. All electrochemical experiments were carried out at room temperature (~22 ˚C). A piece of titanium foil was used as the counter electrode. The first electrolytic solution was an organic solution containing 4 wt% 18 MΩ-cm water and 0.14 *M* NH_4F dissolved in Ethylene Glycol. All samples were first anodized at 60 V for 3 hours. The oxide layer was removed after anodization with ultrasonication and electroplater's masking tape, leaving nanoindentations on the titanium foil. The nanoindented foil samples were then cleaned by rinsing

with acetone, cleaning the enamel paint off with a kimwipe, sonicating in acetone for 5 minutes and drying in an air stream.

The nanoindented foils were then prepared for a second anodization by protecting the backsides from anodization with electroplater's masking tape. The samples were re-anodized, this time in an aqueous electrolytic solution which contained 0.5 *M* H_2SO_4 and 0.14 *M* NaF dissolved in 18 MΩ-cm water. The second anodization was at 20 V for 40 minutes on all samples. By re-anodizing the previous sample, the process was altered because the initial etching of the titanium had already been done. These nanoindentations were used as the framework for the new Super Honeycomb structure seen in Figure 8.1.

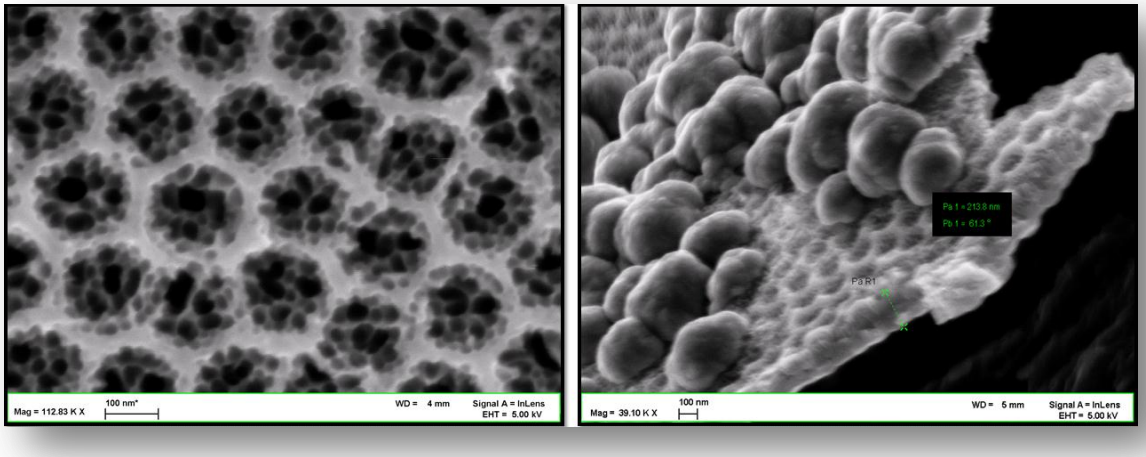

Figure 8.1: TiO_2 Super Honeycomb morphology top view (Left) and side view (with deposited copper crystals) (Right)

Capacitance testing was performed on samples with two different annealing conditions. A Sentro Tech STT-1700-1.5-6 High Temperature Tube Furnace was used to anneal the samples in nitrogen or oxygen environments with a 5 ˚C/min ramp up/down time to/from 450 ˚C and held at 450 ˚C for 2 hours. After annealing, the samples were tested in two solutions: 0.1 *M* LiCl + 0.1 *M* HCl, and 0.1 *M* NaOH, using a Gamry Interface 1000.

The morphology of the samples was examined on a Zeiss Supra 35VP Field Emission Scanning Electron Microscope (FE-SEM). The samples were placed on carbon tape to help prevent charging and were examined at 5 mm working distance and at 5 kV accelerating voltage.

8.4 Results and Discussion

8.4.1 Anodization and Morphology

The creation of the final structure was done through three major steps. The first step was to anodize titanium foil in ethylene glycol at 60 V for 4 hours. Figure 8.2 (Right) shows the morphology of the oxide layer after this step. The TiO_2 nanotubes shown have a diameter of 90-120 nm. The tube length will continue to grow until the anodization process is stopped or the titanium foil is completely oxidized.

The second step in the creation process was to remove the oxide layer and examine the nanoindented structure as can be seen in Figure 8.2 (Left). The nanoindentations have roughly the same diameter as the initial TiO_2 nanotubes that were removed. This surface becomes the template for the anodization in step three.

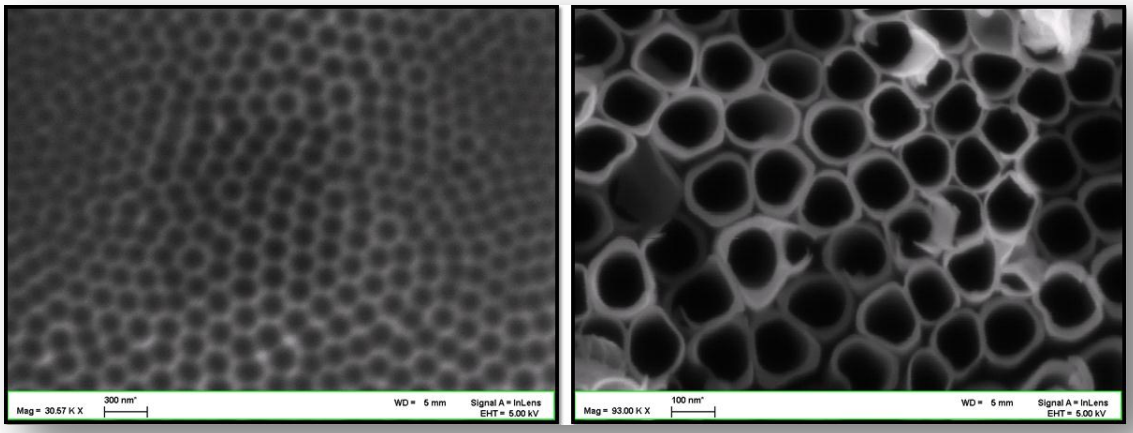

Figure 8.2: (Left) Nanoindentations after 1st oxide layer is removed. (Right) TiO_2 nanotube structure after 1st anodization in EG.

Step three involved re-anodizing the nanoindented foil in an aqueous fluoride solution at 20 V for 40 minutes. This step creates the final Super Honeycomb TiO_2 structure seen in Figure 8.1. This structure has a large format honeycomb structure with honeycomb wells of 110-130 nm in diameter. Each honeycomb well is dotted with 15-20 nanotubes ranging in diameter from 15-40 nm. The surface oxide layer is about 300 nm at its highest points and about 150 nm in the bottom of the honeycomb wells.

There have been several reports of TiO_2 being anodized twice [99], [100], but this morphology has, to the best of the authors' knowledge, never been published. Other reports [101] mention some type of pretreatment to the titanium foils, but their studies did not produce the self-structuring highly organized Super Honeycomb lattice found in this report. A possible mechanism for producing the Super Honeycomb structure is that the water content and fluoride concentration affect the size and clarity of the honeycomb structure, while the voltage applied in the first anodization determines the size of the nanotubes inside of the honeycomb wells.

An additional test was performed to verify this. A piece of titanium foil was anodized in the same EG solution as the other foils but at 40 V. It was then re-anodized after removal of the first oxide layer. The result was the same structural honeycomb lattice with larger nanotubes dotting the honeycomb wells. In all cases, the second anodization stayed exactly the same in all respects. Therefore, it is proposed that the structure is created in the second anodization merely by following a pattern etched into the titanium foil by the first anodization. Other possible reasons for the differences in size of tube and morphology could be the electrode distance and anodization time for the first electrochemical process. More research is needed to understand the exact tunability of the Super Honeycomb features.

It is important to understand the role that crystallinity and defects in the crystal lattice play in the change/discharge cycle. TiO_2 is commonly found in three crystalline forms: brookite, the

rarest, rutile and anatase. Pure brookite is very hard to synthesis, and therefore little is known about its properties. [102] Rutile is the most stable form, and anatase transforms into rutile when heated to high temperatures. After the samples were annealed, they were assumed to be mostly rutile.

8.4.2 Electrochemical Characterization of TiO_2 Super Honeycomb Structure

In order to further investigate the potential of the Super Honeycomb structure here discovered, several electrochemical experiments were used to determine various electrochemical properties of the oxide layer. The test solutions were 0.1 *M* LiCl + 0.1 *M* HCl and 0.1 *M* NaOH. Figures 8.3 and 8.4 show the cyclic voltammograms (CVs) for both electrolyte solutions in the O_2 annealed condition comparing all three scan rates, 100 mV/s, 500 mV/s and 1000 mV/s. Figures 8.5 and 8.6 shows the cyclic voltammograms (CVs) for both electrolyte solutions in the N_2 annealed condition comparing all three scan rates, 100 mV/s, 500 mV/s and 1000 mV/s. The Super Honeycomb annealed in a nitrogen atmosphere at 450 ˚C for 2 hours shows a larger cycle than the O_2 annealed Super Honeycomb or the regular TiO_2 nanotubes, which should lead to higher capacitances. Specific capacitance can be calculated by taking the sum of the lengths between the upper and lower curves at each point and multiplying it by the time difference between each point. Once you have the area under the curve, the area is divided by the voltage difference between the scan limits. This number can easily be normalized to cm^{-2}. The resulting capacitance graphs comparing standard TiO_2 nanotube capacitance to the capacitance obtained in the two electrolytes can be seen in Figures 8.7 and 8.8.

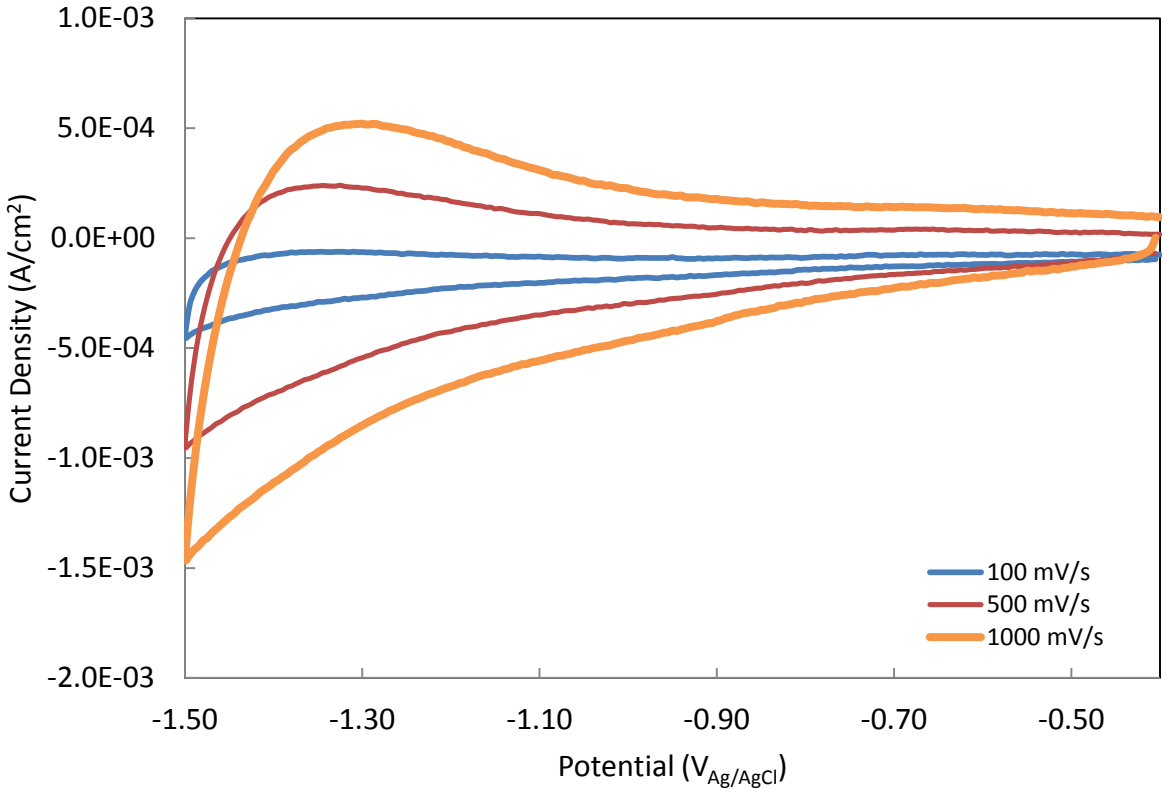

Figure 8.3: Capacitance CVs, Super Honeycomb, EG/NaF anodized, 0.1 *M* NaOH, O_2 annealed.

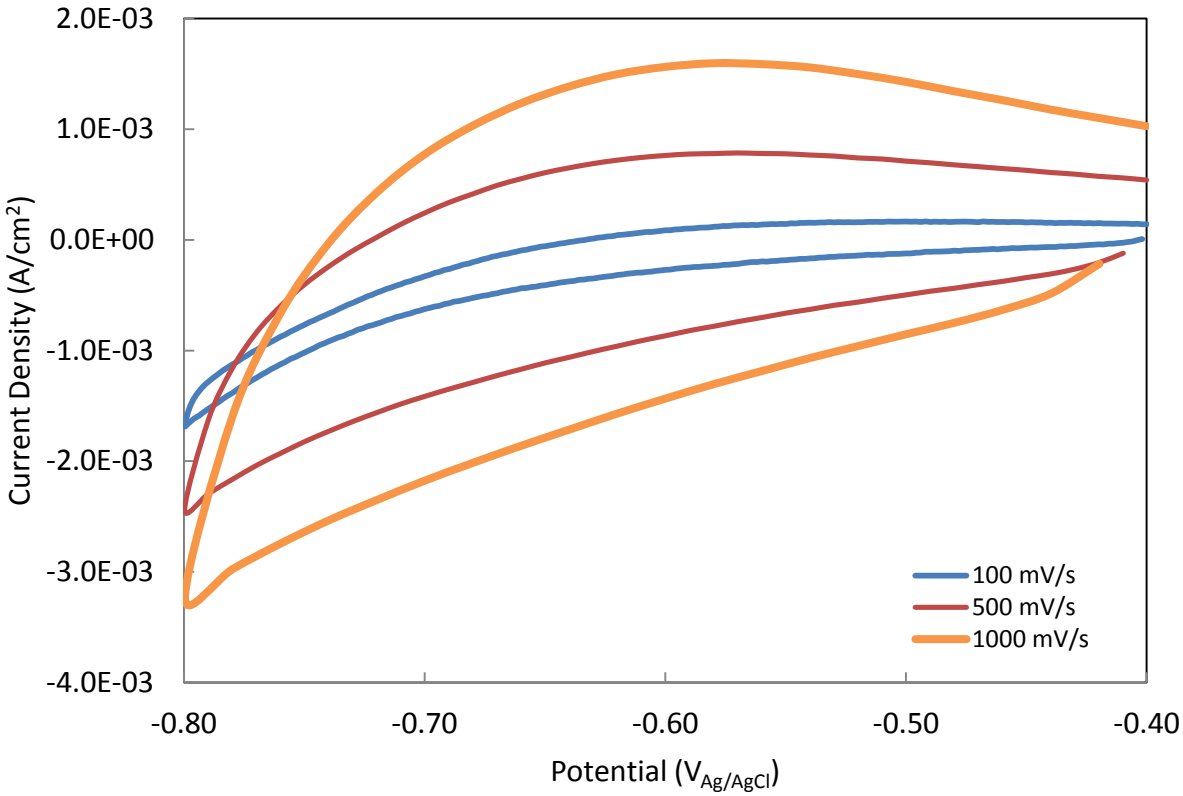

Figure 8.4: Capacitance CVs, Super Honeycomb, EG/NaF anodized, 0.1 *M* LiCl + 0.1 *M* HCl O_2 annealed.

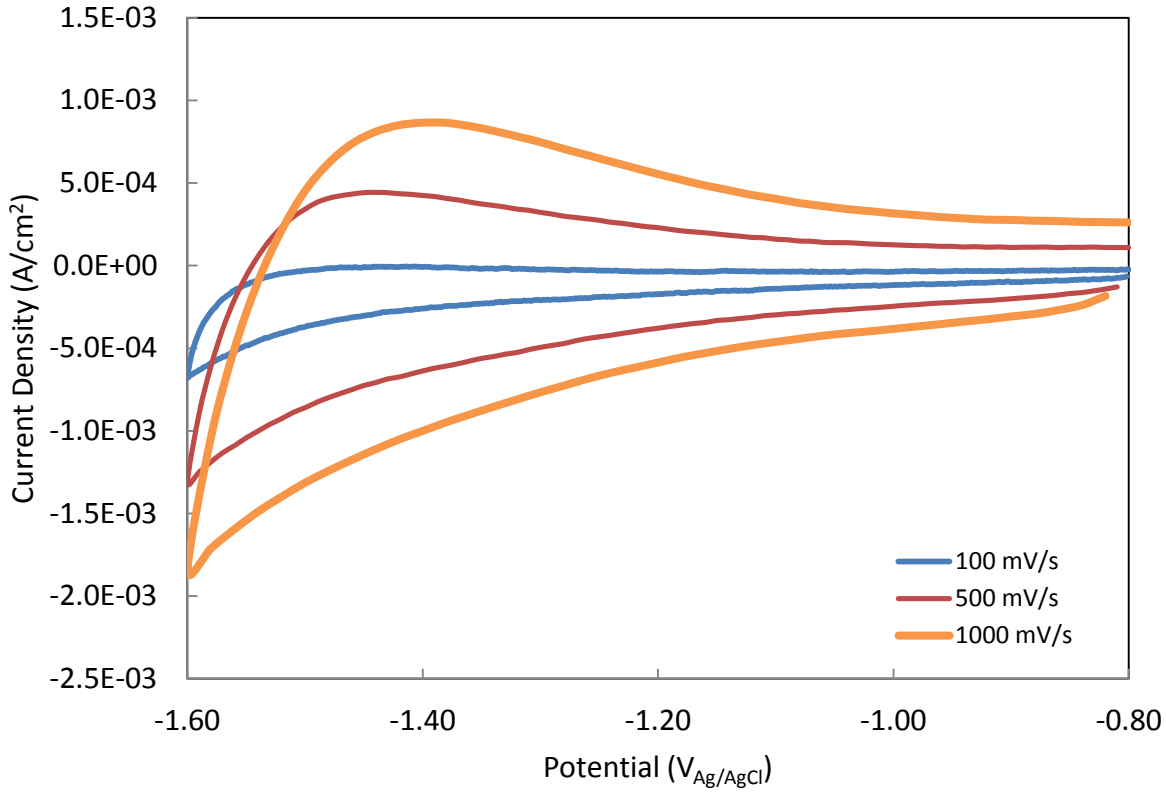

Figure 8.5: Capacitance CVs, Super Honeycomb, EG/NaF anodized, 0.1 *M* NaOH, N_2 annealed.

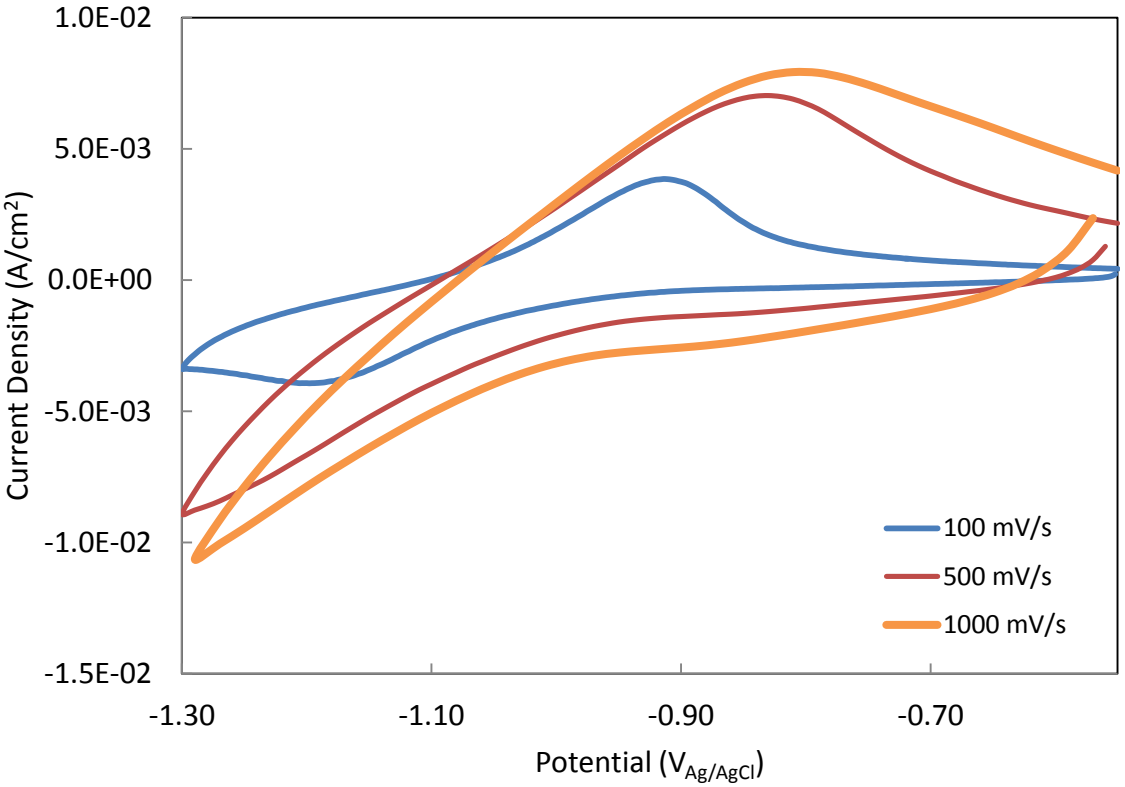

Figure 8.6: Capacitance CVs, Super Honeycomb, EG/NaF anodized, 0.1 *M* LiCl + 0.1 *M* HCl, N_2 annealed.

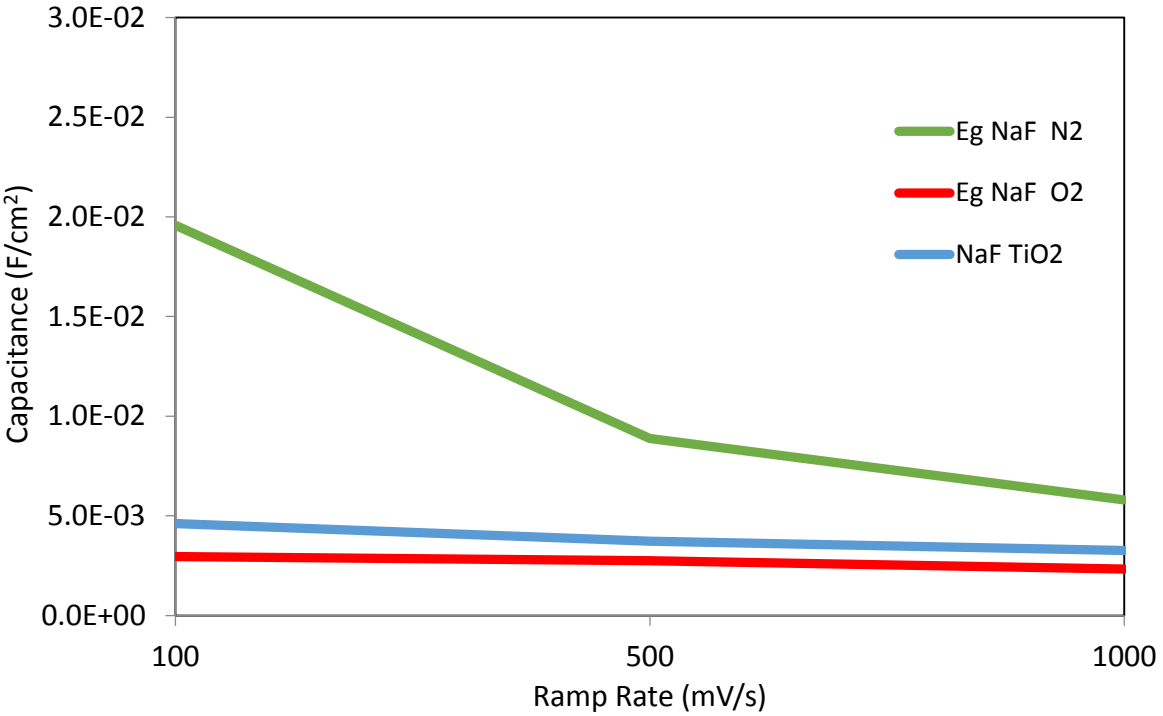

Figure 8.7: Average capacitance 0.1 *M* LiCl + 0.1 *M* HCl, EG/NaF anodized.

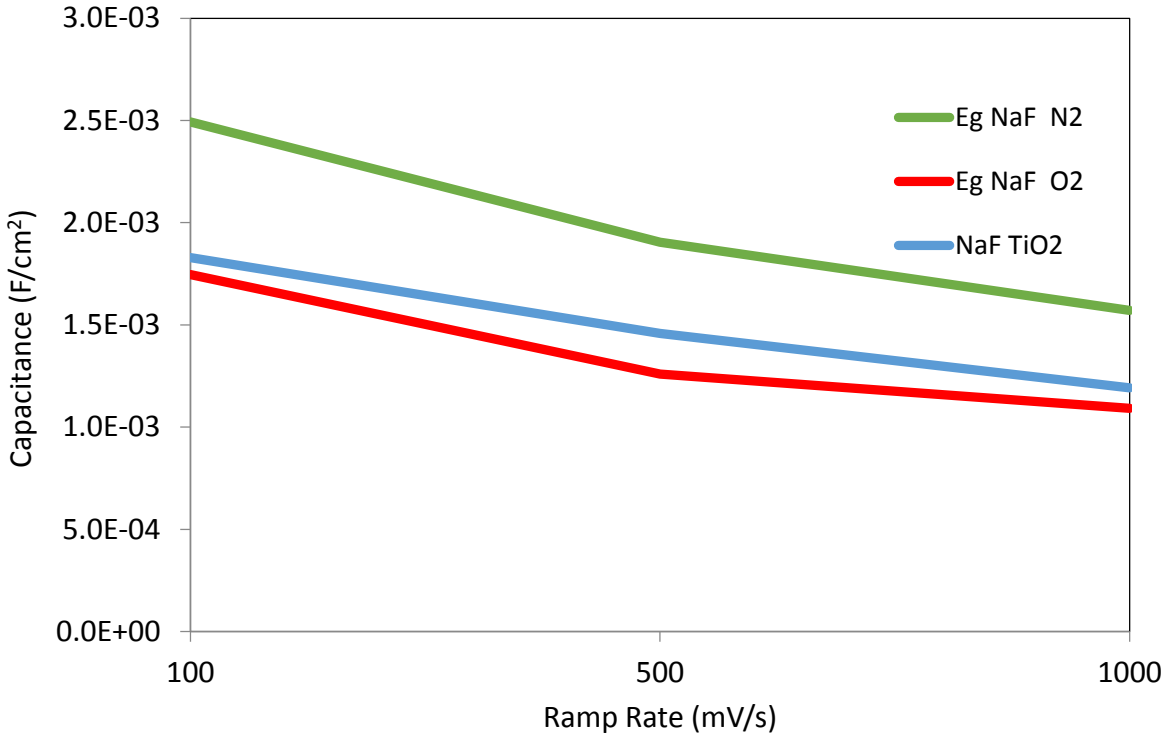

Figure 8.8: Average capacitance 0.1 *M* NaOH, EG/NaF anodized.

Another electrochemical experiment that sheds light on the capacitance activity for the oxide layer is called Electrochemical Impedance Spectroscopy (EIS). These measurements were carried out with no DC bias using a signal of 10 mV with a signal range of 0.1 to 100,000 Hz. The EIS data were analyzed with Nyquist plots as shown in Figure 8.9. The lack of a semicircle indicates that the material is likely a good candidate for supercapacitor use. The closer the line is to being parallel to the imaginary Z" axis, the more suggestive the plot is to showing ideal capacitive behavior. Also, if the values of Z_{img} stay low, as is this case in this plot, it is a good indicator that the material will be a good capacitor. Figure 6 shows the Nyquist plot from the oxygen annealed sample tested in 0.1 *M* LiCl + 0.1 *M* HCl as an example, showing that the TiO_2 Super Honeycomb structure is a good candidate for supercapacitor use.

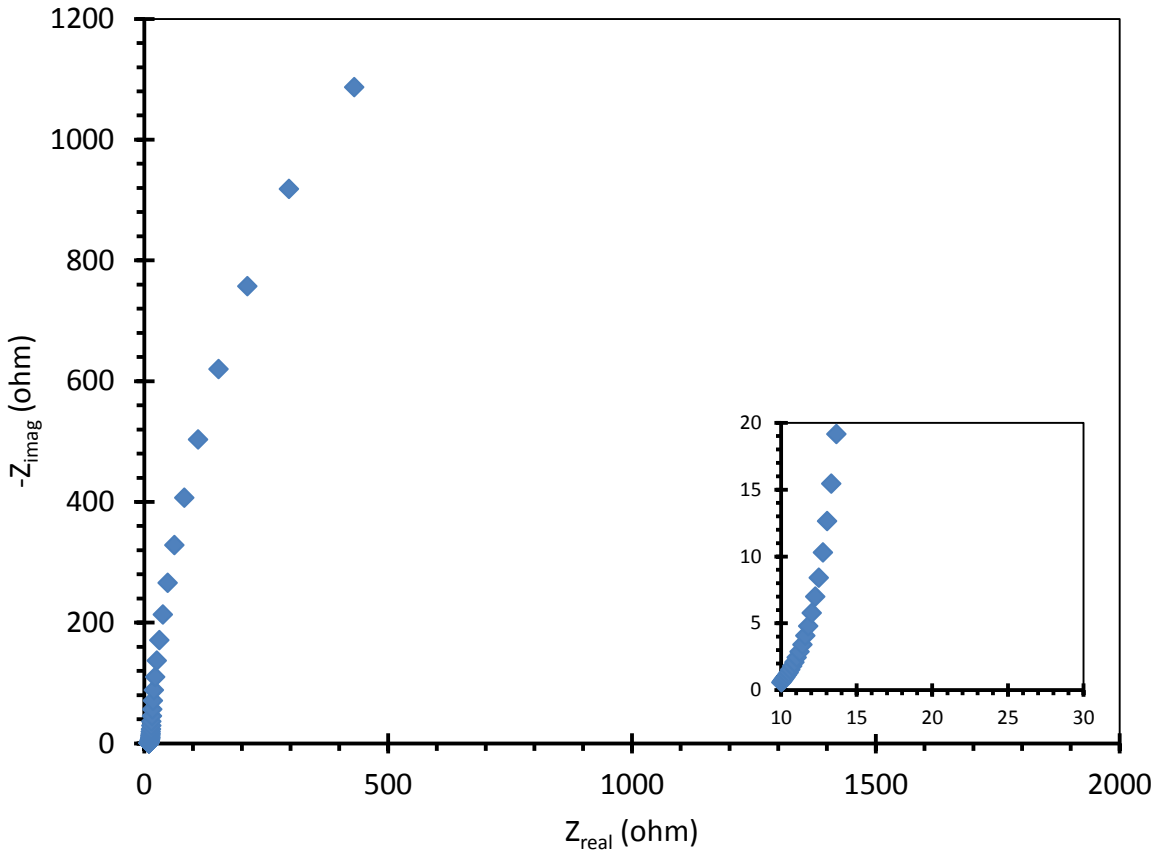

Figure 8.9: Nyquist plot of nitrogen annealed sample in 0.1 *M* LiCl + 0.1 *M* HCl electrolye

8.5 Conclusions

In the present study, a new highly-ordered morphology of TiO_2 has successfully been prepared using a simple and inexpensive electrochemical anodization technique. The new morphology was shown to have good specific capacitance with the highest value of 19.6 mF/cm^2 at a scan rate of 100 mV/s, more than 6 times the highest value known by the authors to have been reported to date for any TiO_2 structure. FE-SEM images showed the new highly-ordered morphology as close-packed TiO_2 nanotubes vertically aligned to the titanium substrate, with an ordered height distribution following the previously etched nanoindentations. The main benefit to the new structure is its large surface area due to long narrow nanotubes. It is also likely to be stable based on its structure. This report shows that this new morphology of TiO_2 is a worthy candidate for further study in industrial uses for supercapacitors.

REFERENCES

[1] R. J. Dillon, J. B. Joo, F. Zaera, Y. Yin, and C. J. Bardeen, "Correlating the excited state relaxation dynamics as measured by photoluminescence and transient absorption with the photocatalytic activity of Au@TiO_2 core–shell nanostructures," *Phys. Chem. Chem. Phys.*, vol. 15, no. 5, pp. 1488–1496, Jan. 2013.

[2] L. Han, C. Zhu, P. Hu, and S. Dong, "One-pot synthesis of a Au@TiO_2 core–shell nanocomposite and its catalytic property," *RSC Adv.*, vol. 3, no. 31, pp. 12568–12570, Jul. 2013.

[3] R. Liu and A. Sen, "Controlled synthesis of heterogeneous metal–titania nanostructures and their applications," *J. Am. Chem. Soc.*, vol. 134, no. 42, pp. 17505–17512, Oct. 2012.

[4] J. M. Macak, B. G. Gong, M. Hueppe, and P. Schmuki, "Filling of TiO_2 nanotubes by self-doping and electrodeposition," *Adv. Mater.*, vol. 19, no. 19, pp. 3027–3031, 2007.

[5] T. Gandhi, K. S. Raja, and M. Misra, "Templated growth of cadmium zinc telluride (CZT) nanowires using pulsed-potentials in hot non-aqueous solution," *Electrochimica Acta*, vol. 51, no. 26, pp. 5932–5942, Aug. 2006.

[6] T. Gandhi, K. S. Raja, and M. Misra, "Synthesis of ZnTe nanowires onto TiO_2 nanotubular arrays by pulse-reverse electrodeposition," *Thin Solid Films*, vol. 517, no. 16, pp. 4527–4533, Jun. 2009.

[7] A. Kar, K. S. Raja, and M. Misra, "Electrodeposition of hydroxyapatite onto nanotubular TiO_2 for implant applications," *Surf. Coat. Technol.*, vol. 201, no. 6, pp. 3723–3731, Dec. 2006.

[8] L. E. Greene, M. Law, B. D. Yuhas, and P. Yang ."ZnO-TiO_2 core-shell nanorod/P3HT solar cells," *J. Phys. Chem. C*, vol. 111, no. 50, pp. 18451–18456, Dec. 2007.

[9] W. Zhu, G. Wang, X. Hong, and X. Shen, “One-step fabrication of Ni/TiO_2 core/shell nanorod arrays in anodic aluminum oxide membranes,” *J. Phys. Chem. C*, vol. 113, no. 14, pp. 5450–5454, Apr. 2009.

[10] S. K. Mohapatra, S. Banerjee, and M. Misra, “Synthesis of Fe_2O_3/TiO_2 nanorod–nanotube arrays by filling TiO_2 nanotubes with Fe,” *Nanotechnology*, vol. 19, no. 31, p. 315601, 2008.

[11] S. K. Kim, D. Josell, and T. P. Moffat, “Electrodeposition of Cu in the PEI-PEG-Cl-SPS additive system,” *J. Electrochem. Soc.*, vol. 153, no. 9, p. C616, 2006.

[12] W. Zhu, G. Wang, X. Hong, and X. Shen, “Synthesis of various metal/TiO_2 core/shell nanorod arrays,” *Chin. J. Chem. Phys.*, vol. 24, no. 1, p. 91, 2011.

[13] G. Sahu, S. W. Gordon, and M. A. Tarr, “Synthesis and application of core-shell Au–TiO_2 nanowire photoanode materials for dye sensitized solar cells,” *RSC Adv.*, vol. 2, no. 2, p. 573, 2012.

[14] D. Fang, K. Huang, S. Liu, and D. Qin, “High density copper nanowire arrays deposition inside ordered titania pores by electrodeposition,” *Electrochem. Commun.*, vol. 11, no. 4, pp. 901–904, Apr. 2009.

[15] S. K. Kim and J. J. Kim, “Additive-free superfilling in Damascene Cu electrodeposition using microcontact printing,” *Electrochem. Solid-State Lett.*, vol. 7, no. 9, pp. C101–C103, Sep. 2004.

[16] P. M. Vereecken, R. A. Binstead, H. Deligianni, and P. C. Andricacos, “The chemistry of additives in Damascene copper plating,” *IBM J. Res. Dev.*, vol. 49, no. 1, pp. 3–18, 2005.

[17] T. P. Moffat, D. Wheeler, S. K. Kim, and D. Josell, “Curvature enhanced adsorbate coverage mechanism for bottom-up superfilling and bump control in Damascene processing,” *Electrochimica Acta*, vol. 53, no. 1, pp. 145–154, Nov. 2007.

[18] T. P. Moffat, D. Wheeler, and D. Josell, “Electrodeposition of copper in the SPS-PEG-Cl additive system,” *J. Electrochem. Soc.*, vol. 151, no. 4, p. C262, 2004.

[19] T. P. Moffat, D. Wheeler, W. H. Huber, and D. Josell, “Superconformal electrodeposition of copper,” *Electrochem. Solid-State Lett.*, vol. 4, no. 4, p. C26, 2001.

[20] Y. Jin, Y. Sui, L. Wen, F. Ye, M. Sun, and Q. Wang, “Competitive adsorption of PEG and SPS on copper surface in acidic electrolyte containing Cl-,” *J. Electrochem. Soc.*, vol. 160, no. 1, pp. D20–D27, 2013.

[21] S. K. Kim, D. Josell, and T. P. Moffat, “Electrodeposition of Cu in the PEI-PEG-Cl-SPS additive system,” *J. Electrochem. Soc.*, vol. 153, no. 9, p. C616, 2006.

[22] W. P. Dow, M. Y. Yen, W. B. Lin, and S. W. Ho, “Influence of molecular weight of polyethylene glycol on microvia filling by copper electroplating,” *J. Electrochem. Soc.*, vol. 152, no. 11, p. C769, 2005.

[23] J. M. Casas, F. Alvarez, and L. Cifuentes, “Aqueous speciation of sulfuric acid–cupric sulfate solutions,” *Chem. Eng. Sci.*, vol. 55, no. 24, pp. 6223–6234, Dec. 2000.

[24] V. S. Bryantsev, M. S. Diallo, A. C. T. van Duin, and W. A. Goddard III, “Hydration of copper(II): new insights from density functional theory and the COSMO solvation model,” *J. Phys. Chem. A*, vol. 112, no. 38, pp. 9104–9112, Sep. 2008.

[25] T. P. Moffat and D. Josell, “Extreme bottom-up superfilling of through-silicon-vias by Damascene processing: suppressor disruption, positive feedback and turing patterns,” *J. Electrochem. Soc.*, vol. 159, no. 4, pp. D208–D216, Jan. 2012.

[26] N. Vasiljevic, M. Wood, P. J. Heard, and W. Schwarzacher, “The influence of specific anion adsorption on the surface roughness of electrodeposited polycrystalline Cu films,” *J. Electrochem. Soc.*, vol. 157, no. 4, p. D193, 2010.

[27] O. M. Magnussen, “Ordered anion adlayers on metal electrode surfaces,” *Chem. Rev.*, vol. 102, no. 3, pp. 679–726, Mar. 2002.

[28] D. M. Soares, S. Wasle, K. G. Weil, and K. Doblhofer, “Copper ion reduction catalyzed by chloride ions,” *J. Electroanal. Chem.*, vol. 532, no. 1–2, pp. 353–358, Sep. 2002.

[29] J. W. Halley, B. B. Smith, S. Walbran, L. A. Curtiss, R. O. Rigney, A. Sutjianto, N. C. Hung, R. M. Yonco, and Z. Nagy, “Theory and experiment on the cuprous–cupric electron transfer rate at a copper electrode,” *J. Chem. Phys.*, vol. 110, no. 13, pp. 6538–6552, Apr. 1999.

[30] W. Shao, G. Pattanaik, and G. Zangari, “Influence of chloride anions on the mechanism of copper electrodeposition from acidic sulfate electrolytes,” *J. Electrochem. Soc.*, vol. 154, no. 4, pp. D201–D207, Apr. 2007.

[31] N. T. M. Hai, T. T. M. Huynh, A. Fluegel, M. Arnold, D. Mayer, W. Reckien, T. Bredow, and P. Broekmann, “Competitive anion/anion interactions on copper surfaces relevant for Damascene electroplating,” *Electrochimica Acta*, vol. 70, pp. 286–295, May 2012.

[32] P. Broekmann, A. Fluegel, C. Emnet, M. Arnold, C. Roeger-Goepfert, A. Wagner, N. T. M. Hai, and D. Mayer, “Classification of suppressor additives based on synergistic and antagonistic ensemble effects,” *Electrochimica Acta*, vol. 56, no. 13, pp. 4724–4734, May 2011.

[33] Y. Jin, M. Sun, D. Mu, X. Ren, Q. Wang, and L. Wen, “Investigation of PEG adsorption on copper in Cu^{2+}-free solution by SERS and AFM,” *Electrochimica Acta*, vol. 78, pp. 459–465, Sep. 2012.

[34] T. P. Moffat, B. Baker, D. Wheeler, and D. Josell, “Accelerator aging effects during copper electrodeposition,” *Electrochem. Solid-State Lett.*, vol. 6, no. 4, pp. C59–C62, Apr. 2003.

[35] S. Armini, “Cu electrodeposition on resistive substrates in alkaline chemistry: effect of current density and wafer RPM,” *J. Electrochem. Soc.*, vol. 158, no. 6, pp. D390–D394, 2011.

[36] S. Armini, Z. El-Mekki, K. Vandersmissen, H. Philipsen, S. Rodet, M. Honore, A. Radisic, Y. Civale, E. Beyne, and L. Leunissen, “Void-free filling of HAR TSVs using a wet alkaline Cu seed

on CVD Co as a replacement for PVD Cu seed," *J. Electrochem. Soc.*, vol. 158, no. 2, p. H160, 2011.

[37] A. Joi, R. Akolkar, and U. Landau, "Additives for bottom-up copper plating from an alkaline complexed electrolyte," *J. Electrochem. Soc.*, vol. 160, no. 12, pp. D3001–D3003, 2013.

[38] W. P. Dow, H. S. Huang, M. Y. Yen, and H. H. Chen, "Roles of chloride ion in microvia filling by copper electrodeposition: Studies using EPR and galvanostatic measurements," *J. Electrochem. Soc.*, vol. 152, no. 2, pp. C77–C88, Feb. 2005.

[39] J. C. Ballesteros, E. Chainet, P. Ozil, Y. Meas, and G. Trejo, "Electrodeposition of copper from non-cyanide alkaline solution containing tartrate," *Int J Electrochem Sci*, vol. 6, pp. 2632–2651, 2011.

[40] E. P. Serjeant and B. Dempsey, *Ionisation Constants of Organic Acids in Aqueous Solution (IUPAC chemical data series)*. Pergamon Pr, 1979.

[41] H. K. Chang, B.-H. Choe, and J. K. Lee, "Influence of titanium oxide films on copper nucleation during electrodeposition," *Mater. Sci. Eng. A*, vol. 409, no. 1–2, pp. 317–328, Nov. 2005.

[42] A. V. Rosário, M. C. Santos, L. H. Mascaro, L. O. S. Bulhões, and E. C. Pereira, "Copper underpotential deposition on TiO_2 electrodes: A voltammetric and electrochemical quartz crystal nanobalance study," *Thin Solid Films*, vol. 518, no. 10, pp. 2669–2673, Mar. 2010.

[43] L. Pauling, *General Chemistry (Dover Books on Chemistry)*, 3rd ed. Dover Publications, 1988.

[44] M. Paunovic and M. Schlesinger, *Fundamentals of Electrochemical Deposition (The ECS Series of Texts and Monographs)*, 2nd ed. Wiley-Interscience, 2006.

[45] Y. D. Chiu and W. P. Dow, "Accelerator screening by cyclic voltammetry for microvia filling by copper electroplating," *J. Electrochem. Soc.*, vol. 160, no. 12, pp. D3021–D3027, 2013.

[46] E. Garcia-Cardona, E. H. Wong, and D. P. Barkey, “NMR spectral studies of interactions between the accelerants SPS and MPS and copper chlorides,” *J. Electrochem. Soc.*, vol. 158, no. 3, pp. D143–D148, Mar. 2011.

[47] T. P. Moffat and L. Y. O. Yang, “Accelerator surface phase associated with superconformal Cu electrodeposition,” *J. Electrochem. Soc.*, vol. 157, no. 4, pp. D228–D241, Apr. 2010.

[48] X. Lu, G. Wang, T. Zhai, M. Yu, J. Gan, Y. Tong, and Y. Li, “Hydrogenated TiO_2 nanotube arrays for supercapacitors,” *Nano Lett.*, vol. 12, no. 3, pp. 1690–1696, Mar. 2012.

[49] L. Zaraska, G. D. Sulka, and M. Jaskuła, “Fabrication of free-standing copper foils covered with highly-ordered copper nanowire arrays,” *Appl. Surf. Sci.*, vol. 258, no. 19, pp. 7781–7786, Jul. 2012.

[50] W. Wang, N. Li, X. Li, W. Geng, and S. Qiu, “Synthesis of metallic nanotube arrays in porous anodic aluminum oxide template through electroless deposition,” *Mater. Res. Bull.*, vol. 41, no. 8, pp. 1417 – 1423, 2006.

[51] R. Bertholdo, M. C. Assis, P. Hammer, S. H. Pulcinelli, and C. V. Santilli, “Controlled growth of anodic aluminium oxide films with hexagonal array of nanometer-sized pores filled with textured copper nanowires,” *J. Eur. Ceram. Soc.*, vol. 30, no. 2, pp. 181–186, Jan. 2010.

[52] S. Kumar, D. Saini, G. S. Lotey, and N. K. Verma, “Electrochemical synthesis of copper nanowires in anodic alumina membrane and their impedance analysis,” *Superlattices Microstruct.*, vol. 50, no. 6, pp. 698–702, Dec. 2011.

[53] W. Zhu, G. Wang, X. Hong, and X. Shen, “One-step fabrication of Ni/TiO_2 core/shell nanorod arrays in anodic aluminum oxide membranes,” *J. Phys. Chem. C*, vol. 113, no. 14, pp. 5450–5454, Apr. 2009.

[54] S. So, K. Lee, and P. Schmuki, “High-aspect-ratio dye-sensitized solar cells based on robust, fast-growing TiO_2 nanotubes,” *Chem. – Eur. J.*, vol. 19, no. 9, pp. 2966–2970, 2013.

[55] X. Feng, K. Zhu, A. J. Frank, C. A. Grimes, and T. E. Mallouk, "Rapid charge transport in dye-sensitized solar cells made from vertically aligned single-crystal rutile TiO_2 nanowires," *Angew. Chem. Int. Ed.*, vol. 51, no. 11, pp. 2727–2730, 2012.

[56] K. Zhu, N. R. Neale, A. Miedaner, and A. J. Frank, "Enhanced charge-collection efficiencies and light scattering in dye-sensitized solar cells using oriented TiO_2 nanotubes arrays," *Nano Lett.*, vol. 7, no. 1, pp. 69–74, Jan. 2007.

[57] L. Tsui and G. Zangari, "Modification of TiO_2 nanotubes by Cu_2O for photoelectrochemical, photocatalytic, and photovoltaic devices," *Electrochimica Acta*, Oct. 2013.

[58] X. S. Yang and H. Kim, "Improved photoelectrochemical properties of Cu-loaded TiO_2 nanotubes," *Adv. Mater. Res.*, vol. 148–149, pp. 1083–1086, Oct. 2010.

[59] V. K. Mahajan, M. Misra, K. S. Raja, and S. K. Mohapatra, "Self-organized TiO_2 nanotubular arrays for photoelectrochemical hydrogen generation: effect of crystallization and defect structures," *J. Phys. Appl. Phys.*, vol. 41, no. 12, p. 125307, Jun. 2008.

[60] J. M. Macak, B. G. Gong, M. Hueppe, and P. Schmuki, "Filling of TiO_2 nanotubes by self-doping and electrodeposition," *Adv. Mater.*, vol. 19, no. 19, pp. 3027–3031, 2007.

[61] S. K. Kim, D. Josell, and T. P. Moffat, "Electrodeposition of Cu in the PEI-PEG-Cl-SPS additive system," *J. Electrochem. Soc.*, vol. 153, no. 9, p. C616, 2006.

[62] M. Hasegawa, Y. Negishi, T. Nakanishi, and T. Osaka, "Effects of additives on copper electrodeposition in submicrometer trenches," *J. Electrochem. Soc.*, vol. 152, no. 4, pp. C221–C228, Apr. 2005.

[63] M. L. Walker, L. J. Richter, and T. P. Moffat, "Competitive adsorption of PEG, Cl, and SPS/MPS on Cu: An in situ ellipsometric study," *J. Electrochem. Soc.*, vol. 153, no. 8, p. C557, 2006.

[64] P. Kar, K. S. Raja, M. Misra, and B. N. Agasanapur, “Formation and stability of anatase phase of phosphate incorporated and carbon doped titania nanotubes,” *Mater. Res. Bull.*, vol. 44, no. 2, pp. 398–402, Feb. 2009.

[65] C. A. Grimes, “Synthesis and application of highly ordered arrays of TiO_2 nanotubes,” *J. Mater. Chem.*, vol. 17, no. 15, pp. 1451–1457, Apr. 2007.

[66] T. P. Moffat and D. Josell, “Extreme bottom-up superfilling of through-silicon-vias by damascene processing: Suppressor disruption, positive feedback and turing patterns,” *J. Electrochem. Soc.*, vol. 159, no. 4, pp. D208–D216, 2012.

[67] L. Johansson, “Complex formation and stereoselective effects in the copper(II) +-and rac-tartrate systems in acid and neutral aqueous solution,” *Acta Chemica Scandinavica A*, vol. 34, pp. 495-506, Feb. 1980.

[68] K. G. Kumar, C. Pavithran, and P. K. Rohatgi, “Preparation of copper-coated titania particles for composites,” *J. Mater. Sci.*, vol. 15, no. 6, pp. 1588–1592, Jun. 1980.

[69] U. Diebold, “The surface science of titanium dioxide,” *Surf. Sci. Rep.*, vol. 48, no. 5–8, pp. 53–229, Jan. 2003.

[70] P. Hoyer, “Formation of a titanium dioxide nanotube array,” *Langmuir*, vol. 12, no. 6, pp. 1411–1413, Jan. 1996.

[71] V. Zwilling, E. Darque-Ceretti, A. Boutry-Forveille, D. David, M. Y. Perrin, and M. Aucouturier, “Structure and physicochemistry of anodic oxide films on titanium and TA6V alloy,” *Surf. Interface Anal.*, vol. 27, no. 7, pp. 629–637, 1999.

[72] D. Gong, C. Grimes, O. K. Varghese, W. Hu, R. S. Singh, Z. Chen, and E. C. Dickey, “Titanium oxide nanotube arrays prepared by anodic oxidation,” *J. Mater. Res.*, vol. 16, no. 12, pp. 3331–3334, 2001.

[73] H. Mirabolghasemi, N. Liu, K. Lee, and P. Schmuki, “Formation of ‘single walled’ TiO_2 nanotubes with significantly enhanced electronic properties for higher efficiency dye-sensitized solar cells,” *Chem. Commun.*, vol. 49, no. 20, pp. 2067–2069, Feb. 2013.

[74] Z. Liu and M. Misra, “Bifacial dye-sensitized solar cells based on vertically oriented TiO_2 nanotube arrays,” *Nanotechnology*, vol. 21, no. 12, p. 125703, Mar. 2010.

[75] G. K. Mor, K. Shankar, M. Paulose, O. K. Varghese, and C. A. Grimes, “Use of highly-ordered TiO_2 nanotube arrays in dye-sensitized solar cells,” *Nano Lett.*, vol. 6, no. 2, pp. 215–218, Feb. 2006.

[76] J. Kim, S. Choi, J. Noh, S. Yoon, S. Lee, T. Noh, A. J. Frank, and K. Hong, “Synthesis of CdSe−TiO_2 nanocomposites and their applications to TiO_2 sensitized solar cells,” *Langmuir*, vol. 25, no. 9, pp. 5348–5351, May 2009.

[77] S. I. In, K. P. Almtoft, H. S. Lee, I. H. Andersen, D. Qin, N. Bao, and C. A. Grimes, “Low temperature synthesis of transparent, vertically aligned anatase TiO_2 nanowire arrays: application to dye sensitized solar cells,” *Bull. Korean Chem. Soc.*, vol. 33, no. 6, pp. 1989–1992, Jun. 2012.

[78] M. Yang, G. Yang, E. Spiecker, K. Lee, and P. Schmuki, “Ordered ‘superlattice’ TiO_2/Nb_2O_5 nanotube arrays with improved ion insertion stability,” *Chem. Commun.*, vol. 49, no. 5, pp. 460–462, Dec. 2012.

[79] C. Guan, X. Xia, N. Meng, Z. Zeng, X. Cao, C. Soci, H. Zhang, and H. J. Fan, “Hollow core–shell nanostructure supercapacitor electrodes: Gap matters,” *Energy Environ. Sci.*, vol. 5, no. 10, p. 9085, 2012.

[80] M. Salari, S. H. Aboutalebi, A. T. Chidembo, I. P. Nevirkovets, K. Konstantinov, and H. K. Liu, “Enhancement of the electrochemical capacitance of TiO_2 nanotube arrays through controlled

phase transformation of anatase to rutile," *Phys. Chem. Chem. Phys.*, vol. 14, no. 14, pp. 4770–4779, Mar. 2012.

[81] A. Ramadoss and S. J. Kim, "Vertically aligned TiO_2 nanorod arrays for electrochemical supercapacitor," *J. Alloys Compd.*, vol. 561, pp. 262–267, Jun. 2013.

[82] M. Salari, S. H. Aboutalebi, K. Konstantinov, and H. K. Liu, "A highly ordered titania nanotube array as a supercapacitor electrode," *Phys. Chem. Chem. Phys.*, vol. 13, no. 11, p. 5038, 2011.

[83] J. C. Cardoso, C. A. Grimes, X. Feng, X. Zhang, S. Komarneni, M. V. B. Zanoni, and N. Bao, "Fabrication of coaxial TiO_2/Sb_2S_3 nanowire hybrids for efficient nanostructured organic–inorganic thin film photovoltaics," *Chem. Commun.*, vol. 48, no. 22, pp. 2818–2820, Feb. 2012.

[84] D. Sarauli, M. Riedel, C. Wettstein, R. Hahn, K. Stiba, U. Wollenberger, S. Leimkühler, P. Schmuki, and F. Lisdat, "Semimetallic TiO_2 nanotubes: New interfaces for bioelectrochemical enzymatic catalysis," *J. Mater. Chem.*, vol. 22, no. 11, pp. 4615–4618, Feb. 2012.

[85] D. Kim, H. Tsuchiya, S. Fujimoto, F. Schmidt-Stein, and P. Schmuki, "Nitrogen-doped TiO2 mesosponge layers formed by anodization of nitrogen-containing Ti alloys," *J. Solid State Electrochem.*, vol. 16, no. 1, pp. 89–92, Jan. 2012.

[86] K. Lee, D. Kim, S. Berger, R. Kirchgeorg, and P. Schmuki, "Anodically formed transparent mesoporous TiO_2 electrodes for high electrochromic contrast," *J. Mater. Chem.*, vol. 22, no. 19, pp. 9821–9825, Apr. 2012.

[87] N. Liu, I. Paramasivam, M. Yang, and P. Schmuki, "Some critical factors for photocatalysis on self-organized TiO_2 nanotubes," *J. Solid State Electrochem.*, vol. 16, no. 11, pp. 3499–3504, Nov. 2012.

[88] A. Kahnt, C. Oelsner, F. Werner, D. M. Guldi, S. P. Albu, R. Kirchgeorg, K. Lee, and P. Schmuki, "Excited state properties of anodic TiO_2 nanotubes," *Appl. Phys. Lett.*, vol. 102, no. 23, pp. 233109–233109–5, Jun. 2013.

[89] J. M. Macak, H. Tsuchiya, L. Taveira, S. Aldabergerova, and P. Schmuki, "Smooth anodic TiO_2 nanotubes," *Angew. Chem. Int. Ed.*, vol. 44, no. 45, pp. 7463–7465, Nov. 2005.

[90] D. Kim, A. Ghicov, S. P. Albu, and P. Schmuki, "Bamboo-type TiO_2 nanotubes: Improved conversion efficiency in dye-sensitized solar cells," *J. Am. Chem. Soc.*, vol. 130, no. 49, pp. 16454–16455, Dec. 2008.

[91] S. P. Albu, D. Kim, and P. Schmuki, "Growth of aligned TiO_2 bamboo-type nanotubes and highly ordered nanolace," *Angew. Chem. Int. Ed.*, vol. 47, no. 10, pp. 1916–1919, Feb. 2008.

[92] N. Liu, H. Mirabolghasemi, K. Lee, S. P. Albu, A. Tighineanu, M. Altomare, and P. Schmuki, "Anodic TiO_2 nanotubes: Double walled vs. single walled," *Faraday Discuss.*, Jul. 2013.

[93] S. K. Mohapatra, M. Misra, V. K. Mahajan, and K. S. Raja, "Synthesis of Y-branched TiO_2 nanotubes," *Mater. Lett.*, vol. 62, no. 12–13, pp. 1772–1774, Apr. 2008.

[94] P. Roy, S. Berger, and P. Schmuki, "TiO_2 nanotubes: Synthesis and applications," *Angew. Chem. Int. Ed.*, vol. 50, no. 13, pp. 2904–2939, 2011.

[95] S. Sarangapani, B. V. Tilak, and C.-P. Chen, "Materials for electrochemical capacitors theoretical and experimental constraints," *J. Electrochem. Soc.*, vol. 143, no. 11, pp. 3791–3799, Nov. 1996.

[96] J. P. Zheng, "Ruthenium oxide-carbon composite electrodes for electrochemical capacitors," *Electrochem. Solid-State Lett.*, vol. 2, no. 8, pp. 359–361, Aug. 1999.

[97] G. Wang, Z. Y. Liu, J. N. Wu, and Q. Lu, "Preparation and electrochemical capacitance behavior of TiO_2-B nanotubes for hybrid supercapacitor," *Mater. Lett.*, vol. 71, pp. 120–122, Mar. 2012.

[98] Z. Endut, M. Hamdi, and W. J. Basirun, "An investigation on formation and electrochemical capacitance of anodized titania nanotubes," *Appl. Surf. Sci.*, vol. 280, pp. 962–966, Sep. 2013.

[99] S. P. Albu, A. Ghicov, S. Aldabergenova, P. Drechsel, D. LeClere, G. E. Thompson, J. M. Macak, and P. Schmuki, "Formation of double-walled TiO_2 nanotubes and robust anatase membranes," *Adv. Mater.*, vol. 20, no. 21, pp. 4135–4139, 2008.

[100] W. Xuelai, C. Rui, Z. Jun, N. Pan, X. Hao, and Z. Xiujian, "Two-step anodization of maltilayer TiO_2 nanotube and its photocatalytic activity under UV light," *J. Wuhan Univ. Technol.-Mater. Sci. Ed.*, vol. 27, no. 5, pp. 866–870, Oct. 2012.

[101] T. Xu, J. Lin, J. Chen, and X. Chen, "The effect of pre-pattern on the morphology and growth speed of TiO_2 nanotube," *Appl. Surf. Sci.*, vol. 258, no. 1, pp. 76–80, Oct. 2011.

[102] Q. Deng, M. Wei, X. Ding, L. Jiang, B. Ye, and K. Wei, "Brookite-type TiO_2 nanotubes," *Chem. Commun.*, no. 31, p. 3657, 2008.